DOCTOR OF PHILOSOPHY

Mathematical modelling of the innate and adaptive immune response to solid tumours

Al-Tameemi, Mohannad Musa Eisa

Award date:
2011

DOCTOR OF PHILOSOPHY

Mathematical modelling of the innate and adaptive immune response to solid tumours

Mohannad Musa Eisa Al-Tameemi

2011

University of Dundee

Mathematical Modelling of the Innate and Adaptive Immune Response to Solid Tumours

By

Mohannad Musa Eisa Al-Tameemi

Doctor of Philosophy

Division of Mathematics

University of Dundee

Dundee

December 2011

To my wife ...

To my sons (Saif - Ayman)

Contents

List of Figures

List of Tables

Acknowledgements

Praise be to ALLAH, the Almighty, whose gracious help made it easy to accomplish successfully this project. Foremost I would like to express my deep thanks and appreciation to my supervisor, Professor Mark Chaplain whose support, constant guidance and continuous encouragements made my thesis work possible. He has always been available to advise me. I wish to thank him for his understanding, patience, motivation, enthusiasm and his immense knowledge. I owe him lots of gratitude for having shown me this way of research. He could not even realise how much I have learned from him. Thank you again Mark for these extremely fruitful four years and I hope that our routes will cross again soon in the future.

I wish also to thank Dr Alberto d'Onofrio for the numerous helpful discussion concerning various aspects of the tumour-immune-system interactions. These discussions were of great importance in the development of my understanding of these issues.

I would like to thank all the members of staff of the Department of Mathematics, in particular Mr Nick Dawes for providing me with many software packages and solving any technical problems I encountered.

I am greatly indebted to my father, mother, brother, and the rest of my family for encouragement, prayers and support they have provided me during my studies. My sincere thanks to my wonderful wife, Emman, for her understanding and love during the past few years. Her support and encouragement was in the end what made this thesis possible. She has managed patiently to look after our little stars, Saif and Ayman, and support me all the time so that I could concentrate on my studies.

Special thanks go to all the PhD students here in Dundee. In particular, I would like to mention the names of Ebraheem Alzahrani, Ali Al-Taie, Faik Mayah, Asad Al-Defae, Marc Sturrock, and Vivi Andasari. I thank you all for being such great friends to me.

Last, but not least, I would like to thank the Iraqi government (Ministry of Higher Education and Scientific Research) and the Iraqi Cultural Attaché in London for sponsoring and helping me during my studying. Also I would like to thank the University of Basrah and College of Education. In particular, all members in my first house, the department of mathematics.

Declaration

I declare that the following thesis is my own composition and that it has not been submitted before in application for a higher degree.

Mohannad Al-Tameemi

Certification

This is to certify that Mohannad Al-Tameemi has complied with all the requirements for the submission of this Doctor of Philosophy thesis to the University of Dundee.

Prof. Mark A. J. Chaplain

Abstract

In this thesis mathematical models describing the growth of a solid tumour in the presence of an immune response are presented. Specifically, attention is focused on the interactions between cytotoxic T-lymphocytes (CTLs) and tumour cells in a small, avascular multicellular tumour. At this stage of the disease the CTLs and the tumour cells are considered to be in a state of dynamic equilibrium or cancer dormancy. The precise biochemical and cellular mechanisms by which CTLs can control a cancer and keep it in a dormant state are still not completely understood from a biological and immunological point of view. The mathematical models focus on the spatio-temporal dynamics of tumour cells, immune cells, chemokines and "chemo-repellors" in an immunogenic tumour. The CTLs and tumour cells are assumed to migrate and interact with each other in such a way that lymphocyte-tumour cell complexes are formed. These complexes result in either the death of the tumour cells (the normal situation) or the inactivation of the lymphocytes and consequently the survival of the tumour cells. In the latter case, we assume that each tumour cell which survives its "brief encounter" with the CTLs undergoes certain beneficial phenotypic changes. We explore the dynamics of the model under these assumptions and show that the process of the immuno-evasion can arise as a consequence of these encounters.

Our computational simulations suggest that the proposed mechanism is able to mimic

various dynamics of immunoevasion during the lifespan of a mouse. We also highlight the differential spatiotemporal contributions to evasion due, respectively, to: *i)* a decrease in the probability p_i of being lethally hit; *ii)* a decrease in the probability, embedded in k_i^+, that a tumour cell is recognized by a CTL. In particular, our model suggests that a decrease in the parameters p_i is needed to produce evasion, which does not occur in the case where p_i remains constant at its baseline level inferred from the experimental data. However, the role of the parameters k_i^+ is important since it can greatly accelerate the simulated process. Moreover, our computational simulations also show that the proposed mechanism can also deeply affect the spatial patterning of the tumour. In particular, our model suggests that to have a uniform invasion profile for the tumour cells necessitates also having a decrease in the recognition rate, embedded in the parameters k_i^+. These parameters also differentially shape the spatial distribution of the various classes of tumour cells.

Also in this thesis, we discuss mathematical models of the interactions between a tumour and both the innate and the cellular part of the adaptive immune system. We have developed and formulated spatiotemporal models of the interactions between macrophages, natural killer cells, cytotoxic T lymphocytes and tumour cells. In addition to presenting computational simulations of our ODE and PDE models, we investigate the linear stability analysis of steady states of the model and the effect of the initial conditions on the behaviour of the ODE solution. We show that limit cycle behaviour could be obtained by making some changes in the parameter values, which gave us oscillations in the solution of the ODE and PDE systems. We observe that there is a slowly damped oscillation in the behaviour of the tumour, natural killer and CTL cells. Also we note that the solution converges to the second steady state where the tumour size is small (dormant state).

A model of cancer invasion and metastasis is also discussed in this thesis. This model attempts to describe the interactions between cancer cells, urokinase plasminogen activator (uPA), plasminogen activator inhibitor-1 (PAI-1), plasmin, extracellular matrix (ECM) and the immune response. The mathematical model focuses on the effect of the immune response on cancer invasion by assuming that there is some form of limit cycle behaviour between the cancer cells and the effector cells. The work we present in this chapter develops a mathematical model for tumour invasion with an immune response using a continuum model in 1 and 2 space dimensions. This model consists of a system of nonlinear partial differential equations and examines the effector cell response the tumour invasion. This model consists of effector cells, tumour cells, ECM, uPA, PAI-1, and plasmin. First, we set all spatial components of the model to zero and consider only the reaction kinetics in order to compare between the behaviour of our model and the original Chaplain and Lolas model (Chaplain and Lolas, 2005). The spatially homogeneous simulation shows the behaviour of solutions have regular oscillations because there is a closed orbit. Second, we present the computational results of the spatio-temporal model, and we note from these simulations that the tumour size of our model is smaller than the tumour size of the Chaplain and Lolas model because the immune cells are interacting with the tumour cells, and also the degradation of ECM is less than that in the Chaplain and Lolas model. In addition, the number of tumour cell clusters in our model is less than those in the Chaplain and Lolas model. Also we found the tumour clusters of the mathematical model which was discussed in this chapter to have the same range than the tumour clusters of the Chaplain and Lolas model.

The final model presented in this thesis is a mathematical model of cancer cells and effector cells which exhibit standing-wave behaviour between them. We show tha the wave of invading cancer cells can be stopped by the wave of effector cells or ECM.

This model also focuses on the effect of the mutation of cancer cells to another sub-population which is more malignant and which has the ability to invade the ECM or the effector cells to occupy space. The numerical simulations discussed in this chapter are essentially associated with an initial model of two equations representing the effector cells and tumour cells, such that there is a standing wave between these species. We note that the solution of the mathematical model is a travelling wave and also has a standing wave solution (i.e. the wave of effector cells stops the wave of tumour cells when they meet). This phenomenon occurs when the two diffusion coefficients are the same. We calculate the wave speed to illustrate that the speed tends to zero when the two waves meet - a positive speed of tumour cells refers to an invading tumour, and a negative speed refers to the decreasing of effector cells. After this we modify the model by adding an equation for a second cancer cell population T_2, which is a sub-population 2 of tumour cells. This is to reflect the fact that cancer is a progressive disease, and as such it becomes more malignant as the cancer cells undergo successive mutations. We show in this case how the new type of cancer cells start to invade the effector cells after the failure of the first type. The third model discussed in this chapter is arrived at by adding an ECM equation to the second model, and it explains how the standing wave arise from two types of equations - the first one contains diffusion, and the second one has no diffusion.

All the mathematical models in this thesis use numerical analysis of nonlinear partial differential equations and computational simulations to obtain insight into the underlying biological systems. The systems of nonlinear partial differential equations were numerically solved by a PDE solver in MATLAB for 1D and COMSOL for 2D. We used the MATLAB PDE solver *pdepe* which uses the method described in Skeel and Berzins (1990) for the spatial discretisation and the MATLAB routine *ode15s* for the

time integration.The numerical simulations demonstrate the existence of cell distributions that are quasi-stationary in time and heterogeneous in space. A linear stability analysis of the underlying (spatially homogeneous) ordinary differential equation (ODE) kinetics coupled with a numerical investigation of ODE system. Our approach may lead to a deeper understanding of the phenomenon of interactions between cancer cells and the immune response and may be helpful in the future development of more effective anti-cancer vaccines.

Publications

1. M. Al-Tameemi, M. Chaplain, A. d'Onofrio (2011). Evasion of tumours from the control of the immune system: consequences of brief encounters. *In preparation*.

2. M. Al-Tameemi, M. Chaplain, A. d'Onofrio (2011). A mathematical model of the innate and adaptive immune response to cancer. *In preparation*

Chapter 1

Introduction

Tumours interact at different levels with the host organism, and in particular with the host immune system. These interactions are complex, and therefore is important to model them mathematically. Mathematical models can help us to better understand these interactions. The immune system comprises two parts: the innate immune system which protects the body from a large number of pathogens using defences that are quickly mobilised and triggered by receptors that recognise a broad spectrum of pathogens; and the adaptive immune system which develops specific cells to combat infections by viral agents. The aim of this thesis is to characterise the main aspects of the tumour-immune system interactions, by studying the interactions between tumours and cytotoxic T lymphocytes (CTLs), macrophages, and natural killer cells.

In vivo experiments are crucial for the understanding of the interactions between the immune system and tumours. However, they are usually very costly and can take months for an experienced team to perform. They are also very complex to follow since it is difficult to observe them without disrupting the ongoing process. So, in vivo experiments can usefully be complemented by a mathematical and statistical approach.

Computer Science can help and enhance our understanding of the immune system-tumour interactions by allowing us to simulate complex systems and behaviours that cannot be observed directly. Computer models can simulate experiments lasting years in real time in a far shorter time and give access to information which is normally hidden during in vivo studies. The precision of these simulations depends on the model used to represent the tumour-immune response interactions. In this thesis, we will present four mathematical models, three for tumour-immune response interactions, and one for a cancer invasion model. The three tumour-immune interactions models are: (i) a model of tumour-CTLs interactions which develops the original work of Matzavinos et al. (2004); (2) a model of macrophage-tumour interactions which develops the work of (Owen and Sherratt, 1997, 1999), and (3) a model of natural killer cell-tumour interactions which develops the work of de Pillis et al. (2005). The invasion model is focussed on the role of the uPA plasminogen activation system and it's role in cancer invasion and develops work by Chaplain and Lolas (2005).

The remaining chapters are organised as follows.

Chapter 2 presents a biological overview of the immune system and its interactions with cancer cells. The aim of this chapter is to give some basic information about the main components of the immune system, especially macrophages, natural killer cells, and CTLs, in addition to explaining the process of immune evasion.

Chapter 3 gives an overview of general reaction-diffusion equations, and explains the important processes which can be applied to analyse mathematical models such as linear stability analysis to determine the stability of the steady states, the non-dimensionalisation of a model with its importance and steps, travelling wave analysis, diffusion-driven instability to check the effect of adding a diffusion term to a system

of ODEs, and limit cycle dynamics arising from Andronov-Hopf bifurcations.

In chapter 4 a review of the various mathematical models that have been developed over the past few decades for the immune-response-tumour interactions is given. Also some general mathematical models of cancer are reviewed.

A spatio-temporal model concerning the evasion of a tumour from the control of the immune system is examined in chapter 5. In particular, we focus on the interactions between CTLs and tumour cells in a small, avascular multicellular tumour, and we assume that each tumour cell which survives its "brief encounter" with the CTLs undergoes certain beneficial phenotypes changes. We show the process of immuno-evasion can arise as a consequence of these encounters.

In chapter 6, we present a mathematical model of the interplay between a tumour and both the innate and the cellular part of the adaptive immune system. We include in this model three types of cell of the immune system: macrophages, natural killer cells and CTLs.

In chapter 7, we present a mathematical model of cancer invasion with an immune response. This model consists of a growing tumour and its interactions with urokinase plasminogen activator, plasminogen activator inhibitor-1, plasmin, extracellular matrix and an immune response.

Chapter 8, we describe a model of solid tumour development where competition for space between the cancer cells, effector cells and ECM is important, and discuss the possible dynamics of standing waves between the effector cells and the tumour cells.

We conclude the thesis with a final chapter concerning discussions and future work.

Chapter 2

Biological Background

In this chapter we review the biological background of cancer and the immune system, and the interactions between them. We also describe the phenomenon of tumour evasion from the immune response.

2.1 What is Cancer?

Cancer is not a single disease, but actually a collection of different diseases. It is "*a new growth of tissue resulting from a continuous proliferation of abnormal cells that have the ability to invade and destroy other tissues*" (King, 2000). In a now famous review paper, Hanahan and Weinberg attribute six key phenotypic differences, or "hallmarks", which distinguish cancer cells from healthy cells (Hanahan and Weinberg, 2000). These are:

- Self-sufficiency in growth signals,
- Insensitivity to growth-inhibitory (i.e. anti-growth) signals,

- Evasion of programmed cell death (apoptosis),
- Limitless replicative potential,
- Sustained angiogenesis,
- Tissue invasion and metastasis.

Recently Fang et al. (2008), also included low levels of oxygen:

- Hypoxia

Cancers are classified in two ways: by the type of tissue from which the cancer originated (histological type) and by the primary site, or the location in the body where the cancer first developed (Alberts et al., 1994). Another term for cancer is "tumour". Tumour literally means "swelling" or mass. After carcinogenesis the development of any cancer is a multi-step process. The initial mutations cause hyperplasia, where the appearance of the cells remains normal but they reproduce too much. At this stage the tumour is benign or non-invasive. Such tumours are not normally life-threatening. They do not have a blood supply and therefore the size is limited, to a diameter of approximately 2mm, because all the nutrients they require to grow must diffuse in from outside the tumour. Benign tumours are unable to destroy normal tissue but can compress it as they grow. Before becoming malignant, or invasive, the tumours go through more mutations. Tumours may also induce the host's blood vessel system to supply them with the nutrients the tumour needs to grow, a process known as angiogenesis. Malignant or invasive tumours are far less differentiated than benign ones. They also have different adhesive properties. Benign cells are strongly homotypic which means they stick to cells of their own kind. Malignant cells become heterotypic which means that individual cells break away from the tumour and adhere to the surrounding connective tissue. Malignant cells may invade the tissue and form secondary growths by a multi-step process known as metastasis.

Table 2.1: Cells of the immune system

Cell type	Type of immunity
Neutrophils	Innate
Eosinophils	Innate
Basophils	Innate
Mast cells	Innate
Monocytes/macrophages	Innate
Dendritic cells	Innate
Natural killer cells	Innate
Cytotoxic T lymphocytes	Adaptive
Helper T lymphocytes	Adaptive
B lymphocytes	Adaptive

2.2 The Immune System Response

The Immune System is a collection of cells, tissues, and molecules that mediate resistance to disease, specifically infectious disease. The coordinated reaction of these cells and molecules to infectious microbes is the immune response. Immunology is the study of the immune system and its response to invading pathogens (Abbas and Lichtman, 2009). The immune system's cellular components can be considered as mediators of either innate or adaptive immunity (see Table 2.1) (Todd and Spickett, 2005).

2.2.1 Innate and Adaptive Immunity

Innate immunity (also called natural or native immunity) refers to the fact that this type of host defence is always present in healthy individuals, prepared to block the entry of microbes and to rapidly eliminate microbes that do succeed in entering host tissue.
Adaptive immunity (also called specific or acquired immunity) is the type of host defence that is stimulated by microbes that invade tissue, that is, it adapts to the presence of microbial invaders (Abbas and Lichtman, 2009).

The first line of defence in innate immunity is provided by epithelial barriers and by specialised cells and natural antibiotics present in epithelia, all of which function to block the entry of microbes. If microbes do breach the epithelia and enter the tissue or circulation system, they are attacked by phagocytes, specialised lymphocytes called natural killer cells, and several plasma proteins, including the proteins of the complement system. Innate immunity is rapidly activated in the early stages of an infection and its defensive properties can limit the proliferation and spread of a pathogen within the body. However, it is only moderately efficient in clearing infection, and its capabilities remain the same on repeated exposure to the same microbe.

The resolution of an infection usually requires an additional adaptive immune response by T-lymphocytes and B-lymphocytes (also referred to as T-cells and B-cells). The adaptive immune response takes longer to activate than an innate immune response but generates a more effective defence which improves upon repeated exposure to the same microbe.

2.2.2 Cells of the Immune System

Both innate and adaptive immune responses depend upon the activities of white blood cells or leukocyets. These cells all originate in the bone marrow, and many of them also develop and mature there (Murphy et al., 2008). In this section we describe some types of immune cells, which we will use in the mathematical models of the next chapters:

Macrophages

Macrophages are resident in almost all tissue and are the mature form of monocytes, which circulate in the blood and continually migrate into tissues where they differentiate. Macrophages are relatively long-lived cells and perform several different functions

throughout the innate immune response and the subsequent adaptive immune response. One is to engulf and kill invading microorganisms. In this phagocytic role they are an important first defence in innate immunity and also dispose of pathogens and infected cells targeted by an adaptive immune response. An additional and crucial role of macrophages is to orchestrate the immune response: they help induce inflammation, which is a prerequisite to a successful immune response, and they secrete signalling proteins that activate other immune-system cells and recruit them into an immune response (Murphy et al., 2008).

Lymphocytes

The common lymphoid progenitor in the bone marrow gives rise to the antigen-specific lymphocytes of the adaptive immune system and also to a type of lymphocyte that responds to the presence of infection but is not specific for a given antigen, and is thus considered to be part of the innate immune system. This latter is a large cell with a distinctive granular cytoplasm and is called a natural killer (NK) cell. There are two types of lymphocytes: B-lymphocytes (B cells) and T-lymphocytes (T cells) each with quite different roles in the immune system and distinct type of antigen receptors (Murphy et al., 2008).

Natural Killer Cells

Natural killer cells are a part of the innate immune system, and are able to recognise and kill some abnormal cells, for example some tumour cells and cells infected with herpes viruses.

Natural killer cells are a class of lymphocytes that recognise infected and stressed cells

and respond by killing these cells and by secreting the macrophage-activating cytokine (Abbas and Lichtman, 2009). Natural Killer cells make up approximately 10% of the lymphocytes in the blood and peripheral lymphoid organs. The cytotoxic mechanism of NK cells is the same as the mechanism used by CTLs to kill infected cells.

T lymphocytes

T-cells are lymphocytes that originate from bone marrow stem cells but emigrate to mature in the thymus, which they enter at the outer margin of the cortex, and are then known as thymocytes. There are three main types of T-cells: killer T-cells (frequently called cytotoxic lymphocytes or CTLs for short), helper T-cells, and regulatory T-cells. The killer T-cells are a potent weapon that can destroy virus-infected cells. The second type of T-cells is the helper T-cell, and this cell serves as the "quarterback" of the immune system team. It directs the action by secreting protein molecules called cytokines that have dramatic effects on other immune system cells. The third type of T-cell, the regulatory T-cell, is still quite mysterious. Although it is believed that regulatory T-cells help keep other T-cells under control, it still isn't clear exactly how they do this or what "under control" means in this context (Sompayrac, 2008).

2.3 Cancer Immune System Interactions

For over a century, cancer immunologists have sought to harness a patient's immune system to augment conventional therapies. Although ideas for boosting cancer immunity have been regularly shown to work to some extent in animal models, the development of useful routine immunotherapies for human cancer is still at an early stage. In some cases, the immune response will be able to control or even eliminate the cancer,

but in others the tumour load will be so great that the immune system will be overwhelmed.

The result of interactions between immune system cells and tumour cells is equally dependent on the functional state of the immune system cells, and on biological patterns of tumour cells. The biological properties of tumour cells are reflected in: 1)recognition of tumour antigens; 2) the character of the immune response (growth inhibition or stimulation, tolerance); 3) the expression of antitumour action of CTLs; 4) the formation of immunosuppression; 5) the influence of tumour cell patterns on the formation of the microenvironment; 6) the development of resistance to CTLs action and drug resistance; 7) the efficacy of immunotherapy etc. (Berezhnaya, 2010).

In mice which have been engineered so that one or more components of their immune system is defective, an increased incidence of lymphoma, leukaemia, and virus-associated cancer is well documented. However, the evidence that mice with compromised immune systems experience an increase in solid tumours that do not involve a virus infection is not compelling. Likewise, in humans there is strong evidence that a weakened immune system can increase one's chances of getting blood-cell and virus-associated cancer.

2.3.1 Macrophages and NK Cells Against Cancer

Macrophage and natural killer cells may provide surveillance against some cancers. Hyperactivated macrophages secrete tumour necrosis factor (TNF) and express it on their surface. Either form of TNF can kill certain types of tumour cells in the best tube. NK cells target cells that express low levels of class I Major histocompatibility complex protein (MHC) molecules, and which display unusual surface molecules (e.g. proteins which indicate that the target cells are "stressed"). There would be a number

of advantage to having macrophages and NK cells provide surveillance against potential cancer cells. First, unlike CTLs, which take a week or more to become fully functional, macrophage and NK cells are fast-acting. This is an important consideration, because the longer abnormal cells have to proliferate, the greater is the likelihood they will mutate to take on the characteristic of metastatic cancer cells. Second, both NK cells and macrophages recognise diverse target structures, so the chance of them being fooled by a single mutation is small. In addition, macrophage are located out in the tissue where most tumours arise, so they can intercept cancer cells at an early stage. NK cells do not need to be activated to kill, since natural killer cells that are circulating in the blood may be able to destroy either blood-cell cancers or cancer cells that are metastasising through the blood from a primary tumour (Sompayrac, 2008).

2.3.2 CTLs Against Cancer

We describe the interactions between CTLs and some types of cancers: spontaneous tumours, cancerous blood cells, and virus-associated tumours.

CTLs and spontaneous tumours

The majority of human cancers are spontaneous tumours that are not of blood-cell origin, and it has been proposed that killer cells might provide surveillance against these cancers. A CTL would have to perform an "unnatural act" to be activated by a tumour out in the tissues i.e. it would have to break the "traffic laws", and somehow avoid being energised or killed. This could happen, but it would be very inefficient in comparison to the activation of CTLs in response to viral infection. Another possible scenario is that cancer cells from the primary tumour might metastasis to a lymph node, where T-cells could be activated. However, by the time this happens, the original

tumour probably will have become quite large and this poses an additional problem. A tumour cell's high mutation rate is its greatest advantage over the immune system, and usually keeps these cells one step ahead of surveillance by CTLs. So even when it occurs, CTL surveillance is usually a case of "too little, too late" (Sompayrac, 2008).

CTLs and cancerous blood cells

One of the difficulties that CTLs have in providing surveillance against tumours that arise in tissues is that these tumours simply are not on the normal traffic pattern of the virgin T-cells, and it is hard to imagine how a CTL could be activated by a cancer it doesn't see. In contrast, most blood cell cancers are found in the blood, lymph, and secondary lymphoid organs, and this is ideal for viewing by CTLs, which pass through these all the time. Thus, in the case of blood-cell cancers, the traffic pattern of cancer cells and virgin T-cells actually intersect. Moreover, in contrast to tumours in tissues, which usually are unable to supply the co-stimulation required for activation of virgin T-cells, some cancerous blood cells actually express high levels of B7, and therefore can provide the necessary co-stimulation. These properties of blood-cell cancers suggest that CTLs may provide surveillance against some of them. Unfortunately this surveillance must be incomplete, because people with otherwise healthy immune systems still get leukemias and lymphomas (Sompayrac, 2008).

CTLs and virus-associated tumours

Most viruses cause "acute" infections in which all the virus-infected cells are rather quickly destroyed by the immune system. Since a dead cell is not going to make a tumour, viruses which only cause acute infection do not play role in cancer. This explains why most viral infections are not associated with human cancer.

There are viruses, however, which can evade the immune system, and establish long-term infections. Importantly, all viruses which have been shown to play a role in causing cancer are able to establish long-term infections during which they "hide" from the immune system. Because CTLs cannot destroy virus-infected cells while they are hiding, and because these hidden cells are the very ones that eventually become cancer cells, it can be argued that CTLs cannot provide significant surveillance against virus-associated cancers. Also CTLs cannot provide significant surveillance against virus-infected cells once they have become cancerous, because these cancers only result from long-term viral infections i.e. infections which CTLs cannot detect or cannot deal with (Sompayrac, 2008).

2.4 Tumour Immune Evasion

The immune response often fails to check tumour growth, because these responses are ineffective or because tumours evolve to evade an immune attack. The immune system faces a daunting challenge if it is to be effective against malignant tumours, because any immune responses must kill all tumour cells and tumours grow rapidly. Often, the growth of the tumour simply outstrips immune defences. The immune response against tumours may be weak because many tumour antigens are weakly immunogenic, perhaps because they differ only slightly from self-antigens. Growing tumours also develop mechanisms for evading immune responses. Some tumours stop expressing the antigens that are the targets of immune attack. These tumours are called "antigen loss variants". If the lost antigen is not involved in maintaining the malignant properties of the tumour, the variant tumour cells continue to grow and spread (Abbas and Lichtman, 2009).

Cytotoxic CD8 T-cells are the best effector cells for killing tumour cells. One way in

which tumour cells escape a cytotoxic T-cell is to stop expressing the autologous HLA class I molecule that presents the tumour antigen to the T-cell. Between one-third and one-half of all human tumours have a defective expression of one or more of their HLA class I allotypes. That is, many patients have made a CD8 T-cells response against their cancer but variant cells lacking particular HLA class I allotypes have escaped that immune response and expanded to keep the cancer going (Parham, 2009). Loss of HLA class I expression can in some circumstances make a tumour susceptible to attack by NK cells. The killing of acute myelogenous leukaemia cells by alloreactive NK cells in an HLA-haploidentical bone marrow transplant occurs because the recipient's tumour cells lack an HLA class I allotype that the donor-derived NK-cells see as "self". This is an example of NK-cells attacking a cell that is 'missing self'.

As well as evading the immune response, tumours can also manipulate the immune response in their favour. In the absence of inflammation, tumour-cell antigens can be processed and presented to cells by dendritic cells that lack B7 co-stimulators. As a result, the tumour secretes cytokines such as TGF-β that create an immunosuppressive environment in the tumour, which can be reinforced by the recruitment of regulatory cells (Parham, 2009).

Chapter 3

Mathematical Background

A mathematical model is an abstract, simplified mathematical construction to part of the "real world" and is created for a specific purpose, i.e., it is designed to mimic reality by using the language of mathematics. Mathematical models contribute to an understanding of the real system which is being modelled. Such simulation helps us to look at reality more deeply and with a heightened understanding. A good mathematical model can be used to: (1) help confirm or reject hypotheses about complex systems; (2) reveal contradictions or incompleteness of data and/or hypotheses; (3) predict system performance under untested or presently untestable conditions; (4) predict and supply information on the value of experimentally inaccessible variables; and finally, (5) a good mathematical model may suggest the existence of new unobserved phenomena. Modelling can help us avoid, or reduce the need for costly, undesirable or impossible experiments in the real world. In this chapter, we present some technical background we will use to analyse our mathematical models, especially reaction-diffusion models and we will explain travelling wave solutions of these models. Also we will describe the phenomenon of diffusion-driven instability and then limit cycle behaviour through Andronov-Hopf bifurcations.

3.1 Reaction Diffusion Equations

The dynamics of reactive mixtures results from local transformation process, chemical reactions, and transport in space, diffusion. These process are typically modelled by a standard reaction-diffusion equation

$$\frac{\partial \rho}{\partial t} = D\frac{\partial^2 \rho}{\partial x^2} + F(\rho), \tag{3.1}$$

where ρ is a vector of concentration of the diffusing species, D is the diffusion matrix, and F is a kinetic term describing reactions or interactions between the species. Reaction-diffusion models are not limited to the field of chemistry and chemical engineering. They can describe the dynamics of nonchemical systems, and reaction-diffusion equations provide a general theoretical framework for the study of phenomena in areas such as biology, ecology, physics, and materials science (Mendez et al., 2010).

3.1.1 Rate Equations

If spatial effects can be neglected, many systems in chemistry, biology, ecology, physics, and other areas can be described by rate equations, i.e. a set of ordinary differential equations. Systems may be homogeneous because the system is small enough and transport is efficient enough to eliminate spatial gradients, or the spatial homogeneity may be imposed from the outside. We consider systems consisting of individuals, e.g., microorganism or animals, or particles, e.g., molecules of n different species. We assume that the system is large enough that a continuum, mean-field description is valid, i.e., the internal fluctuations due to the discrete nature of the constituents can be neglected. The evolution of the densities or concentrations is governed by the kinetic

equations:

$$\frac{\partial \rho}{\partial t} = F(\rho, \mu), \tag{3.2}$$

where $\rho \in \mathbb{R}^n$ and F : $\mathbb{R}^n \to \mathbb{R}^n$. For systems of particles, the coefficients or parameters of the rate terms, μ, are real numbers. Evolution equations for systems of particles must posses certain properties to be acceptable descriptions. The densities ρ_i, i=1,...,n, cannot be negative. Therefore the kinetic Equations must preserve positivity, i.e., $\rho_i(0) \geq 0$ at time $t = 0$ implies $\rho_i(t) \geq 0$ for all times $t > 0$.
Equations (3.2) have this property if

$$F_i(\rho_1, ..., \rho_{i-1}, 0, \rho_{i+1}, ..., \rho_n) \geq 0.$$

It is sometimes convenient to split the rate function F_i into its positive and negative parts, i.e., write it in production-loss form:

$$F_i(\rho) = F_i^+(\rho) - F_i^-(\rho),$$

where $F_i^+(\rho) \geq 0$ and $F_i^-(\rho) \geq 0$. The first term, F_i^+, is the production or birth term and captures the processes that increase the chemical concentration or population density. The second term, F_i^-, is the loss or death term and captures the processes that decrease the concentration or density.

3.1.2 Linear Stability Analysis

Studies of the dynamics of a system generally pay little attention to transient behaviour and focus instead on the ultimate fate of the system, the asymptotic state it attains as time goes to infinity. These can be stationary state, time-dependent periodic states, or

time-dependent aperiodic or chaotic states. Our interest here is the former, the stationary or steady states and their properties.

Let $\bar{\rho}$ be a stationary state of (3.2):

$$F(\bar{\rho}) = 0.$$

The stationary state $\bar{\rho}$ is stable if trajectories that start sufficiently close to it stay close to the steady state. This is more formally stated in the following definition:

Definition 3.1.1 *The Stationary state $\bar{\rho}$ is Lyapunov stable if for any $\varepsilon > 0$, there exists a $\delta > 0$ (depending on ε) such that for all initial condition $\rho(0) = \rho_0$ with $|\rho_0 - \bar{\rho}| < \delta$ we have $|\rho(t) - \bar{\rho}| < \varepsilon$ for all $t > 0$.*

This definition states only that a stationary state is stable if the system does not wander too far away when starting close enough to the steady state. The next definition is a stronger notion of stability, namely that the system actually returns to the steady state after a sufficiently small perturbation (Mendez et al., 2010).

Definition 3.1.2 *The Stationary state $\bar{\rho}$ is asymptotically stable in the sense of Lyapunov, if there exists an η such that if $|\rho_0 - \bar{\rho}| < \eta$ then*

$$\lim_{t \to \infty} |\rho(t) - \bar{\rho}| = 0.$$

The stationary state $\bar{\rho}$ is globally asymptotically stable if η can be arbitrarily large (Mendez et al., 2010). Let $\delta(t) = \rho(t) - \bar{\rho}$. The evolution of the perturbation $\delta(t)$ is given by

$$\frac{d\delta}{dt} = J\delta + N(\delta),$$

where $N(\delta) = o(\delta)$ as $\delta \to 0$, i.e., $|N(\delta)/\delta| \to 0$ as $|\delta| \to 0$. The $n \times n$ matrix J is the Jacobian matrix of the system evaluated at the steady state $\bar{\rho}$ and is given by

$$\left.\frac{\partial F_i}{\partial \rho_j}\right|_{\bar{\rho}}.$$

Neglecting the small nonlinear terms $N(\delta)$, we obtain the linearised system, with respect to the steady state $\bar{\rho}$, for (3.2):

$$\frac{d\delta}{dt} = J\delta. \tag{3.3}$$

Let λ_i, i=1,...,n, be the eigenvalues of the Jacobian J and Φ_i, i=1,...,n, the associated eigenvectors. For the generic case that all eigenvalues are distinct, the solution of (3.3) is given by

$$\delta(t) = \sum_{i=0}^{n} a_i \Phi_i exp(\lambda_i t),$$

where a_i are constants determined by the initial condition $\delta(0)$. If all eigenvalues of the Jacobian have a negative real part, $Re\lambda_i < 0$ for i=1,...,n, then the perturbations decay, i.e., the solution of the linearised equation (3.3) approaches 0. If there exists at least one $\lambda_{i'}$ with a positive real part, $Re\lambda_{i'} > 0$ then the system moves away from the steady state. The stability of the steady state $\bar{\rho}$ is determined by the eigenvalues of the Jacobian. That is the content of the following theorem.

Theorem 3.1.1 *(a) if all the eigenvalues λ_i, i=1,...,n, of the Jacobian matrix J have a negative real part, then the steady state $\bar{\rho}$ of the nonlinear evolution (3.2) is asymptotically stable. (b) if at least one eigenvalue of J has a positive real part, then the steady state $\bar{\rho}$ is unstable. (c) If the Jacobian has one or more eigenvalues with zero real part and no eigenvalues with positive real part, then the steady state $\bar{\rho}$ may be stable, unstable, or asymptotically stable depending on the nonlinear terms.*

The eigenvalues λ_i of J are the roots of the nth order characteristic polynomial, $(-1)^n det(J-\lambda I_n)=0$, where I_n is the $n \times n$ identity matrix,

$$\lambda^n + c_1\lambda^{n-1} + c_2\lambda^{n-2} + ... + c_{n-1}\lambda + c_n = 0.$$

3.1.3 Diffusion

In an assemblage of particles, for example, cells, bacteria, chemicals, animals and so on, each particle usually moves around in a random way. The particles spread out as a result of this irregular individual particles motion. When this microscopic irregular movement results in some macroscopic or gross regular motion of the group we can think of it as a diffusion process (Murray, 2002). The classical approach to diffusion considers Fickian diffusion which states that the flux, **J**, of material, which can be cells, concentration of chemical, number of animals and so on, is proportional to the gradient of the concentration of the material. That is, in one-space dimension:

$$J \propto -\frac{\partial \rho}{\partial x} \qquad \Rightarrow \qquad J = -D\frac{\partial \rho}{\partial x}, \tag{3.4}$$

where $\rho(x,t)$ is the concentration of the species and D is its diffusivity. The minus sign simply indicates that diffusion transports matter from a high to a low concentration.
We now write a general conservation equation which says that the rate of change of the amount of material in a region is equal to the rate of flow across the boundary plus any that is created within the boundary. If the region is $x_0 < x < x_1$ and no material is created,

$$\frac{\partial}{\partial t}\int_{x_0}^{x_1} \rho(x,t)dx = J(x_0,t) - J(x_1,t).$$

If we take $x_1 = x_0 + \Delta x$, take the limit as $\Delta x \to 0$ and use (3.4) we get the classical diffusion equation in one dimensional, namely,

$$\frac{\partial \rho}{\partial t} = -\frac{\partial J}{\partial x} = \frac{\partial (D\frac{\partial \rho}{\partial x})}{\partial x},$$

which, if D is constant, becomes

$$\frac{\partial \rho}{\partial t} = D\frac{\partial^2 \rho}{\partial x^2}. \tag{3.5}$$

If we release an amount Q of particles per unit area at x = 0 at t = 0, that is,

$$\rho(x,0) = Q\delta(x).$$

where $\delta(x)$ is the Dirac delta function, then the solution of (3.5) is

$$\rho(x,t) = \frac{Q}{2(\pi DT)^{1/2}} e^{-x^2/(4Dt)}, \qquad t > 0.$$

3.1.4 Chemotaxis

A large number of insects and animals (including humans) rely on an acute sense of smell for conveying information between members of the species. Chemicals which are involved in this process are called pheromones. For example, the female silk moth Bombyx mori exudes a pheromone, called bombykol, as a sex attractant for the male, which has a remarkably efficient antenna filter to measure the bombykol concentration, and it moves in the direction of increasing concentration. In this thesis we model chemically directed movement, which is called chemotaxis, which, unlike diffusion, directs the motion up a concentration gradient. It is not only in animal and insect ecology that chemotaxis is important. It can be equally crucial in biological processes

where there are numerous examples. For example, when a bacterial infection invades the body it may be attacked by movement of cells towards the source as a result of chemotaxis. Convincing evidence suggests that leukocyte cells in the blood move towards a region of bacterial inflammation, to counter it, by moving up a chemical gradient caused by the infection.

Let us suppose that the presence of a gradient in an attractant, a(x,t), gives rise to a movement, of the cells say, up the gradient. The flux of cells will increase with the number of cells, $\rho(x,t)$, present. Thus we may reasonably take as the chemotactic flux

$$J = \rho\chi(a)\nabla a, \tag{3.6}$$

where $\chi(a)$ is a function of the attractant concentration. In the general conservation equation for $\rho(x,t)$, namely

$$\frac{\partial\rho}{\partial t} + \nabla\cdot J = f(\rho),$$

where $f(\rho)$ represents the growth term for the cells, the flux

$$J = J_{diffusion} + J_{chemotaxis}$$

where the diffusion contribution is from $J = -D\nabla\rho$, with the chemotaxis flux from (3.6). Thus a basic reaction-diffusion-chemotaxis equation is

$$\frac{\partial\rho}{\partial t} = f(\rho) - \nabla\cdot\rho\chi(a)\nabla a + \nabla\cdot D\nabla\rho,$$

where D is the diffusion coefficient of the cells.

Since the attractant a(x,t) is a chemical it also diffuses and is produced, by the amoebae, for example, so we need a further equation for a(x, t). Typically

$$\frac{\partial a}{\partial t} = g(a,\rho) + \nabla\cdot D_a\nabla a,$$

where D_a is the diffusion coefficient of a and $g(a,\rho)$ is the kinetics/source term, which may depend on ρ and a. Normally we would expect $D_a > D$ (Murray, 2002).

3.1.5 Non-Dimensionalisation

Non-dimensionalisation is the partial or full removal of units from an equation involving physical quantities by a suitable substitution of variables. It is the first and arguably the most important step in the analysis of a system of differential equations. It involves scaling each variable (dependent and independent) by a typical or reference value, leaving a non-dimensional variable whose typical scale is $O(1)$. Non-dimensionalisation or problem normalisation has several important uses:

1. It identifies the dimensionless groups (ratios of dimensional parameters) which control the solution behaviour.

2. Terms in the equations are now dimensionless and so allows comparison of their sizes.

   This allows the identification of the important (i.e. dominant) terms in the equations and their interactions in different regimes, giving insight into the structure of solutions and the dominant physical mechanisms at work.

   In particular, negligible terms can be identified leading to simplification in many circumstances.

3. It allows estimates of the effects of a additional features to the original model through the new dimensional group(s) associated with the additional term(s). This allows measuerment of the effect of the physical feature(s) in the model.

4. Finally, it can reduce the number of parameters occurring in the problem by formation the nondimensional parameters or dimensionless groups.

Non-dimensionalisation steps

To non-dimensionalise a system of equations, one must do the following:

1. Identify all the independent and dependent variables;
2. Replace each of them with a quantity scaled relative to a characteristic unit of measure to be determined;
3. Divide through by the coefficient of the highest order polynomial or derivative term;
4. Choose judiciously the definition of the characteristic unit for each variable so that the coefficients of as many terms as possible become 1;
5. Rewrite the system of equations in terms of their new dimensionless quantities.

3.2 Travelling Wave Solutions

Travelling wave solutions are solutions of special type. They can be usually characteristic as solution invariant with respect to translation in space. A travelling wave is taken to be a wave which travels *without change of shape*, and If a solution $\rho(x,t)$ represents a travelling wave, the shape of the solution will be the same for all time and the speed of propagation of this shape is a constant, which we denote by c (Adam and Bellomo, 1997). A mathematical way of saying this is that if the solution

$$\rho(x,t) = \rho(x-ct) = \rho(z), \qquad z = x-ct, \tag{3.7}$$

then $\rho(x,t)$ is a travelling wave, and it modes at constant speed c in the positive x-direction. A wave which moves in the negative x-direction is of the form $\rho(x+ct)$.

When we look for travelling wave solutions of an equation or system of equations in x and t in the form (3.7), we have $\partial\rho/\partial t = -c\, d\rho/dz$, and $\partial\rho/\partial x = d\rho/dz$. So partial differential equations in x and t become ordinary differential equations in z.
It is part of the classical theory of linear parabolic equations, such as (3.5), that there are no physically realistic travelling wave solutions. Suppose we look for solutions in the form (3.7); then (3.5) becomes

$$D\frac{\partial^2\rho}{\partial z^2} + c\frac{\partial\rho}{\partial z} = 0 \quad \Rightarrow \quad \rho(z) = A + Be^{-cz/D},$$

where A and B are integration constants. Since ρ has to be bounded for all z, B must be zero since the exponential becomes unbounded as $z \to \infty$. $\rho(z) = A$, a constant, is not a wave solution. In marked contrast the parabolic reaction diffusion equation (3.1) can exhibit travelling wave solutions, depending on the form of the reaction/interaction term $f(\rho)$. This solution behaviour was a major factor in starting the whole mathematical field of reaction diffusion theory. Although most realistic models of biological interest involve more than one dimension and more than one dependent variable, whether concentration or population, there are several multi-species systems which reasonably reduce to a one-dimensional single- species mechanism which captures key features.

3.3 Diffusion-Driven Instability

A reaction diffusion system exhibits diffusion-driven instability, sometimes called Turing instability, if the homogeneous steady state is stable to small perturbations in the absence of diffusion but unstable to small spatial perturbations when diffusion is present. The concept of instability in biology is often in the context of ecology, where a uniform steady state becomes unstable to small perturbations and the populations typically exhibit some temporal oscillatory behaviour. The instability we are

concerned with here is of a quite different kind. The main process driving the spatially inhomogeneous instability is diffusion: the mechanism determines the spatial pattern that evolves. How the pattern or mode is selected is an important aspect of the analysis, a topic we discuss in this (and later) chapters. We derive here the necessary and sufficient conditions for diffusion-driven instability of the steady state and the initiation of spatial pattern for the general system

$$\begin{aligned} \frac{\partial u}{\partial t} &= \nabla^2 u + \gamma f(u,v), \\ \frac{\partial v}{\partial t} &= d\nabla^2 v + \gamma g(u,v), \\ (n.\nabla)\begin{pmatrix} u \\ v \end{pmatrix} &= 0, \qquad r \text{ on } \partial B; \qquad u(r,0), v(r,0) \text{ given} \end{aligned} \tag{3.8}$$

where ∂B is the closed boundary of the reaction diffusion domain B and n is the unit outward normal to ∂B. The relevant homogeneous steady state (u_0, v_0) of (3.8) is the positive solution of

$$f(u,v) = 0, \qquad g(u,v) = 0.$$

With no spatial variation u and v satisfy

$$u_t = \gamma f(u,v), \qquad v_t = \gamma g(u,v) = 0. \tag{3.9}$$

Linearising about the steady state (u_0, v_0), we set

$$\begin{pmatrix} u - u_0 \\ v - v_0 \end{pmatrix} \tag{3.10}$$

and (3.9) becomes, for $| w |$ small,

$$w_t = \gamma A w, \qquad A = \begin{pmatrix} f_u & f_v \\ g_u & g_v \end{pmatrix}_{u_0, v_0} \tag{3.11}$$

where A is the stability matrix. We now look for solutions in the form

$$w \propto e^{\lambda t}, \tag{3.12}$$

where λ is the eigenvalue. The steady state w = 0 is linearly stable if Re $\lambda < 0$ since in this case the perturbation w$\rightarrow$0 as t$\rightarrow \infty$. Substituation of (3.12) into (3.11) determines the eigenvalues λ as the splutions of

$$\begin{aligned} | \gamma A - \lambda I | &= \begin{vmatrix} \gamma f_u - \lambda & \gamma f_v \\ \gamma g_u & \gamma g_v - \lambda \end{vmatrix} = 0 \qquad (3.13) \\ \Rightarrow \qquad & \lambda^2 - \gamma(f_u + g_v)\lambda + \gamma^2(f_u g_v - f_v g_u) = 0, \end{aligned}$$

so

$$\lambda_1, \lambda_2 = \frac{1}{2}\gamma \left[(f_u + g_v) \pm \{(f_u + g_v)^2 - 4(f_u g_v - f_v g_u)\}^{1/2} \right].$$

Linear stability, that is , Re $\lambda < 0$, is guaranteed if

$$trA = f_u + g_v < 0, \qquad | A | = f_u g_v - f_v g_u > 0. \tag{3.14}$$

Now consider the full reaction diffusion system (3.8) and again linearise about the steady state, which with (3.10) is w = 0, to get

$$w_t = \gamma Aw + D\nabla^2 w, \qquad D = \begin{pmatrix} 1 & 0 \\ 0 & d \end{pmatrix}. \tag{3.15}$$

To solve this system of equations subject to the boundary conditions (3.8) we first define W(r) to be the time-independent solution of the spatial eigenvalue problem defined by

$$\nabla^2 W + k^2 W = 0, \qquad (n.\nabla)W = 0 \quad for \quad r\ on\ \partial B \tag{3.16}$$

where k is the eigenvalue. For example, if the domain is one-dimensional, say, $0 \leq x \leq a$, $W \propto cos(n\pi x/a)$ where n is an integer; this satisfies zero flux conditions at $x = 0$ and $x = a$. The eigenvalue in this case is $k = n\pi/a$. So $1/k = a/n\pi$ is measure of the wavelike pattern: the eigenvalue k is called the wavenumber and $1/k$ is proportional to the wavelength $\omega; \omega = 2\pi/k = 2a/n$ in this example.

Let $W_k(r)$ be the eigenfunction corresponding to the wavenumber k. Each eigenfunction W_k satisfies zero flux boundary conditions. Because the problem is linear we now look for solutions w(r, t) of (3.15) in the form

$$w(r,t) \quad = \quad \sum_k c_k e^{\lambda t} W_k(r), \tag{3.17}$$

where the constants c_k are determined by a Fourier expansion of the initial conditions in terms of $W_k(r)$. λ is the eigenvalue which determines temporal growth. Substituting this form into (3.15) with (3.16) and cancelling $e^{\lambda t}$, we get, for each k,

$$\begin{aligned} \lambda W_k &= \gamma A W_k + D\nabla^2 W_k \\ &= \gamma A W_k - Dk^2 W_k. \end{aligned} \tag{3.18}$$

We require nontrivial solution for W_k so the λ are determined by the roots of the characteristic polynomial

$$| \lambda I - \gamma A + Dk^2 | = 0.$$

Evaluating the determinant with A and D from (3.11) and (3.15) we get the eigenvalues $\lambda(k)$ as functions of the wavenumber k as the roots of

$$\begin{aligned} \lambda^2 + \lambda[k^2(1+d) - \gamma(f_u + g_v)] + h(k^2) = 0, \\ h(k^2) = dk^4 - \gamma(df_u + g_v)k^2 + \gamma^2 | A | . \end{aligned} \tag{3.19}$$

The steady state (u_0, v_0) is linearly stable if both solutions of (3.19) have Re $\lambda < 0$. We have already imposed the constraints that the steady state is stable in the absence of any spatial effects; that is, Re $\lambda(k^2 = 0) < 0$. The quadratic (3.19) in this case is (3.12) and the requirement that Re $\lambda < 0$ gave conditions (3.14). For the steady state to be unstable to spatial disturbances we require Re $\lambda(k) > 0$ for some $k \neq 0$. This can happen if either the coefficient of λ in (3.19) is negative, or if $h(k^2) < 0$ for some $k \neq 0$. Since $(f_u + g_v) < 0$ from conditions (3.14) and $k^2(1+d) > 0$ for all $k \neq 0$ the coefficient of λ, namely,

$$[k^2(1+d) - \gamma(f_u + g_v)] > 0,$$

so the only way Re $\lambda(k^2)$ can be positive is if $h(k^2) < 0$ for some k.

3.4 Limit Cycles and Andronov-Hopf bifurcations

Most dynamical systems contain parameters in addition to the dependent and independent variables. A general system of ordinary differential equations (ODEs) could

therefore be written

$$\dot{x} = f(x,k),$$

where k is a set of parameters on which the equations, and thus their solutions, depend. If we solve a set of differential equations at different parameter values, we often find that, qualitatively, not much changes. However, in some models, we can find sets of parameter values which are close to each other but where the behaviour of the model is in some way qualitatively different for one set or the other. For instance, a stable equilibrium point might have become unstable. We then say that the system has undergone a bifurcation. Bifurcations often change the attractors of a dynamical system. Informally, an attractor is a solution which is approached at long times. Stable equilibrium points are attractors, but they are not the only possibility. We will engage in some simple numerical discovery exercises in which we will see a few important bifurcations and their consequences. We will use the dynamical systems software xpp-paut (xpp for short). One very important kind of bifurcation is the Andronov-Hopf bifurcation (formerly known in the West as a Hopf bifurcation). In an Andronov-Hopf bifurcation, a stable focus becomes an unstable focus as a parameter is varied, and the attractor becomes a limit cycle. A limit cycle is an asymptotically stable, periodic solution which can be pictured as a closed curve in phase space. Limit cycles differ from conservative oscillations in mechanical systems in that the former have fixed shapes and sizes at given parameter values, while the corresponding quantities in a conservative mechanical oscillator depend on the total energy, i.e. on the initial conditions. There are two qualitatively different kinds of Andronov-Hopf bifurcations, supercritical Andronov-Hopf bifurcation and subcritical Andronov-Hopf bifurcation. In a supercritical Andronov-Hopf bifurcation, the limit cycle grows out of the equilibrium point. In other words, right at the parameters of the Andronov-Hopf bifurcation, the limit cycle has zero amplitude, and this amplitude grows as the parameters move further into the limit-cycle regime. Pictorially, think of it this way:

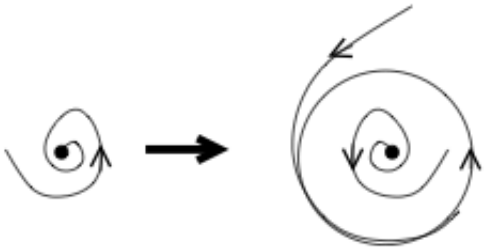

In a subcritical Andronov-Hopf bifurcation, there is an unstable limit cycle surrounding the equilibrium point, and a stable limit cycle surrounding that. The unstable limit cycle shrinks down to the equilibrium point, which becomes unstable in the process. For systems started near the equilibrium point, the result is a sudden change in behaviour from approach to a stable focus, to large-amplitude oscillations. Here is the corresponding picture: Because the stable limit cycle exists even when the equilibrium

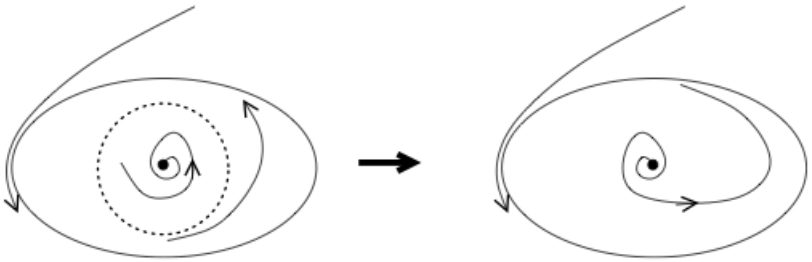

point is stable, if we imagine slowly varying a system parameter back-and-forth across the Andronov-Hopf bifurcation, we wouldnt expect to jump back to the equilibrium point at the same parameter value of the parameter from which this point lost stability. This is called hysteresis, and is associated with bistability, the fact that the system actually has two attractors over a range of parameters. In both cases, Andronov-Hopf bifurcations occur when an equilibrium point changes from being a stable to an unstable focus. We therefore detect Andronov-Hopf bifurcations through linear stability analysis.

3.5 Numerical Methods

In this thesis, we are normally going to simulate the models we have developed by using four different software packages, i.e., MATLAB, MAPLE, COMSOL and XPPAUT. In MATLAB we will use the ODE solver *ode45* to find the numerical solutions to ordinary differential equations, and the PDE solver *pdepe* to find the numerical solutions of partial differential equations. *ode45* is a standard solver for ordinary differential equations. This function implements a Runge-Kutta method with a variable time step for efficient computation. It is design to handle the following general problem:

$$\frac{\partial x}{\partial t} = f(t,x), \qquad x(t_0) = x_0,$$

where t is the independent variable, x is a vector of dependent variables to be found and f(t,x) is a function of t and x. *pdepe* solves a class of parabolic/elliptic PDE systems by converting the PDEs to ODEs using a second-order accurate spatial discretisation based on a set of nodes specified by the user. The time integration is done with the routine *ode15s*. These systems involve a vector-valued unknown function u that depends on a scalar space variable, x, and a scalar time variable, t. The general class to which *pdepe* applies has the form:

$$c(x,t,u,\frac{\partial u}{\partial x})\frac{\partial u}{\partial t} = x^{-m}\frac{\partial}{\partial x}(x^m f(x,t,u,\frac{\partial u}{\partial x})) + s(x,t,u,\frac{\partial u}{\partial x}),$$

where $a \leq x \leq b$ and $t_0 \leq t \leq t_f$. The integer m can be 0, 1, or 2, corresponding to slab, cylindrical, and spherical symmetry, respectively. The function c is a diagonal matrix and the flux and source functions f and s are vector valued. We using MAPLE to solve algebraic equations which are obtained by removing all the temporal and spatial derivative terms of the mathematical models. These solutions give us the steady states of the models. Also we use MAPLE to make a linearisation of the model by calculating

the Jacobian matrix at the steady state, which determine the stability of the steady states. We use COMSOL to calculate the numerical simulation of partial differential equations in 2D, by using the Finite Element Method. XPPAUT is used to find any Hopf-bifurcations.

Chapter 4

Literature Review

In this chapter we review some of the key papers in the mathematical modelling of cancer, and we focus specifically on the mathematical modelling of tumour-immune interactions. Also we give a brief review of mathematical models of invasion and angiogenesis.

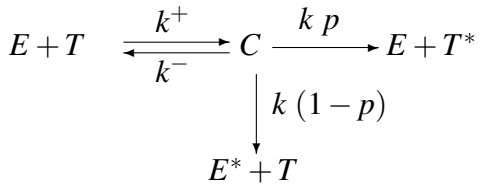

Figure 4.1: Schematic diagram of the basic local lymphocyte-cancer cell interactions

4.1 Immune Response-Cancer Interaction Models

The Model of Matzavinos et al.

In the work of Matzavinos et al., the authors proposed a spatiotemporal model of the interactions between tumour cells and cytotoxic T-lymphocytes (CTLs) (Matzavinos et al., 2004; Chaplain and Matzavinos, 2006) by including the spatial motility of both tumour cells and CTLs, as well as chemotactic motion of the CTLs. They focused mainly on the role of the immune system in determining dormant states of the tumour, by showing, through a series of simulations, that a dormant state is reached, but the tumour cells are spatially distributed in an irregular pattern, which also temporally oscillates in a non-periodic fashion.

The interplay between tumour cells and tumour-infiltrating cytotoxic-T-lymphocytes can be modelled as shown in figure 4.1 (see: Matzavinos et al. (2004)), where T denotes a tumour cell, E denotes an effector cell (CTL), C denotes the complex formed, T^* denotes a dead tumour cell and E^* denotes a dead effector cell. The following assumptions are made:

- the complexes C consist of a tumour cell and a CTL forming at a rate k^+. The parameter k^+ consists of the encounter rate between a tumour cell and a CTL, the probability that the CTL recognizes the tumour cell as a "non-self" entity, and also the probability that the tumour cell forms a complex with the CTLs
- the break-up of complexes can lead to a situation where both the tumour cell and the CTLs are alive with a rate k^-
- the break-up of complexes can lead to a situation where either the immune cell or the tumour cell survives the encounter with a rate k

- the probability that a tumour cell is killed is p, and correspondingly the probability that a CTL is killed (i.e. the tumour cells survives) is $(1-p)$

Using the Law of Mass Action, this leads to the following system of differential equations describing these specific kinetic interactions (figure 4.1):

$$\begin{aligned} \partial_t C &= k^+ ET - (k^- + k)C \\ \partial_t T &= -k^+ ET + k^- C + k(1-p)C \\ \partial_t E &= -k^+ ET + k^- C + kpC \end{aligned} \tag{4.1}$$

The authors added the diffusion terms to the system (4.1) and considered diffusion of the chemokine. They assumed all random motility, chemotaxis and diffusion coefficients are constant. The numerical simulation of this model demonstrated the existence of dynamics that are quasi-stationary in time but heterogeneous in space. A subsequent linear stability analysis of the underlying (spatially homogeneous) ODE kinetics coupled with the numerical investigation of the ODE system revealed the existence of a stable limit cycle in the corresponding phase space. This was verified by the bifurcation analysis.

The Model of Owen and Sherratt

As far as spatial aspects are concerned, Owen and Sherrat (Owen and Sherratt, 1997, 1999) developed a detailed spatiotemporal model focused on the role of macrophages. They showed that the presence of chemo-attraction of macrophages towards the tumour cells implies both the onset of traveling waves and a heterogeneous spatial distribution of the tumour cells. In Owen and Sherratt (1997), the authors presented the main properties and interactions of such tumour-associated macrophages, leading to a description of a mathematical model for the spatial interactions of macrophages, tumour cells and

$$f + l + m \xrightarrow{k_1} c + f \qquad\qquad c \xrightarrow{k_2} l + debris$$

Figure 4.2: Schematic diagram of the macrophage-cancer cell interactions

normal tissue cells, and they focused on the ability of macrophages to kill mutant cells (figure. 4.2).

The authors showed that the rapid diffusion of chemical regulators in comparison to cell movement, combined with the anti-tumour effects of macrophages, can lead to the onset of instability and the appearance of hot-spots of tumour cell density. Also they showed that while the tumouricidal activity of macrophages is insufficient to eliminate tumours, it can have important implications for their structure. They demonstrated that chemotaxis can stabilise the homogeneous tumour steady state behind the wave, but can also initiate spatiotemporally irregular solutions. These results raise a key question about the effect of chemotaxis in the more realistic two and three dimensional setting. In Owen and Sherratt (1999), the authors presented a mathematical model of reaction-diffusion form, which represents the influx of macrophage into a small avascular tumour, and their dynamics within the tumour as it grows. This model predicts that macrophages are unable to spontaneously eliminate whole tumours, in keeping with the conventional view that without intervention, the immune system is an ineffective weapon against the majority of cancers. Nevertheless, this model predicts that the ability of macrophages to selectively kill tumour cells has a extremely significant effect on tumour development, since it is able to induce spatial inhomogeneities. This work suggested that the anti-tumour activity may nevertheless be crucial in establishing the spatial structure that is able later, to induce angiogenesis. From the numerical bifurcation study, the authors suggested that the mechanism by which these occur is that a stationary spatial (Turing) pattern becomes unstable via a Hopf bifurcation, while the homogeneous equilibrium from which the turing pattern bifurcated remains kinetically stable.

The Model of dePillis et al.

de Pillis et al. (2005) described tumour-immune interactions and focussed on the role of natural killer (NK) and $CD8^+$T cells in tumour surveillance, with the goal of understanding the dynamics of immune-mediated tumour rejection. The functions of the model describing tumour-immune growth, response, and interactions rates, as well as associated variables, are developed using a least-squares method combined with a numerical differential equations solver. Also the authors discussed the variable sensitivity analysis. The model assumptions are as follows:

1. The tumour cells grow logistically in the absence of an immune response.
2. Both NK and $CD8^+$T cells can kill tumour cells.
3. Tumour cells have the potential to engender cytocidal activity in previous naive and noncytotoxic cells.
4. As a part of the innate immunity, NK cells are always present and active in the system, even in the absence of tumour cells.
5. As a part of the specific immunity, tumour specific $CD8^+$T cells are recruited once tumour cells are present.

The mathematical model suggests the value in continuing to research the mechanisms by which NK cells and $CD8^+$T cells induce tumour cells lysis. The authors hypothesise that the more effective the immune cell kill is, the more closely it follows a rational law dynamics. Model results seem to indicate that to promote tumour regression, it may be necessary to focus on increasing $CD8^+$T cell activity. The authors propose that the there may be a direct positive correlation between the patient-specific efficacy of the $CD8^+$T cell response, as measured by cytotoxicity assays, and the likelihood of a patient favourably responding to immunotherapy treatments.

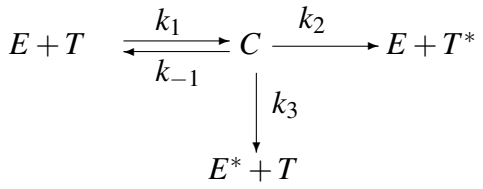

Figure 4.3: Schematic diagram of the basic local lymphocyte-cancer cell interactions from the paper of Kuznetsov et al.

The Model of Kuznetsov et al.

Kuznetsov et al. (1994) presented a mathematical model of cytotoxic T-lymphocyte (CTL) response to an immunogenic tumour. They described the kinetics of growth and regression of the B-lymphoma BCL_1 in the spleen of mice. Figure 4.3 shows the interactions between effector cells (E) and tumour cells (T) in vitro, where C is the effector cell-tumour cell conjugate, E^* is inactivated effector cells, and T^* is "lethally hit" tumour cells.

This model has four steady states, the low tumour steady state is stable, and it refers to the "dormant tumour" steady state. The high tumour and low effector level steady state is also stable, and it corresponds to relatively "uncontrolled" tumour growth or "tumour escape".

Also the authors used bifurcation analysis to explore the critical parameter values where the qualitative behaviour predicted. $\mu = k_3/k_2$ is a critical parameter in the model. With small μ the model predicts that BCL_1 tumours do not efficiently inactivate effector cells. They also show the model does have stable spirals, but the Dulac-Bendixson criterion demonstrates there are no stable closed orbits.

This model show that there may be a connection between the phenomenon of immunostimulation of tumour growth, the "sneaking through" of a tumour, and the formation of the tumour "dormant state".

From this model one can speculate that even in the presence of a cell-mediated immune response, which in this model does not totally eliminate even highly immunogenic tumours, a multitude of dormant tumours could accumulate in body tissue with increasing age. This model can be applicable to other processes in biology such as the infection of T-cells by HIV.

The Model of Webb et al.

Webb et al. (2002) developed a mathematical model based on tumour cell-lymphocyte interactions and the cell surface expression of Fas and FasL, and also extended the model to include the involvement of Matrix Metalloproteinases (MMP) and the catalysed soluble degradation product of the ligand (sFasL). This model consisted of ordinary differential equations which represent the interactions of two cell types: armed effector T-cells, and FasL positive tumour cells. They based the model upon the demonstration that the certain type of human tumours can produce functional FasL and can induce the apoptotic killing of activated lymphocytes in vitro. The key features in the model are the constitutive expression and engagement of membrane bound FasL on tumours with Fas expressed on the surface of activated lymphocytes, and the down-regulation of the cell surface Fas in tumours.

The authors predict that the production of soluble forms of Fas and FasL will lead to down-regulation of the immune response by neutralising the Fas ligand or receptor. Moreover, the inclusion of MMP inactivation in the model results in increased transmembrane FasL and leads to a higher rate of Fas-mediated apoptosis for lymphocytes that for tumour cells. The clinical implications of this model are two-fold. Firstly, elevated levels of MMPs in tumours and their association with invasion and angiogenesis have led to the development of board spectrum MMP inhibitors as potential therapeutic agents, and several compounds are undergoing clinical trails in cancer patients. Such

therapies could be compromised by the predicted adverse effect of MMP inactivation on FasL and lymphocyte apoptosis. On the other hand, MMP-7 inactivation would effectively lead to decreased levels of sFasL and this down-regulation may abrogate the suppressive effect of the soluble ligand on neutrophilic inflammation and could result in tumour regression. Secondly, many tumours cell types are resistant to Fas-mediated apoptosis and these cells often have the capability of killing activated lymphocytes via expression of FasL. They suggest, therefore, that the Fas/FasL system may have an important impact on the outcome of numerous ongoing immunotherapeutic trials based upon, for example, antigenic peptide presentation, costimulation and activation of lymphocytes/dendritic cells.

The Model of Kirschner et al.

Immunotherapy with the cytokine interleukin-2 (IL-2) may boost the immune system to fight tumours. Kirschner and Panetta (1998) showed by the mathematical model the dynamics between the tumour cells, immune-effector cells, and IL-2. These efforts are able to explain both short tumour oscillations in tumour size as well as long-term tumour relapse. Also they explored the effect of adoptive cellular immunotherapy on the model and described under what circumstances the tumour can be eliminated. The model consist of three populations, E(t) the activated immune-system cells; T(t) tumour cells; and $I_L(t)$, the concentration of IL-2. This model have four steady state, the trivial steady state is saddle, from the bifurcation diagram, they found the parameter c, the tumour antigenicity is the bifurcation parameter. The antigenicity of the tumour play the key role of the dynamics. For low antigenic tumours immune system is not able to clear the tumour, while, for highly antigenic tumours, reduction to a small dormant tumour is the best case scenario. This model has a stable limit cycles which imply that the tumour and the immune system undergo oscillations. If the tumour has

a low to medium antigenicity these cycles are relatively long with large amplitudes and the tumour is in a dormant state during most of the period. This may explain long term recurrence of tumour. If the tumour has medium to high antigenicity the period of cycles are short with small amplitudes.

Also the authors studied the treatment of the tumour-immune system with immunotherapy. Two type of treatment are explored individually and together, Adoptive cellular immunotherapy (ACI) and administration of the cytokine IL-2. Treatment with IL-2 alone does not offer a satisfactory outcome; if IL-2 administration is low there is no tumour-free state. However, if IL-2 input is high the tumour can be clear but the immune system grow without bounds causing problems such as capillary leak syndrome. Treatment with ACI and IL-2 that gives the combined effects obtained from the monotherapy regimes. Cytokine-enhanced immune function can play a significant role in treatment of cancer.

The Model of Eftimie et al.

Eftimie and Bramson (2011) reviewed spatially homogeneous mechanistic mathematical models describing the interactions between a malignant tumour and the immune system. They showed some models with, one, two , three, and four equations. In the one equation model they take simple model to described the tumour growth patterns, involving a single ordinary differential equation (ODE). These model describe only one cell population (cancer cell), which are subject to self-regulation by density dependent processes. In the two equation model, the authors added the effector equation to the model of first equation. they consider a generic effector cell population interacting with tumour cells. These interactions are described by two equations, which are of predator pray type. The immune cells play the role of the predator, while the tumour cells are the prey. This model is very helpful for elucidating basic (generic) mechanisms that

can induce observed behaviour, such as tumour regression and tumour dormancy. In the three equations model, the authors consider how the three-equation models help to uncover the possible mechanism underlying such interactions. They used three model: Tumour growth modulated by two effector cell type, Tumour growth modulated by effector cells and normal cells through competition for resources, and tumour growth modulated by effector cells and cytokines. The interactions between cancer cells, effector cells, and cytokines (especially IL-2) can explain long-term tumour relapse. Finally, In the four equations model, the authors add a new equation to the model of three equations. This extra equation describe, for example the dynamics of a cytokine concentration, or the dynamics of chemokine concentration. They show two examples, Two types of cells and two types of cytokines, and three type of cells and one cytokine or chemokine. These model indicate that including the effects of the additional component of the tumour microenvironment does not lead to any new behaviour. The patterns are similar to those obtained with three-equation models. exponential growth of tumour cells, oscillatory growth, or oscillatory decay. This suggests that the most essential mechanisms have already been captured with three equations.

The Models of Bellomo et al.

Bellomo and Delitala (2008) reviewed the mathematical kinetic theory of active particles applied to the modelling of the very early stage of cancer phenomena, specifically mutations, onset, progression of cancer cells, and their competition with the immune system. The mathematical theory described the dynamics of large systems of interacting entities whose microscopic state includes not only geometrical and mechanical variables, but also specific biological functions. Applications of this model are focused of complex biological system where two scales at the levels of genes and cells interact generating the heterogeneous onset of cancer phenomena, and the analysis refers to the

derivation of tissue level models from underlying description at the lower scales. The modelling aspects of the interactions with lower and higher scale have been treated.
The authors consider a biological system viewed as a complex network of various interacting subsystems, each of them expressing a well defined function. The state of each subsystem is described at a specific scale, molecular, cellular or tissue. The overall representation within each subsystem, labelled by the subscript i, is statically described by the distribution functions:

$$f_i = f_i(t,u) : [0,T] \times D_u \to \mathbb{R}_+, \qquad i = 1,...,n$$

over the microscopic state $u \in D_u$ of the active particles. By definition, $d_{n_i} = f_i(t,u)du$ denotes the number of active particles, which at time t, are in the element [u,u+du] of the space of microscopic state.
Gross average quantities can be computed, when these function are obtained by solution of the resultant equations. For instant, the local number density is calculated, under suitable integrability assumptions on f_i, as follows:

$$v_i = \int_{D_u} f_i(t,u)du,$$

with the following quantities:

$$a_i = a[f_i](t) = \int_{D_u} u f_i(t,u)du$$

and

$$A_i = A[f_i](t) = \frac{a[f_i](t)}{v_i(t)}$$

have been called, respectively, activation and the activation density. These quantities represent, respectively, the overall activity of the cells per unit volume and their mean activity.

The overall evolution of the system is caused by interactions. Specifically, the following phenomena (interactions), focused on cancer modelling, are considered:

- Stochastic modification of the microscopic state of genes or cells due to binary interactions with other cells of the same or different populations. These interactions are called conservative as they do not modify the number density of the interacting populations.
- Genetic alteration of cells which may either increase the progression of tumour cells or even generate, by clonal selection, new cells in a new population of cancer cells with higher level of malignancy.
- Proliferation or destruction of cells due to binary interactions with other cells of the same or of different populations.
- External actions, either therapeutical actions or other external agents, which modify the distribution function

Also the authors defined the probability density destributions:

$$f = f(t,u) : [0,T] \times D_u \to \mathbb{R}_+, \qquad i = 1,...,n$$

and

$$\phi = \phi(t,u) : [0,T] \times D_v \to \mathbb{R}_+, \qquad i = 1,...,n$$

over the microscopic states $u \in D_u$ and $v \in D_v$ of the interacting entities regarded as active particles.

The interaction scheme from the lower to the higher scale can be represented as follows:

$$[\partial_t \phi = N[\phi,\phi]] \quad \to \quad [\partial_t f = M_g[f,\phi]],$$

that corresponding to the following dynamics:

- The evolution of the system at the lower scale is determined by the interaction between genes among themselves and with the outer environment that is supposed known.

- The evolution of the system at the higher scale is determined by the interaction between active particles, of the population, among themselves and with particles of the lower system that is obtained by solution of the evolution equation for such a system.

Also, the authors reviewed when the cancer cells becomes relevant, various space phenomena, including invasion and pattern formation due to aggregation and chemotaxis. They added the space homogeneous description stochastic velocity jump process to the model.

4.1.1 Other Immune-Tumour Interaction Models

Tumour cells are characterized by a large number of genetic and epigenetic events leading to the appearance of specific antigens (e.g. mutated proteins, under/over-expressed normal proteins and many others) triggering reactions by the both the innate and the adaptive immune system (Delves et al., 2006; Kindt et al., 2006; Pardoll, 2003; Swann and Smyth, 2007; Yefenov, 2008; Szymanska, 2003; Garay and Lefever, 1978; Lefever et al., 1992). These observations have provided a theoretical basis to the empirical hypothesis of immune surveillance, i.e. that the immune system may act to eliminate tumours (Ehrlich, 2009), only recently experimentally and epidemiologically confirmed (Dunn et al., 2004). Of course, the competitive interaction between tumour cells and the immune system involves a considerable number of events and molecules, and as such is extremely complex. Thus, the kinetics of the interplay between tumour cells and the immune system is strongly non-linear.

Moreover, to describe fully the immuno-oncological dynamics, one has to take into account a range of spatial phenomena. Indeed, the interplay between tumour cells and the immune system is strongly influenced by the spatial mobility of both tumour cells and cells of the immune system i.e. effector cells (Matzavinos et al., 2004). Indeed, apart from the random motion of both types of cell, a prominent role is played by chemoattraction of effector cells towards the tumour cells. Indeed, chemotactic motion of immune system cells is a hallmark of the defence of the human body against "non-self agents", including tumours, since cells belonging to both the innate and adaptive immune system are able to reach their targets thanks to the gradients of various kinds of chemicals (Delves et al., 2006; Keener and Sneyd, 2003), e.g. inflammation-related substances produced by tumour cells. Thus, chemotaxis is of paramount importance in the interplay between tumours and the immune system, since it influences the control of tumour growth and also the immune surveillance.

However, besides temporal and spatial non-linearities, another important point to stress is that the structure of the above-mentioned interactions is also characterized by a series of evolutionary phenomena. As is self-evident, the immune system is not able to eliminate all neoplasms. In other cases, a dynamic equilibrium may also be established, such that the tumour may survive in a so-called "dormant state" (Koebel et al., 2007; Chaplain and Matzavinos, 2006; d'Onofrio, 2005, 2007), which is undetectable. Until recently this was largely inferred from clinical data, but Koebel et al. (2007) have been able to show experimentally, through an *ad hoc* mouse model, that adaptive immunity can maintain an occult cancer in an equilibrium state. It is quite intuitive that this equilibrium can be disrupted by sudden events affecting the immune system. Indeed, if disease-related impairments of the innate and adaptive immune systems, or immuno-suppressive treatments preceding organ transplantations occur, then tumour regrowth occurs (Dunn et al., 2004; Stewart and Abrams, 2008). This has been shown both by mouse models and through epidemiological studies (Dunn et al., 2004; Stewart

and Abrams, 2008).

However, there is a major class of causes of disruption of the equilibrium that are not related to immuno-suppression. Indeed, over a long period of time Dunn et al. (2004), a neoplasm may develop multiple strategies to circumvent the action of the immune system (Pardoll, 2003; Dunn et al., 2004), which may allow it to recommence growing (Dunn et al., 2004; d'Onofrio, 2007) into clinically apparent tumours (Koebel et al., 2007), which theoretically can reach their maximum carrying capacity (d'Onofrio, 2007). From an ecological point of view, we could say that the tumour has adapted to survive in a hostile environment, in which the anti-tumour immune response is activated (Dunn et al., 2004; d'Onofrio, 2007). For example, the tumour may develop mechanisms to grow and spread by reducing its immunogenicity (Pardoll, 2003; Dunn et al., 2004). In other words, the immunogenic phenotype of the tumour is influenced by the interaction with the immune system of the host. For this reason, the theory of the interactions between a tumour and the immune system has been called immuno-editing theory (Dunn et al., 2004).

An impressive body of research is accumulating on immuno-evasive strategies, and a recent monograph Gabrilovich and Hurwitz (2008) has been devoted to some aspects of this fascinating subject and to its close relationship with the effectiveness of immunotherapies. As far as the mathematical modelling of tumour and immune system interactions is concerned, there are many papers in the current literature which use deterministic models (Stepanova, 1980; Kuznetsov and Knott, 2001; Kogan et al., 2010; Arciero et al., 2004; d'Onofrio, 2005, 2007, 2006, 2008; Kronick et al., 2010; Kim et al., 2008; Lejeune et al., 2008) or stochastic models (Horsthemke and Lefever, 1977; Du and Mei, 2010; Caravagna et al., 2010; d'Onofrio, 2010), as well as models introduced by Bellomo based on the kinetic theories of nonlinear statistical mechanics (Bellomo et al., 2004; Bellomo and Delitala, 2008). The general approach of Bellomo's theory is based on the concept of changes of activities of both the tumour

cells and the effector cells of the immune system after encounters between them. In (d'Onofrio, 2007, 2008), the immuno-editing phenomenon was empirically modelled by allowing the presence of slowly time-varying generic parameters in deterministic models (with time-scales significantly longer than those typical of the tumour-immune system interaction). Recently, in the framework of the above-mentioned kinetic approach, a generic model has been proposed for the learning ability of effector cells and for the hiding of tumour cells (Bellomo, 2010).

4.2 General Cancer Modelling

In this section we will give a brief overview of some important mathematical models of cancer invasion and tumour-induced angiogenesis.

Anderson et al. (2000) presented two types of mathematical model which describe the invasion of host tissue by tumour cells. The first model focusses on the macro-scale structure and considers the tumour as a single mass. This model consists of a system of partial differential equations, describing the production and/or activation of degradative enzymes by the tumour cells, the degradation of the matrix and the migratory response of the tumour cells. The second model focusses on the micro-scale (individual cell) level and uses a discrete technique. This technique enables one to examine the implications of metastatic spread.

Chaplain and Lolas (2005) considered a mathematical model of cancer cell invasion of tissue which focuses on the role of the plasminogen activation system. This model consists of a system of reaction-diffusion-taxis partial differential equations describing

the interactions between cancer cells, urokinase plasminogen activator (uPA), uPA inhibitors, plasmin and the host tissue. It focus of the modelling on the spatio-temporal dynamics of the uPA system and how this influences the migratory properties of the cancer cell through random motility, chemotaxis, and haptotaxis. The main achievement of this model is that fairly simple mathematical model representing the binding interactions of the components of the plasminogen activation system coupled with cell migration were able to capture the main characteristic effects of the system in cancer progression and invasion.

Finally, Chaplain (1995) considered two mathematical models which describe different aspects of solid tumour growth and development- angiogenesis and vascular growth. In this paper, the model of Chaplain and Stuart (1993) was modified and improved qualitative results were obtained with simulations in one spatial dimension. Also the model was extended to two spatial dimensions in order to take into account explicitly the key features of angiogenesis of anastomosis and secondary sprout formation (branching). In the second part of this paper, standard reaction-diffusion theory (turing-type models) was applied to a novel situation- that of the growth of solid tumours. It was shown that the spatially heterogeneous patterns which arise in the case of a spherical geometry may play a part and help to explain certain observed phenomenon in carcinoma and multicell spheroids.

Chapter 5

Evasion of Tumours from the Control of the Immune System: A Consequence of a Brief Encounter

5.1 Introduction

In this chapter, based on the concept introduced by Dunn et al. (2004) that the immune system has the ability of *sculpting the phenotype* of a tumour cell, we propose a cell-centred semi-mechanistic approach aimed at describing a possible immunologically realistic kinetic mechanism through which immuno-evasion begins. Since there is strong experimental evidence that type, density and location of CTLs are predictive of the clinical outcome of some neoplasms, such as colorectal tumours (Galon et al., 2006), and since we are interested in the long-time dynamics, here we shall deal with the interplay of a neoplasm with CTLs. In our model, we suppose that the tumour cells that survive an attack by CTLs have a probability of acquiring (through mutations or even by epigenetic changes) a phenotype that is more resistant to future

attacks by CTLs. In turn, at each new encounter with a CTL, this resistance can be increased further, and after a finite number of encounters a complete or *maximal* resistance to specific immunity is acquired. Moreover, specific spatial effects may be linked to the immuno-evasion of neoplasms. Indeed, recently Vianello et al. (2006) showed experimentally that tumour cells can produce chemicals that act as chemo-repellors for CTLs. We integrate these experimental findings in our model by permitting in the range of features defining the increasingly resistant tumour cell phenotypes an increasing ability to produce such chemorepulsive substances. These two bio-theoretical hypotheses, although new, are in line with the general schema of tumour cell escape from the immune response. Indeed, as stressed by Stewart and Abrams (2008), tumour cells may escape from immune control through two general mechanisms: *(a)* mechanisms that involve the secretion of soluble factors; *(b)* mechanisms that are dependent on the contact between the tumour cells and the effectors and that are aimed at reducing antigen recognition/adhesion and apoptotic resistance. Given the current experimental knowledge the above mentioned factors are primarily aimed - apart from, in many cases, their mitogenic action - at inducing the emergence of immunosuppressive networks (Kim et al., 2007). In our present model, the factors, in line with the animal model by Vianello et al. (2006), are chemicals that repel CTLs.

5.2 The Mathematical Model

Since we are modelling a situation where immuno-evasion of the tumour cells is not considered, the interplay between tumour cells and tumour-infiltrating cytotoxic-T-lymphocytes can be modelled as shown in figure 4.1. We develop the work of Matzavinos et al. (2004), by assuming that a proportion of the tumour cells that survive an encounter with a CTL are more resistant to any future attacks by CTLs. Consequently, the phenotypic properties of these new “enhanced” tumour cells will be different from

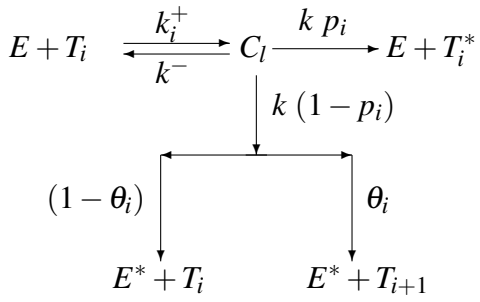

Figure 5.1: Schematic diagram of the extended local lymphocyte-cancer cell interactions

those of the "naive" tumour cells. Specifically, we make the additional assumptions:

- their probability of being killed (previously the parameter p) is smaller
- their probability of being recognized and also of forming a complex with a CTL (embedded in the parameter k^+) is smaller

Moreover, we shall also assume that the recruitment rate of CTLs stimulated by the presence of the complexes is also smaller. We denote the initial naive tumour cells by $T_0(t)$ and the non-naive tumour cells by T_i, where i stands for the number of previous encounters with the CTLs. We assume that the fitness of tumour cells increases up to a maximum number of encounters N, implying that we consider in total $1+N$ "classes" of tumour cells, $T_0, T_1, \ldots, T_N$.

The new kinetic relationships of our model are illustrated in figure 5.1 and are characterized by the following new groups of parameters:

- the rate of formation of complexes $[ET_i]$: k_i^+. We assume that k_i^+ is constant or decreasing with index i, with $k_N^+ \geq 0$;

- the probability that a tumour cell of the i-th class is killed: p_i. We assume that p_i is decreasing with index i, with $p_N \geq 0$;

- the probability of transition $T_i \rightarrow T_{i+1}$ to the state i: ϑ_i. We assume that ϑ_i is increasing for $0 \leq i \leq N-1$. Since we have assumed N classes of tumour cells, $\vartheta_N = 0$.

As far as the temporal dynamics of the tumour cells, CTLs and complexes is concerned, once again using the Law of Mass Action, the kinetic scheme of figure 5.1 can be translated into the following system of ordinary differential equations:

$$\begin{aligned}
\frac{\partial T_0}{\partial t} &= -k_0^+ E T_0 + k^- C_0 + (1-\theta_0)(1-p_0) k C_0 \\
\frac{\partial T_i}{\partial t} &= -k_i^+ E T_i + \theta_{i-1}(1-p_{i-1}) k C_{i-1} + (k^- + k(1-\theta_i)(1-p_i)) C_i \\
\frac{\partial C_l}{\partial t} &= k_l^+ E T_l - (k^- + k) C_l \\
\frac{\partial E}{\partial t} &= -E(\sum_{j=0}^{N} k_j^+ T_j) + (\sum_{j=0}^{N} k^- C_j) + (\sum_{j=0}^{N} k p_j C_j)
\end{aligned} \tag{5.1}$$

where $i = 1, ..., N$, and $l = 0, ..., N$.

However, not only the temporal but also the spatio-temporal properties of the "fitter" tumour cells are likely to be different from those of the baseline tumour cells. Namely:

- the production rates of chemoattractants stimulated by a complex CTL^+ non naive tumour cell' is assumed to be smaller than that of the naive cells

- since recently Vianello et al. (2006) showed in an animal model that tumours produce chemicals that repels the CTLs, here we assume that those chemorepellors are produced by the non-naive cells

- the non-naive cells might be repelled by chemorepellors produced by CTLs

In the following, we provide the full equations for all variables, including the spatial components. As mentioned in the previous section, we have assumed the model of Matzavinos et al. (2004) as our baseline model.

Spatiotemporal Dynamics of the Tumour Cells

Following Matzavinos et al. (2004), we assume that the tumour growth may be described by a logistic law, and that the tumour cells migrate randomly. Thus, it follows that the spatio-temporal dynamics of the naive tumour cells T_0 is as follows:

$$\frac{\partial T_0}{\partial t} = \overbrace{D_{T_0}\nabla^2 T_0}^{random\ motion} + \overbrace{r_1 T_0(1-\beta_1 \sum_{j=0}^{N} T_j)}^{logistic\ growth} - \overbrace{k_0^+ E T_0 + (k^- + k(1-\theta_0)(1-b_0))C_0}^{local\ kinetics}$$

and the dynamics of the non-naive cells T_i is given by:

$$\frac{\partial T_i}{\partial t} = \overbrace{D_{T_i}\nabla^2 T_i}^{random\ motion} + \overbrace{r_1 T_i(1-\beta_1 \sum_{j=0}^{N} T_j)}^{logistic\ growth} - \overbrace{k_i^+ E T_0 + (k^- + k(1-\theta_i)(1-b_i))C_i + k\theta_{i-1}(1-p_{i-1})C_{i-1}}^{local\ kinetics}$$

where $i = 1, \ldots, N$.

Spatiotemporal Dynamics of the CTLs

Considering the CTLs, as in Matzavinos et al. (2004), both random and chemotactic motion of these cells is included. However, as previously discussed, an additional type of motility is included due to the postulated onset of "negative taxis" due to the

production of a chemorepellor ρ by the non-naive tumour cells (Vianello et al., 2006). This results in the following equation:

$$\frac{\partial E}{\partial t} = \overbrace{D_E\nabla^2 E}^{random\ motility} - \overbrace{\chi(\alpha)\nabla.(E\nabla\alpha)}^{chemotaxis} + \overbrace{A(\rho)\nabla.(E\nabla\rho)}^{chemo-repulsion} + \overbrace{sh(x)}^{supply} + \frac{\overbrace{f\sum_{j=0}^{N} q_j C_j}^{proliferation+recruitment}}{g+\sum_{j=0}^{N} T_j}$$

$$-\overbrace{d_1 E}^{decay} - \overbrace{E(\sum_{j=0}^{N} k_j^+ T_j) + (\sum_{j=0}^{N} k^- C_j) + (\sum_{j=0}^{N} kp_j C_j)}^{local\ kinetics}$$

The recruitment rate of the CTLs, E, stimulated by the complexes C_j is embedded in the rate constant q_j, which, as a consequence, must be decreasing with the index j, with $q_N \geq 0$. The external influx of CTLs is, for the sake of the simplicity, modelled as $sh(x)$, where $h(x)$ is a Heaviside function, taken to be zero over a given subregion of the domain of interest cf. Matzavinos et al. (2004). In other words, we assume that there is a subdomain where lymphocytes are not naturally present and which is penetrated by CTLs only thanks to diffusion and chemotaxis.

Chemoattractant

The spatiotemporal dynamics of the chemoattractant α produced by the complexes is given by

$$\frac{\partial \alpha}{\partial t} = \overbrace{D_2\nabla^2\alpha}^{diffusion} - \overbrace{\delta_1\alpha}^{decay} + \overbrace{(\sum_{j=0}^{N} \pi_j C_j)}^{production}$$

where we assume that the production rate constant π_i is decreasing with index i, with $\pi_N \geq 0$, since we assume that complexes between CTLs and non-naive tumour cells are less and less able to produce such a chemoattractant.

Chemorepellor

Adapting the experimental findings by Vianello et al. (2006) to our framework, we suppose that the non-naive tumour cells produce a chemical that repels the CTLs and whose concentration ρ is governed by the equation

$$\frac{\partial \rho}{\partial t} = \overbrace{D_\rho \nabla^2 \rho}^{diffusion} - \overbrace{\delta_2 \rho}^{decay} + \overbrace{(\sum_{j=0}^{N} w_j T_j)}^{production}$$

where the production rate constants w_i are such that: $w_0 = 0$ (absence of production for naive tumour cells) and

$$w_1 < w_2 < \cdots < w_N.$$

Tumour cell-CTL Complexes

Following Matzavinos et al. (2004), we assume that the motility of the complexes is so small that it can be neglected:

$$\frac{\partial C_l}{\partial t} = \overbrace{k_l^+ E T_l - (k^- + k) C_l}^{local\ kinetic}$$

where $l = 0, \ldots, N$.

5.3 Boundary and Initial Conditions

We initially consider the model in a fixed 1-dimensional domain $[0, x_a]$ and close the system by applying appropriate boundary and initial conditions. As far as the boundary conditions are concerned, zero-flux boundary conditions are imposed on all state variables (apart from C): E, α, ρ and T_i, $i = 0, ..., N$. These boundary conditions

are appropriate for the tumour-immune dynamics we are considering. For example, in BCL_1 lymphomas of the spleen tumour cells are spatially contained in the lymph tissue of the spleen, an elongated organ that, in mice, is characterized by a very strong basement membrane, which is only broken when the tumour cells switch to an "invasive phenotype". Since here we are concerned with earlier stage dynamics of tumour cells in a dormant state evading the CTLs, it follows that the zero-flux boundary conditions are adequate for our particular model.

As far as the initial conditions are concerned, we assume an initial front of naive tumour cells encountering a front of CTLs, resulting in the formation of C_0 complexes. We suppose that initially there are no non-naive tumour cells and hence no complexes involving them. No chemicals are initially present in the spatial domain. These assumptions yield:

$$E(x,0) = \begin{cases} 0, & \text{if } 0 \leq x \leq l, \\ E_a(1-\exp(-1000(x-l)^2)), & \text{if } l < x \leq x_a. \end{cases}$$

$$T_0(x,0) = \begin{cases} T_a(1-\exp(-1000(x-l)^2)), & \text{if } 0 \leq x \leq l, \\ 0 & \text{if } l < x \leq x_a. \end{cases}$$

$$T_i(x,0) = 0, \forall x \in [0,x_a].$$

$$C_0(x,0) = \begin{cases} 0, & \text{if } x \notin [l-\varepsilon, l+\varepsilon], \\ C_a \exp(-1000(x-l)^2), & \text{if } x \in [l-\varepsilon, l+\varepsilon]. \end{cases}$$

$$C_i(x,0) = 0, \forall x \in [0,x_a].$$

$$\alpha(x,0) = 0, \forall x \in [0,x_a].$$

$$\rho(x,0) = 0, \forall x \in [0, x_a].$$

where

$$E_a = \frac{s}{d_1}, \;\; T_a = \frac{1}{\beta_1}, \;\; C_a = min(E_a, T_a), \;\; 0 < \varepsilon \ll 1, \;\; i = 1, ..., N.$$

Note that E_a is the the baseline homogenous steady-state value of CTLs in the absence of tumour cells, and that T_a is the the baseline homogenous steady-state value of the naive cells in absence of CTLs.

5.4 Non-dimensionalisation

Before undertaking any computational simulations, we non-dimensionalise our model (as well as the boundary and initial conditions) by adopting the following scaling:

i) space is scaled by adopting a reference value x_a equal to the size of the domain in consideration and we assume $x_a = 1$ *cm*; time is rescaled relative to the diffusion rate of CTLs by setting $t_a = x_a^2 D_E$:

$$\bar{x} = \frac{x}{x_a}, \quad \bar{t} = \frac{t}{t_a};$$

ii) cellular densities are rescaled relative to the maxima of the respective initial conditions:

$$\bar{T}_i = \frac{T_i}{T_a}, \quad \bar{E} = \frac{E}{E_a}, \quad \bar{C}_i = \frac{C_i}{C_a}, \quad i = 0, \ldots, N$$

iii) The concentrations of the chemoattractant and of the chemorepellor are rescaled

relative to the baseline values α_a and ρ_a respectively:

$$\bar{\alpha} = \frac{\alpha}{\alpha_a}, \quad \bar{\rho} = \frac{\rho}{\rho_a}$$

By omitting the bars, for the sake of simplifying the notation, the proposed model becomes:

$$\begin{aligned}
\frac{\partial E}{\partial t} &= \nabla^2 E - \gamma(\alpha)\nabla(E\nabla\alpha) + \xi(\rho)\nabla(E\nabla\rho) + \eta_1 \frac{\sum_{j=0}^{N} q_j C_j}{a + \sum_{j=0}^{N} T_j} - E(\sum_{j=0}^{N} \psi_j T_j) - \sigma E \\
&\quad + k_3(\sum_{j=0}^{N} C_j) + k_4(\sum_{j=0}^{N} p_j C_j) + \sigma h(x), \\
\frac{\partial \alpha}{\partial t} &= D_\alpha \nabla^2 \alpha - \delta_\alpha \alpha + \mu_\alpha(\sum_{j=0}^{N} \pi_j C_j), \\
\frac{\partial \rho}{\partial t} &= D_\rho \nabla^2 \rho - \delta_\rho \rho + \mu_\rho(\sum_{j=0}^{N} w_j T_j), \\
\frac{\partial T_0}{\partial t} &= \nabla^2 T_0 + r T_0(1 - \sum_{j=0}^{N} T_j) - \phi_0 E T_0 + k_1 C_0 + (1-\theta_0)(1-p_0)k_2 C_0, \\
\frac{\partial T_i}{\partial t} &= \nabla^2 T_i + r T_i(1 - \sum_{j=0}^{N} T_j) - \phi_i E T_i + k_1 C_i + \theta_{i-1}(1-p_{i-1})k_2 C_{i-1} \\
&\quad + k_2(1-\theta_i)(1-p_i)C_i, \\
\frac{\partial C_l}{\partial t} &= \psi_l E T_l - \lambda C_l,
\end{aligned} \tag{5.2}$$

where:

$r = r_1 t_a$	$\phi_i = k_i^+ E_a t_a$	$k_1 = \frac{k^- C_a t_a}{T_a}$	$a = \frac{g}{T_a}$
$\lambda = (k^- + k)$	$\psi_i = k_i^+ T_a t_a$	$k_2 = \frac{k C_a t_a}{T_a}$	$\gamma = \alpha_a t_a \chi(\alpha)$
$\eta_1 = \frac{f t_a}{T_a}$	$\sigma = \mu_o t_a$	$k_3 = k^- t_a$	$\mu_\alpha = \frac{C_a t_a}{\alpha_a}$
$D_\alpha = D_2 t_a$	$\delta_\alpha = \delta_1 t_a$	$k_4 = k t_a$	$\mu_\rho = \frac{T_a t_a}{\rho_a}$

After the non-dimensionalisation, the boundary conditions become (in 1-D):

$$\begin{aligned}
&\frac{\partial E}{\partial x}(0,t) = 0, && \frac{\partial E}{\partial x}(1,t) = 0,\\
&\frac{\partial \alpha}{\partial x}(0,t) = 0, && \frac{\partial \alpha}{\partial x}(1,t) = 0,\\
&\frac{\partial \rho}{\partial x}(0,t) = 0, && \frac{\partial \rho}{\partial x}(1,t) = 0,\\
&\frac{\partial T_i}{\partial x}(0,t) = 0, && \frac{\partial T_i}{\partial x}(1,t) = 0,
\end{aligned}$$

which then imply, assuming some smoothness of the solution and the form of C_i equations, that

$$\frac{\partial C_i}{\partial x}(0,t) = 0, \qquad \frac{\partial C_i}{\partial x}(1,t) = 0.$$

and the initial conditions take the form (again in 1-D):

$$E(x,0) = \begin{cases} 0, & \text{if } 0 \le x \le l,\\ (1-\exp(-1000(x-l)^2)), & \text{if } l < x \le 1, \end{cases}$$

$$\alpha(x,0) = 0, \forall x \in [0,1]$$

$$\rho(x,0) = 0, \forall x \in [0,1]$$

$$T_0(x,0) = \begin{cases} (1-\exp(-1000(x-l)^2)), & \text{if } 0 \le x \le l,\\ 0, & \text{if } l < x \le 1, \end{cases}$$

$$T_i(x,0) = 0, \forall x \in [0,1],$$

$$C_0(x,0) = \begin{cases} 0, & \text{if } x \notin [l-\varepsilon, l+\varepsilon], \\ \exp(-1000(x-l)^2), & \text{if } x \in [l-\varepsilon, l+\varepsilon], \end{cases}$$

where : l=0.1, and $\varepsilon = 0.01$.

$$C_i(x,0) = 0, \forall x \in [0,1].$$

5.5 Parameter Values: Baseline Set

To carry out the computational simulations of the proposed model, we used the baseline parameter set reported in Matzavinos et al. (2004), since these were all estimated from experimental data on murine B-cell Lymphoma BCL_1, which is an animal model for the study of tumour dormancy (Uhr and Marches, 2001). In addition to this baseline set, we used the migration parameters proposed in Chaplain and Matzavinos (2006). Thus, the complete parameter set is the following:

$s = 1.36 \times 10^4\ day^{-1} cells\ cm^{-1}$	$f = 0.2988 \times 10^8\ day^{-1} cells\ cm^{-1}$
$g = 2.02 \times 10^7\ cells\ cm^{-1}$	$k_0^+ = 1.3 \times 10^{-7}\ day^{-1} cells^{-1}\ cm$
$k^- = 24\ day^{-1}$	$k = 7.2\ day^{-1}$
$p_0 = 0.9997$	$r_1 = 0.18\ day^{-1}$
$\beta_1 = 2 \times 10^{-9}\ cells^{-1}\ cm$	$d_1 = 0.0412\ day^{-1}$
$D_E = 10^{-6}\ cm^2\ day^{-1}$	$\chi = 1.728 \times 10^6\ cm^2\ day^{-1}\ M^{-1}$
$D_{T_i} = 10^{-6}\ cm^2\ day^{-1}$	$D_2 = 8 \times 10^{-3} cm^2\ day^{-1}$

Hence, from the experimental data above, the non-dimensional values of parameters becomes:

$$\gamma = 1.728 \times 10^2 \qquad \eta_1 = 5.976 \times 10^4 \qquad \psi_0 = 6.5 \times 10^7$$
$$\sigma = 4.12 \times 10^4 \qquad k_3 = 2.4 \times 10^7 \qquad k_4 = 7.2 \times 10^6$$
$$D_\alpha = 8 \times 10^3 \qquad \delta_\alpha = 1.115 \times 10^4 \qquad \mu_\alpha \pi_0 = 10^4$$
$$r = 1.8 \times 10^5 \qquad \phi_0 = 4.29 \times 10^4 \qquad k_1 = 1.584 \times 10^4$$
$$k_2 = 4.752 \times 10^3 \qquad \lambda = 3.12 \times 10^7 \qquad a = 4.04 \times 10^{-2}$$

As far as the spatiotemporal dynamics of the chemorepellor is concerned, we assume that its diffusion coefficient and decay rate is the same as the chemokine α i.e. $D_\rho = D_\alpha$, $\delta_\rho = \delta_\alpha$, $\mu_\rho = \mu_\alpha$, and $\xi = \gamma$.

Concerning the transitions $T_i \rightarrow T_{i+1}$, we assume that they are a linear function of i:

$$\theta_i = \theta_0 + (\theta_{MAX} - \theta_0)\frac{i}{N-1},\ i = 0, \ldots, N-1,$$

$$\theta_N = 0,$$

$$\theta_{MAX} = 10\theta_0,$$

and that their baseline value is sufficiently small: $10^{-5} \leq \theta_0 \leq 10^{-3}$.

The probability p_i that a tumour cell of class T_i is lethally hit is given by:

$$p_i = p_0 + (p_N - p_0)\frac{i}{N},$$

where :

$$0 \leq p_N < p_0.$$

Concerning the rates k_i^+, we assume either that they are constant or that they are linearly decreasing with $k_N^+ = 0$:

$$k_i^+ = k_0^+ \left(1 - \frac{i}{N}\right).$$

The production rate of chemoattractant is also assumed to vary linearly:

$$\pi_i = \pi_0 \left(1 - \frac{i}{N}\right)$$

with:

$$\pi_0 = 20 - 3000 \; molecules \; cells^{-1} \; min^{-1},$$

We suppose that the chemorepellor is produced via a mechanism of "threshold generation", i.e. only after a sufficient number of encounters, yielding:

$$w_i = \begin{cases} 0, & \text{if } 0 \leq i \leq N_*, \\ w_{MAX} \frac{i - N_*}{N - N_*}, & N_* < i \leq N, \end{cases} \tag{5.3}$$

where we can assume:

$$w_{MAX} \approx \pi_0.$$

5.6 Computational Simulation Results

In addition to the baseline parameter set detailed in the previous section, in the following sections all our computational simulations were performed assuming values for key parameters associated with the encounter of CTLs and tumour cells as follows:

$$\theta_0 = 10^{-4}, \; p_N \in \{0, 0.5, 0.75, 0.9997\}, \; k_0^+ = 1.3 \times 10^{-7}$$

and k_i^+ may be either constant or linearly decreasing, with $k_N^+ = 0$.

Since the average lifespan of a chimeric mouse is three years, and since we are interested in assessing the possibility (and spatio-temporal modality) of the onset of immunoevasion of a tumour, all simulations (unless stated) represent an interval of length 1100 days $\approx$ 3 years.

5.6.1 Spatially Homogenous Case

In this first set of simulations, we set all the spatial components of the model to zero and consider only the reaction kinetics in order to ascertain whether the primary mechanism of evasion can be purely temporal. All simulations suggest that our model, with the parameter assumptions and values we used, is able to reproduce the onset of immunoevasion in a biologically realistic time-frame.

Figure 5.2 shows the plots of the growth of the tumour cell population over time where the killing probability at the last stage is zero, i.e. $p_N = 0$, and $k_i^+ = constant = 1.3 \times 10^{-7}$. We observe that if $N = 4$ the onset of evasion is at $t \approx 200$ days, i.e. the tumour remains dormant for 200 days, which is a long period of time. On the contrary, if $N = 10$ then the immunoevasion is delayed even further, with onset at $t \approx 500$ days.

Figure 5.3 shows the plots of the growth of the tumour cell population over time where the killing probability at the last stage is not zero but it is only halved, i.e. $p_N = 0.5$, and as in the previous figure, $k_i^+ = constant = 1.3 \times 10^{-7}$. Also in this case the immunoevasion is reproduced and takes place, respectively, at $t \approx 425$ *days* for $N = 4$ and at $t \approx 950$ *days* for $N = 10$.

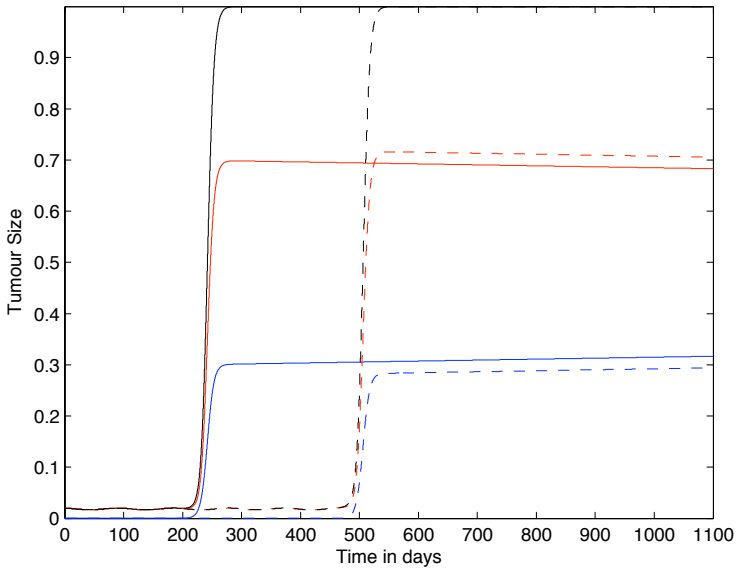

Figure 5.2: Plots showing the growth of the tumour cell population over time in the case where the spatial components of the model (i.e. all diffusion, taxis terms) have been set to zero. The plots show that the tumour can evade the immune system for either approximately 200 days or approximately 500 days depending on the parameter N. Parameter values: $p_N = 0$ and $k_i^+ = constant = 1.3 \times 10^{-7}$ and: $N = 4$ (solid line) and $N = 10$ (dashed lines). The red lines represent the population T_0, the blue lines represent the summed populations $T_1 + ... + T_N$, and the black lines represent the summed populations $T_0 + ... + T_N$. Time t is in days.

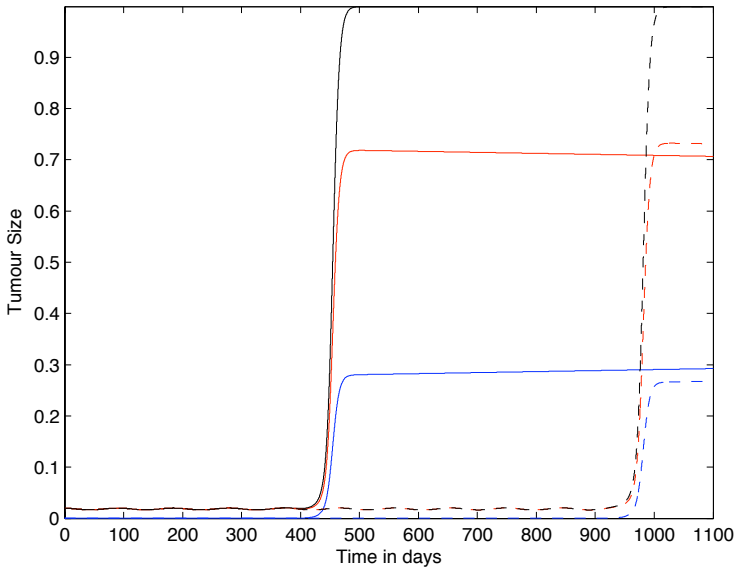

Figure 5.3: Plots showing the growth of the tumour cell population over time in the case where the spatial components of the model (i.e. all diffusion, taxis terms) have been set to zero. The plots show that the tumour can evade the immune system for either approximately 400 days or approximately 950 days depending on the parameter N. Parameter values: $p_N = 0.5$ and $k_i^+ = constant = 1.3 \times 10^{-7}$ and: $N = 4$ (solid line) and $N = 10$ (dashed lines). The red lines represent the population T_0, the blue lines represent the summed populations $T_1 + ... + T_N$, and the black lines represent the summed populations $T_0 + ... + T_N$. Time t is in days.

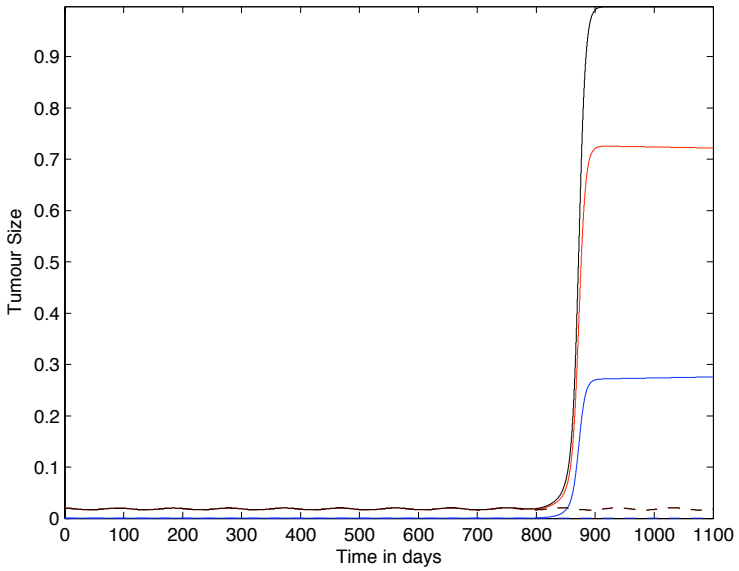

Figure 5.4: Plots showing the growth of the tumour cell population over time in the case where the spatial components of the model (i.e. all diffusion, taxis terms) have been set to zero. The plots show that the tumour can evade the immune system for either approximately 850 days or approximately 1900 days depending on the parameter N. Parameter values: $p_N = 0.75$ and $k_i^+ = constant = 1.3 \times 10^{-7}$ and: $N = 4$ (solid line) and $N = 10$ (dashed lines). The red lines represent the population T_0, the blue lines represent the summed populations $T_1 + ... + T_N$, and the black lines represent the summed populations $T_0 + ... + T_N$. Time t is in days.

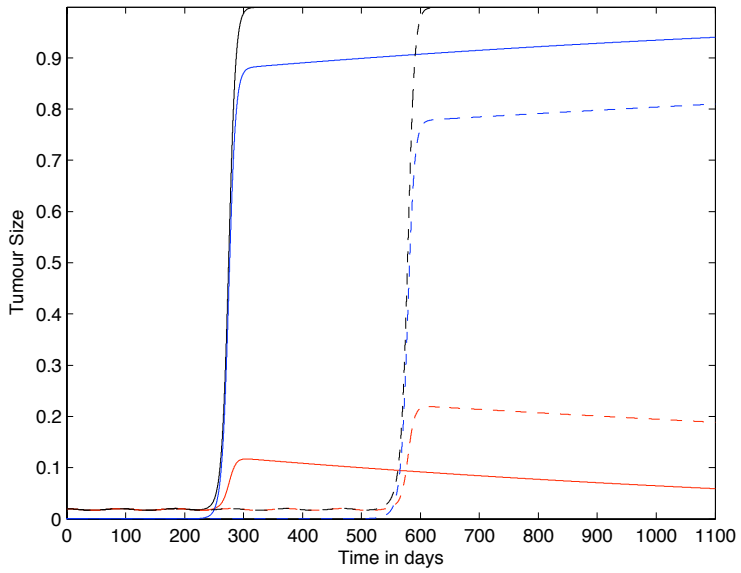

Figure 5.5: Plots showing the growth of the tumour cell population over time in the case where the spatial components of the model (i.e. all diffusion, taxis terms) have been set to zero. The plots show that the tumour can evade the immune system for either approximately 250 days or approximately 550 days depending on the parameter N. Parameter values: $p_N = 0.75$ and k_i^+ are linearly decreasing functions and: $N = 4$ (solid line) and $N = 10$ (dashed lines). The red lines represent the population T_0, the blue lines represent the summed populations $T_1 + ... + T_N$, and the black lines represent the summed populations $T_0 + ... + T_N$. Time t is in days.

Figure 5.4 shows the plots of the growth of the tumour cell population over time where the killing probability at the last stage is $p_N = 0.75$, and as in the previous figure, $k_i^+ = constant = 1.3 \times 10^{-7}$. These results are different from the previous two cases. Here the immunoevasion takes place *in the lifespan of the mouse* only for the case $N = 4$. This suggests that in absence of changes in the parameter k_i^+: *i)* the late stages T_i are the most important to determine the onset of the evasion; *ii)* due to the finite lifespan of chimeric mice and to the slow rate of the transitions, the immunoevasion process requires that the maximum ability of genetic or epigenetic changes in a tumour cell upon complexing with a CTL (embedded in the transition probability whose maximum, we recall, is at $i = N - 1$), is reached in a small number of encounters.

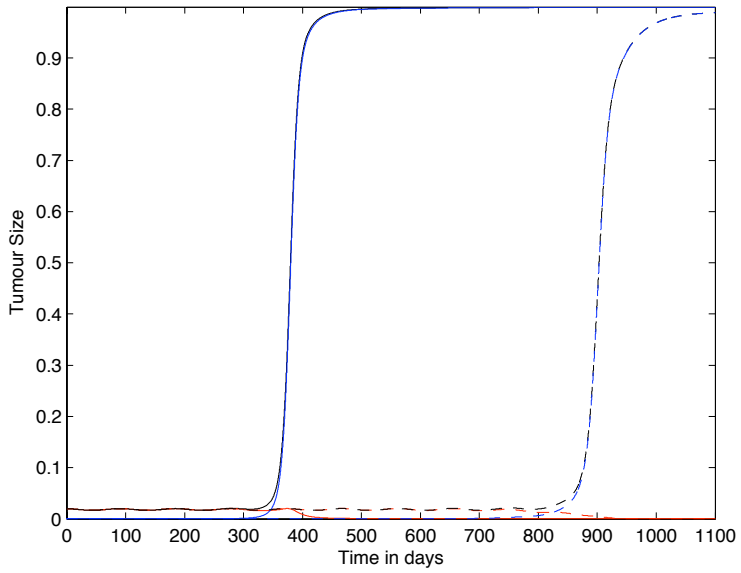

Figure 5.6: Plots showing the growth of the tumour cell population over time in the case where the spatial components of the model (i.e. all diffusion, taxis terms) have been set to zero. The plots show that the tumour can evade the immune system for either approximately 350 days or approximately 850 days depending on the parameter N. In this case however, the initial population T_0 is eradicated. Parameter values: $p_i = constant = 0.9997$ and k_i^+ are linearly decreasing functions and: $N = 4$ (solid line) and $N = 10$ (dashed lines). The red lines represent the population T_0, the blue lines represent the summed populations $T_1 + ... + T_N$, and the black lines represent the summed populations $T_0 + ... + T_N$. Time t is in days.

Figure 5.5 shows the growth of the tumour cell population over time where the parameter $p_N = 0.75$, but in this case the parameters k_i^+ are linearly decreasing with $k_N^+ = 0$. We notice the following differences from the previous case: *i)* here the onset of immunoevasion is for $N = 4$ at $t \approx 250$ *days*, i.e. it is considerably accelerated; *ii)* there is the onset of immunoevasion (at $t \approx 550$ *days*) also for $N = 10$. Thus, this simulation suggests that the role of the decrease of the probability that a tumour cell is recognized by a CTL is important for the timing of the onset of immunoevasion. Moreover, the decrease of the parameters k_i^+ alone is sufficient to induce immunoevasion, as suggested in the simulations shown in figure 5.6, where $p_i = constant = 0.9997$ and k_i^+ are linearly decreasing.

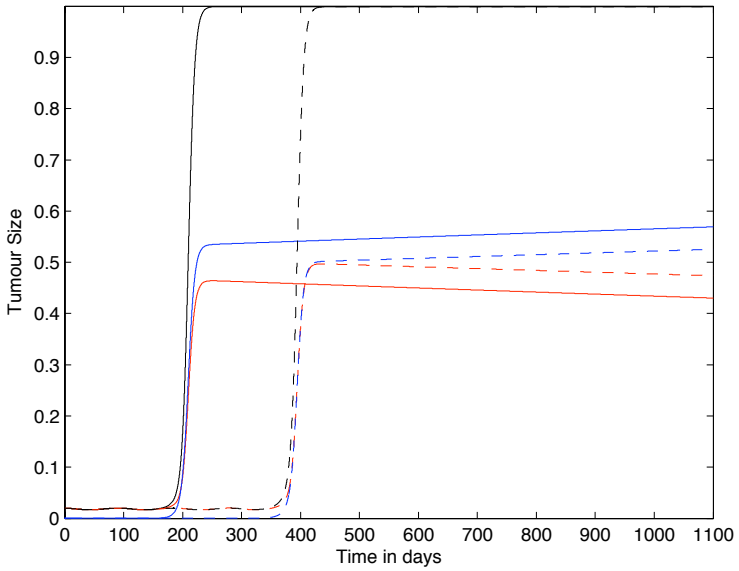

Figure 5.7: Plots showing the growth of the tumour cell population over time in the case where the spatial components of the model (i.e. all diffusion, taxis terms) have been set to zero. The plots show that the tumour can evade the immune system for either approximately 200 days or approximately 400 days depending on the parameter N. Parameter values: $p_N = 0$ and k_i^+ are linearly decreasing functions and: $N = 4$ (solid line) and $N = 10$ (dashed lines). The red lines represent the population T_0, the blue lines represent the summed populations $T_1 + ... + T_N$, and the black lines represent the summed populations $T_0 + ... + T_N$. Time t is in days.

However, as shown in figure 5.7, if $p_N = 0$, then the addition of the mechanism of decreasing k_i^+ does not accelerate the onset of immunoevasion to such a degree with respect to the baseline case of constant k_i^+ shown in the previous figure 5.2.

Finally, comparing the results shown in all the figures we have examined in this section, we note that

$$Max(T_0) < Max(T_1 + \cdots + T_N)$$

holds in the cases where k_i^+ is decreasing. Moreover, $Max(T_0)$ seems to be a decreasing function of p_N. These results might be explained as follows: the decrease of the competition between all the tumour cells and the immune system embedded in the decrease of the parameters k_i^+, might shift the 'internal' competition between the naive and the non-naive tumour cells.

5.6.2 Spatiotemporal Model

1-Dimensional Domain

Before we present the computational simulation results of the new model in this chapter, in figures 5.8 and 5.9 we plot the spatial distribution of tumour cells and CTLs, respectively, in the baseline case of the absence of immunoevasive mechanisms.

Figure 5.8 shows the spatial distribution of tumour cell density within the tissue at times 100, 400, 700, and 1100 days. These results illustrate the basic spatiotemporal dynamics of the tumour cell density induced by its interplay with the distribution of CTLs i.e. a gradual transition between a front of tumour cells to a train of solitary-like traveling waves slowly invading the tissue, finally creating a spatially heterogeneous

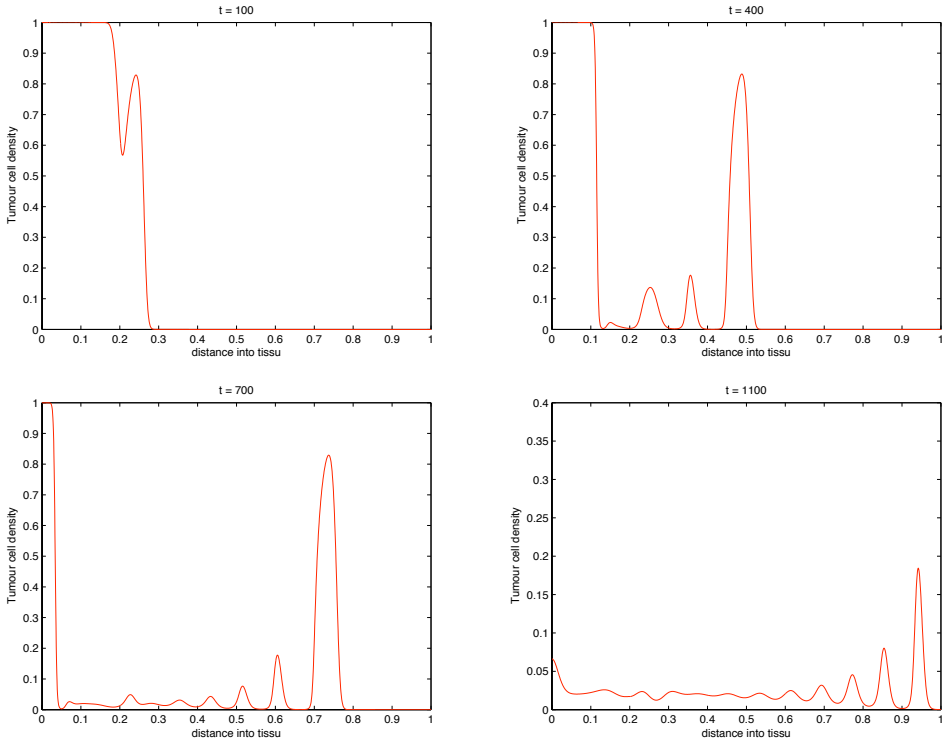

Figure 5.8: Plots showing the spatial distribution of tumour cells within the tissue at times corresponding to 100, 400, 700, and 1100 days, respectively, in the baseline case of absence of the immunoevasive mechanism described in this chapter. This corresponds to the results of Matzavinos et al. (2004).

and time-changing (through irregular temporal oscillations) distribution. Similarly, figure 5.9 shows the corresponding plots of the CTL density.

Figure 5.10 shows the spatial distribution of tumour cell density within the tissue at times 100, 400, 700, and 1100 days where the parameters $p_N = 0.75$ and $k_i^+ = constant$. These results show that if we include the immunoevasive mechanism with a decreased value for the parameter p_N, we obtain a process that is identical to the baseline case for most of the time. Indeed, basically the first three plots of this figure are identical to those of figure 5.8. However, after the onset of the evasion, the tumour cell density distribution changes significantly as can be seen in the left part of the domain. From these observed differences, we may say that in this modelling framework the

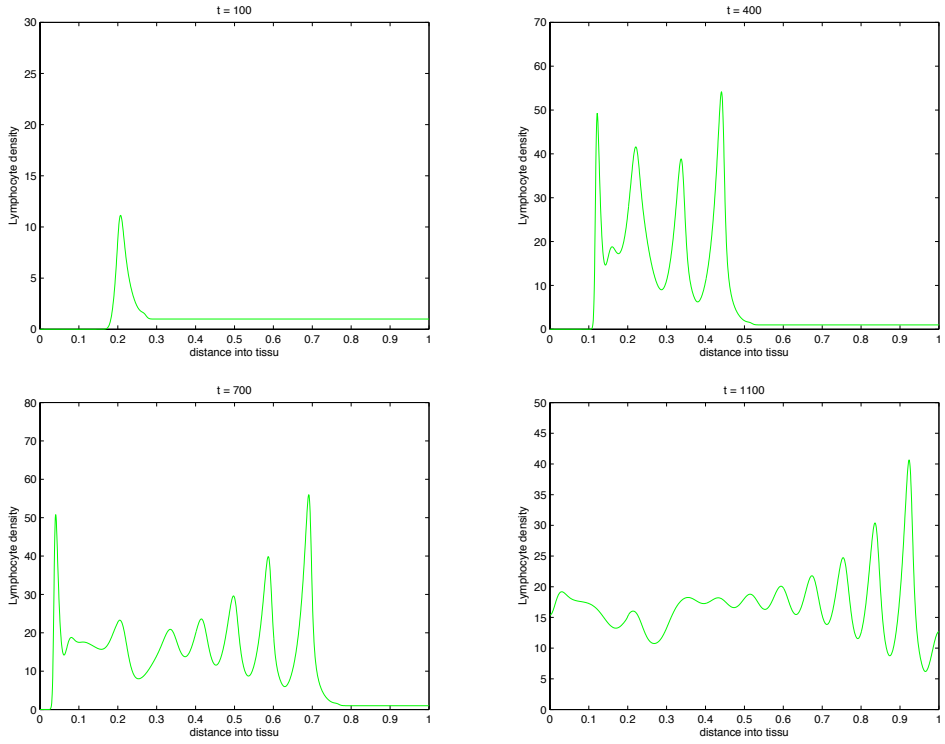

Figure 5.9: Plots showing the spatial distribution of CTLs within the tissue at times corresponding to 100, 400, 700, and 1100 days, respectively, in the baseline case of absence of the immunoevasive mechanism described in this chapter. This corresponds to the results of Matzavinos et al. (2004).

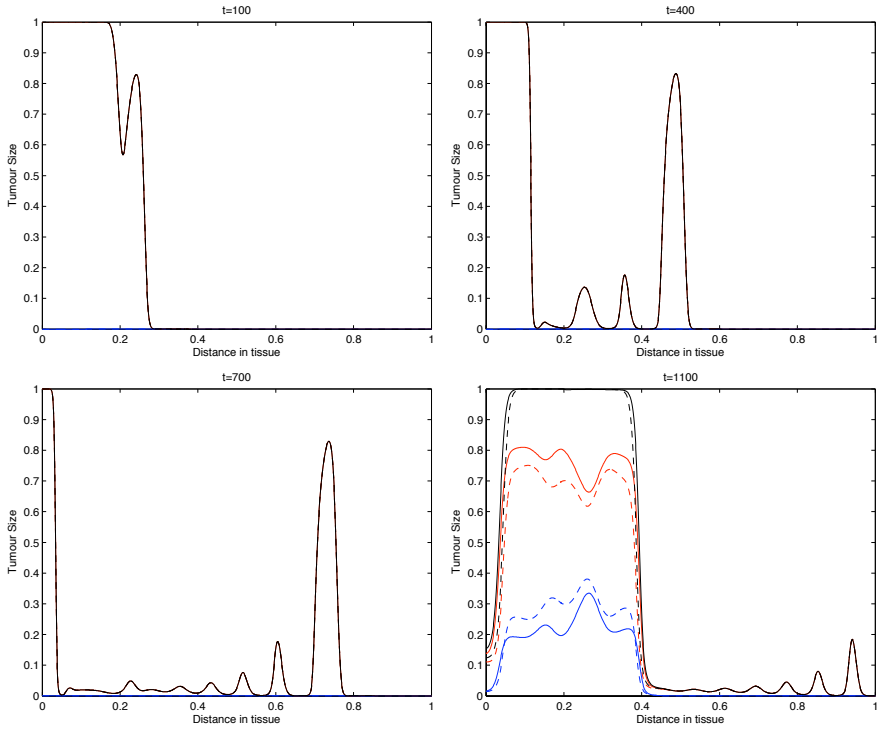

Figure 5.10: Plots showing the distribution of tumour cell density within the tissue at times corresponding to 100, 400, 700, and 1100 days respectively. These plots illustrate the spatiotemporal onset of immunoevasion. The final plot at $t = 1100$ should be compared to the equivalent plot in figure 5.8. Parameter values $p_N = 0.75$ and $k_i^+ = constant$. Solid line with chemorepellor, dashed line without (i.e. $\xi = 0$). The red lines represent the population T_0, The blue lines represent the summed population $T_1 + ... + T_N$, and the black lines represent the summed population $T_0 + ... + T_N$.

effect of immunoevasion on the spatio-temporal dynamics is characterized by a return to a spatially homogeneous steady-state. This transition to the new spatial regimen is illustrated in more detail by the "time-slices" shown in figure 5.11.

Finally, we note that the predicted effect on the tumour cells spatial distribution of the induction of chemorepulsion of CTLs is not detectable if we consider the total density of all tumour cells. However it is noticeable if we consider the density of T_0 versus the density of $T_1 + \cdots + T_N$ (see the fourth plot of figure 5.10).

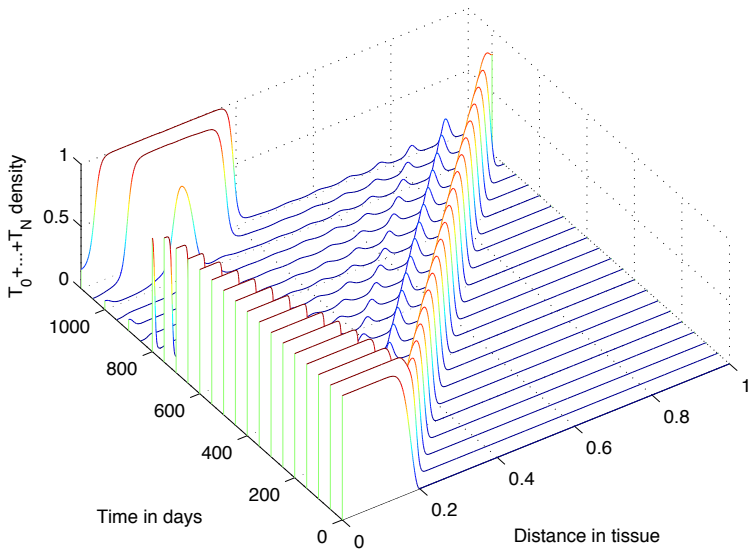

Figure 5.11: Plots showing detailed changes in the spatial distribution of all tumour cells $\sum_{j=0}^{N} T_j$ within the tissue over time in the case of immunoevasion. Parameter values $p_N = 0.75$ and $k_i^+ = constant$.

Figures 5.12 and 5.13 show the corresponding density of CTLs in the tissue. Note that after the onset of immunoevasion, corresponding to the newly reformed invasive front of tumour cells at a high density, the density of CTLs is close to zero.

Figure 5.14 shows the spatial distribution of tumour cell density within the tissue at times 100, 400, 700, and 1100 days in the case where the parameters $p_N = 0.75$ and k_i^+ are decreasing such that $k_N^+ = 0$. Due to the acceleration of the immunoevasion caused by the synergy existing between the variability of p_i and k_i^+, the plots in this figure are substantially different from those in the baseline case in figure 5.8 and also with respect to the plots in figure 5.10. Indeed, in this case the spatio-temporal distribution of the tumour cell density is far more regular, and by $t = 1100$ days almost all of the tissue has been invaded by the tumour cells close to their maximum density. Moreover, here in large regions of the domain we have $T_0 < T_1 + \cdots + T_N$, which is the

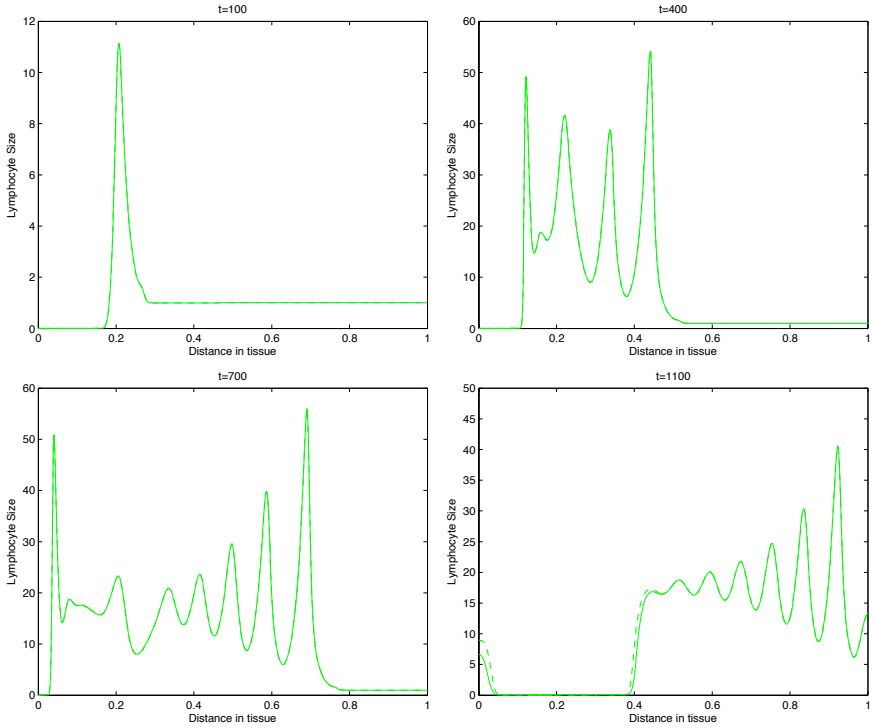

Figure 5.12: Plots showing the distribution of CTLs within the tissue at times corresponding to 100, 400, 700, and 1100 days respectively. These plots illustrate the spatiotemporal onset of immunoevasion. The final plot at $t = 1100$ should be compared to the equivalent plot in figure 5.9. Parameter values $p_N = 0.75$ and $k_i^+ = constant$. Solid line with chemorepellor, dashed line without (i.e. $\xi = 0$).

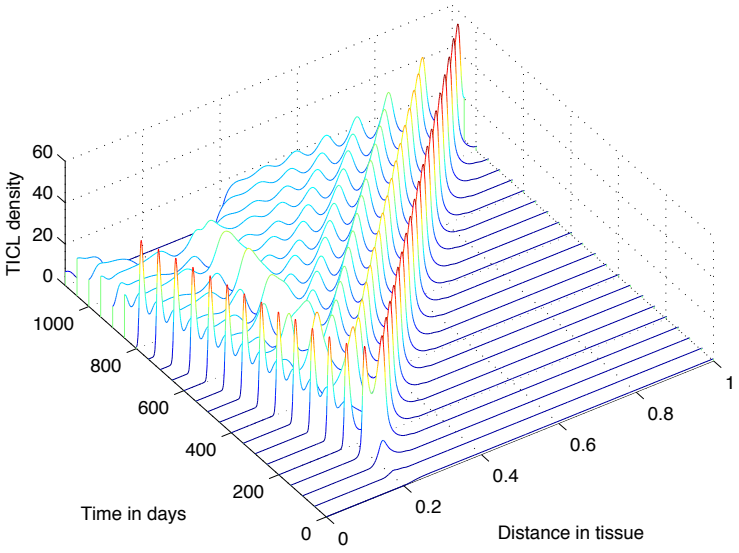

Figure 5.13: Plots showing detailed changes in the spatial distribution of CTLs within the tissue over time in the case of immunoevasion. Parameter values $p_N = 0.75$ and $k_i^+ = constant$.

opposite of the previous case, where the naive tumour cells T_0 were prevalent. Finally, figure 5.14 illustrates the fact that the distributions of naive vs non-naive tumour cells are "mirror-images" of one another and they are complementary, since their sum is a homogeneous front.

In figure 5.15 we show the differential effect of chemorepulsion on the various classes of tumour cells. The plots show the total number $A_i(t)$ of cells in each classes, i.e.

$$A_i(t) = \int_0^1 T_i(x,t)dx,$$

over time, as well as, in the last plot, the grand-total $A_1(t) + \cdots + A_N(t)$. The effect of the chemorepulsion on each sub-population A_i is striking, although overall it is globally compensated (see the last plot).

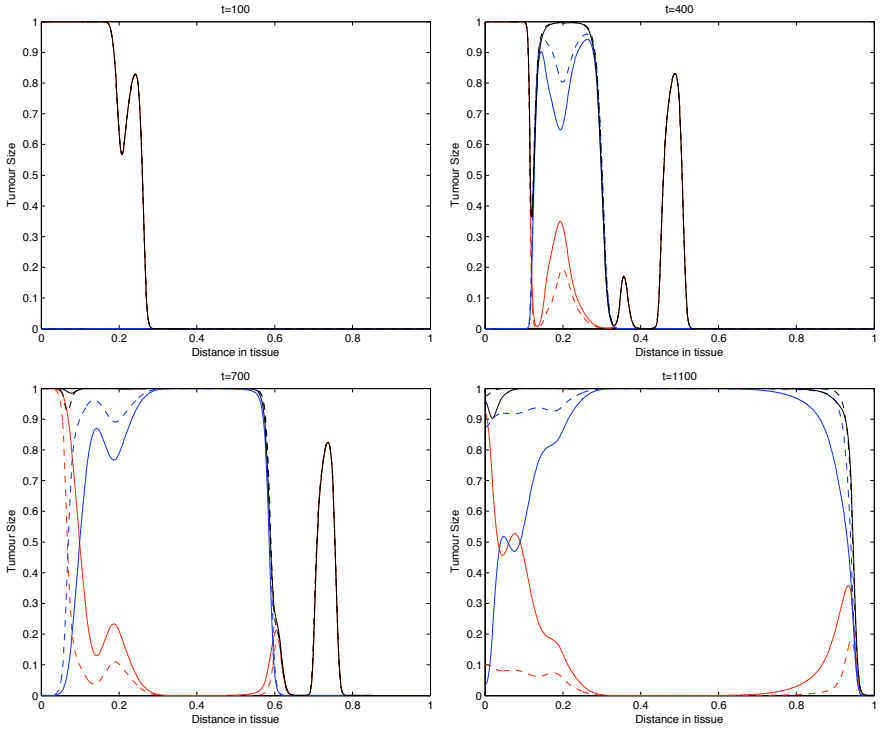

Figure 5.14: Plots showing the distribution of tumour cell density within the tissue at times corresponding to 100, 400, 700, and 1100 days respectively. These plots illustrate the spatiotemporal onset of immunoevasion. Parameter values $p_N = 0.75$ and k_i^+ are decreasing such that $k_N^+ = 0$. Solid line with chemorepellor, dashed line without (i.e. $\xi = 0$). The red lines represent the population T_0, The blue lines represent the summed population $T_1 + ... + T_N$, and the black lines represent the summed population $T_0 + ... + T_N$.

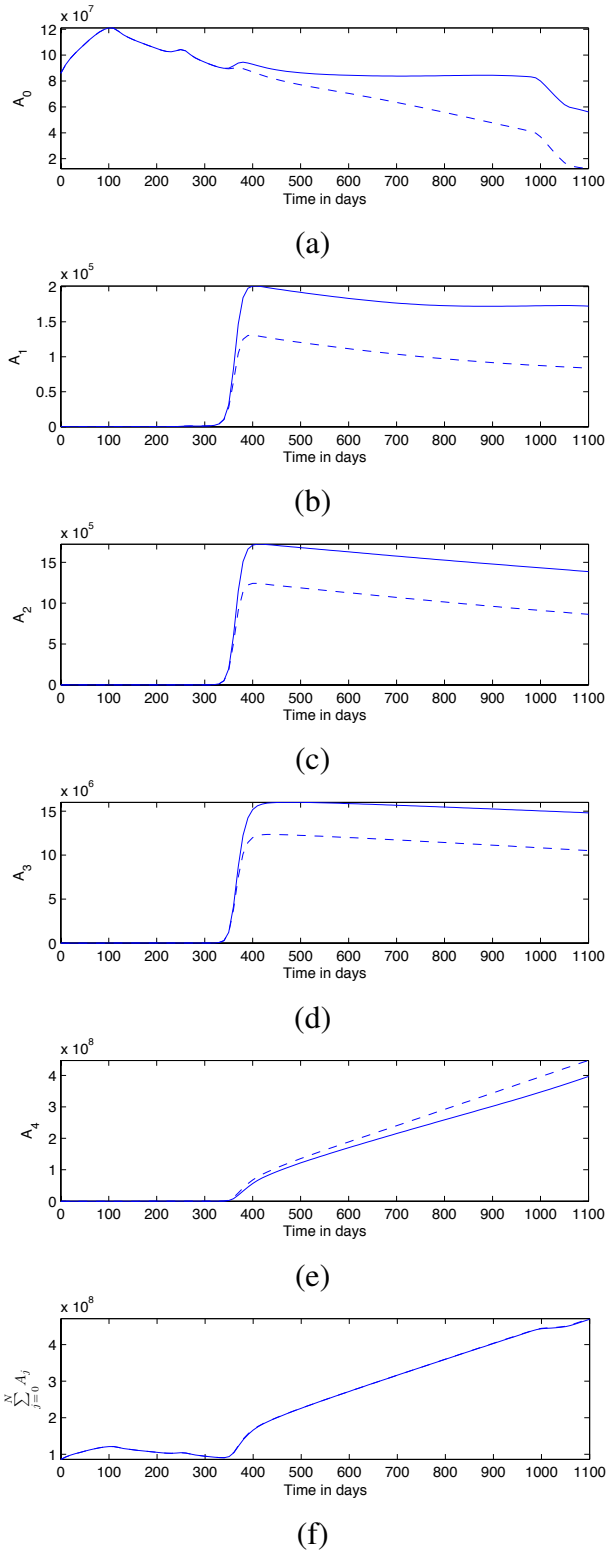

Figure 5.15: Plots showing the effects of chemorepulsion on the total number of spatially distributed classes of tumour cells. Plots of the total number of cells $A_i(t) = \int_0^1 T_i(x,t)dx$. Panels: (a) A_0, (b) A_1, (c) A_2, (d) A_3, (e) A_4, and (f) $\sum_{j=0}^{4} A_j(t)$. Solid line with chemorepellor, dashed line without (i.e. $\xi = 0$). Time is measured in days.

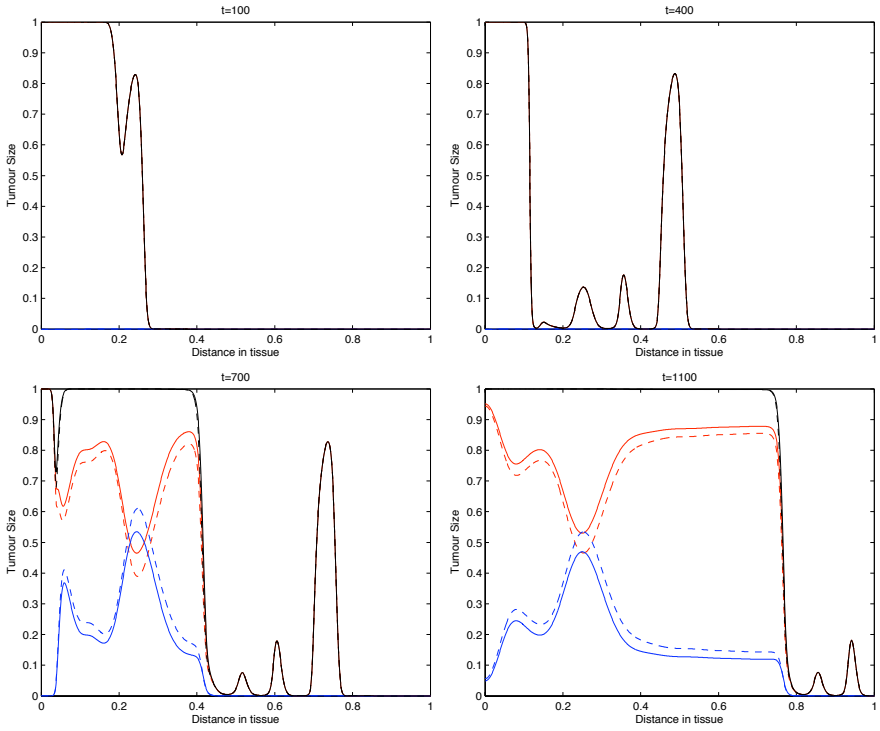

Figure 5.16: Plots showing the distribution of tumour cell density within the tissue at times corresponding to 100, 400, 700, and 1100 days respectively. These plots illustrate the spatiotemporal onset of immunoevasion. Parameter values $p_N = 0.5$ and k_i^+ are constant. Solid line with chemorepellor, dashed line without (i.e. $\xi = 0$). The red lines represent the population T_0, The blue lines represent the summed population $T_1 + ... + T_N$, and the black lines represent the summed population $T_0 + ... + T_N$.

Figure 5.16 shows the distribution of tumour cell density within the tissue at times corresponding to 100, 400, 700, and 1100 days respectively with parameter values $p_N = 0.5$ and $k_i^+ = constant = k_0^+$. Note that in this case, although $p_N = 0.5$, probably due to the constancy of k_i^+, in large parts of the space the number of naive cells exceeds the rest of the classes of other tumour cells, i.e. $T_0 > T_1 + \cdots + T_N$. Note that at the end of the average lifespan of the mouse, the tissue is invaded to a large extent but to a lesser extent that in the case where $p_N = 0.5$ and $k_N^+ = 0$. Figure 5.17 shows a more detailed evolution of the tumour cell density by presenting the "time-slices" from $t = 0$ to $t = 1100$. Figure 5.18 shows the corresponding distribution of CTL density.

Finally, figure 5.19 shows the distribution of tumour cell density within the tissue at

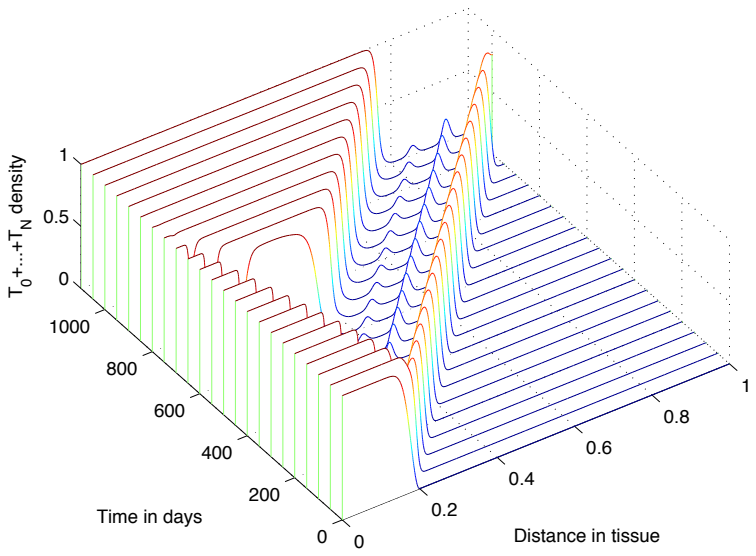

Figure 5.17: Plots showing detailed changes in the spatial distribution of all tumour cells $\sum_{j=0}^{N} T_j$ within the tissue over time in the case of immunoevasion. Parameter values $p_N = 0.5$ and $k_i^+ = constant$.

times corresponding to 100, 400, 700, and 1100 days respectively when the parameters $p_N = 0.5$ and $k_N^+ = 0$. This figure summarizes well the important role of the two parameters p_N and k_N^+ in shaping the spatio-temporal distribution of tumour cells. Indeed, the parameter k_N^+ appears to accelerate the onset and the velocity of propagation of the invasive front, and moreover it also differentially shapes T_0 and $T_1 + \cdots + T_N$.

2-Dimensional Domain

In this section, we undertake computational simulations for our model in the absence of any 'taxis' on a two-dimensional domain i.e. we did not included the chemotaxis and chemorepulsion terms. Moreover, here we also considered a constant influx of CTLs. The simulations were performed using MATLAB enhanced with the tool COMSOL Multiphysics which uses a finite-element approach to solve PDEs. As extension of the

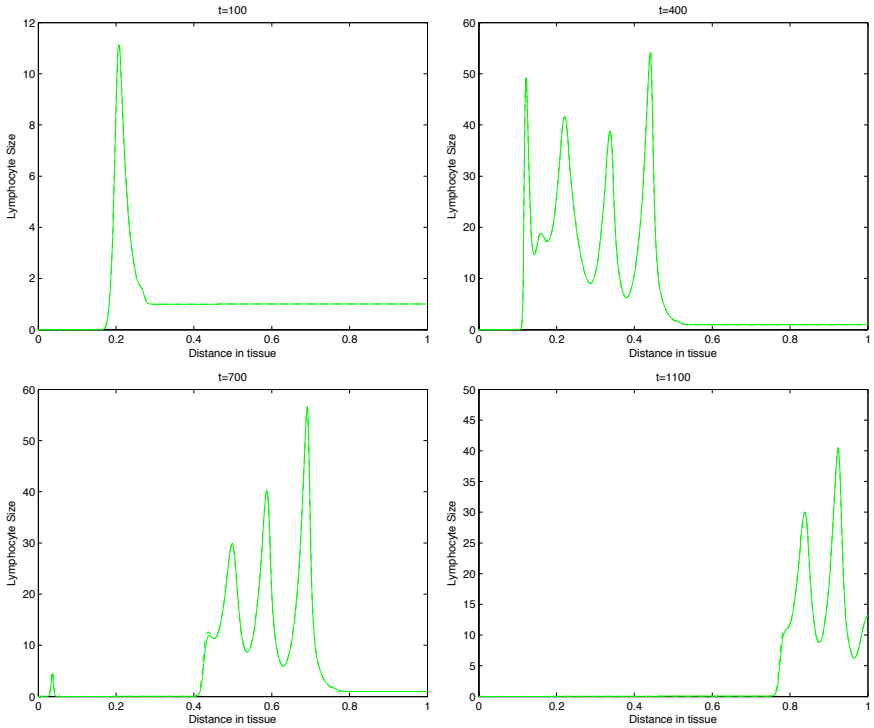

Figure 5.18: Plots showing the distribution of CTLs within the tissue at times corresponding to 100, 400, 700, and 1100 days respectively. These plots illustrate the spatiotemporal onset of immunoevasion. Parameter values $p_N = 0.5$ and k_i^+ are constant. Solid line with chemorepellor, dashed line without (i.e. $\xi = 0$).

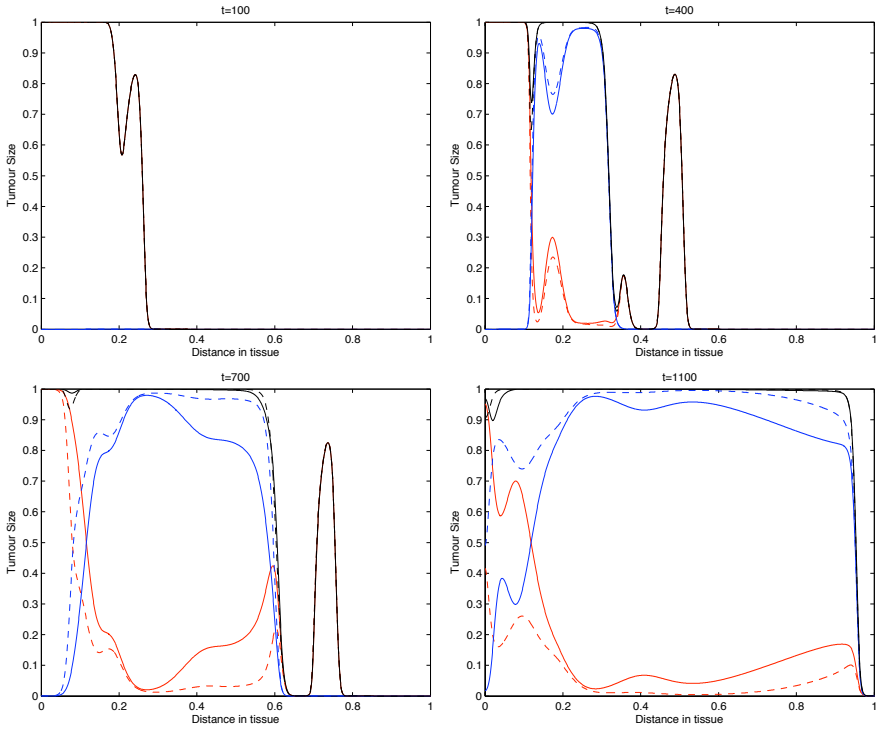

Figure 5.19: Plots showing the distribution of tumour cell density within the tissue at times corresponding to 100, 400, 700, and 1100 days respectively. These plots illustrate the spatiotemporal onset of immunoevasion. Parameter values $p_N = 0.5$ and $k_N^+ = 0$. Solid line with chemorepellor, dashed line without (i.e. $\xi = 0$). The red lines represent the population T_0, The blue lines represent the summed population $T_1 + ... + T_N$, and the black lines represent the summed population $T_0 + ... + T_N$.

1-D settings, we considered the rectangular domain:

$$D = [0,1] \times [0,1] \subset \mathbb{R}^2$$

with zero-flux boundary conditions. The initial conditions are:

$$T_0(x,y) = T(x,y,0) = exp(-100((x-0.5)^2 + (y-0.5)^2)),$$

$$E_0(x,y) = E(x,y,0) = 1 - exp(-100((x-0.5)^2 + (y-0.5)^2)),$$

with the other variables being set to zero initially.

Once again in figures 5.20, 5.21 we first of all plot the spatial distribution of tumour cells and CTLs, respectively, in the baseline case of the absence of immunoevasive mechanisms (cf. figures 5.8 and 5.9).

Following the 1-dimensional results, figures 5.22 and 5.23 show the spatial distribution of, respectively all tumour cells and of CTLs in the case $p_N = 0.75$ and constant k_i^+. Figures 5.24 and 5.25 show the spatial distribution of, respectively, all tumour cells and of CTLs in the case $p_N = 0.75$ and $k_N = 0$.

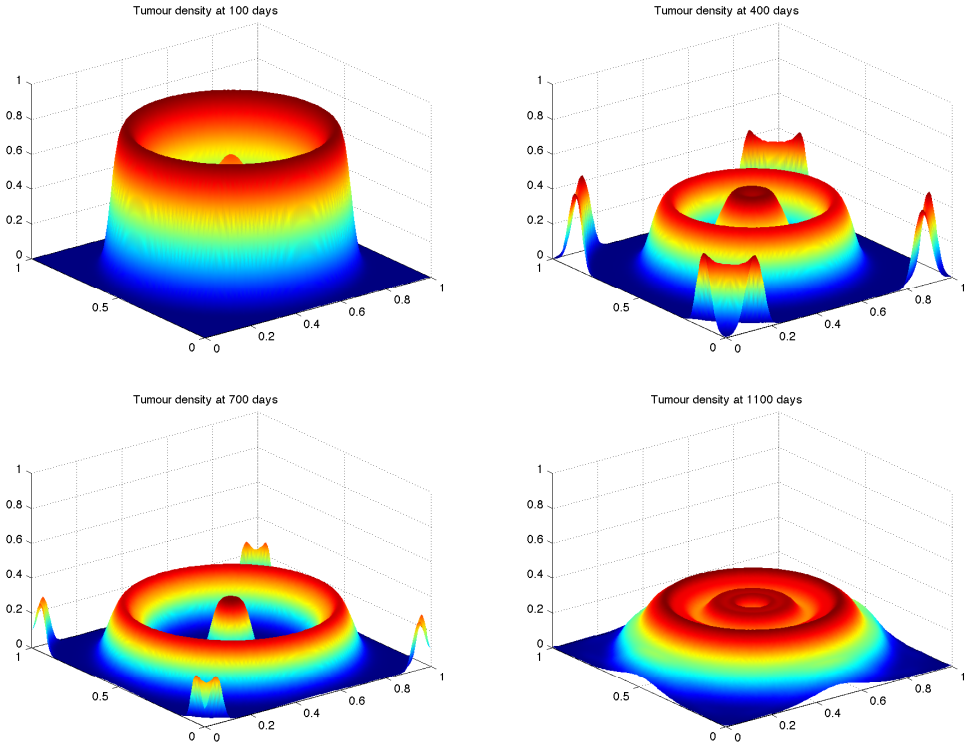

Figure 5.20: Plots showing the spatial distribution of the total tumour cell density ($\sum_{j=0}^{N} T_j$) within the tissue in a 2-dimensional spatial domain at times corresponding to 100, 400, 700, and 1100 days, respectively, in the baseline case of absence of the immunoevasive mechanism described in this chapter.

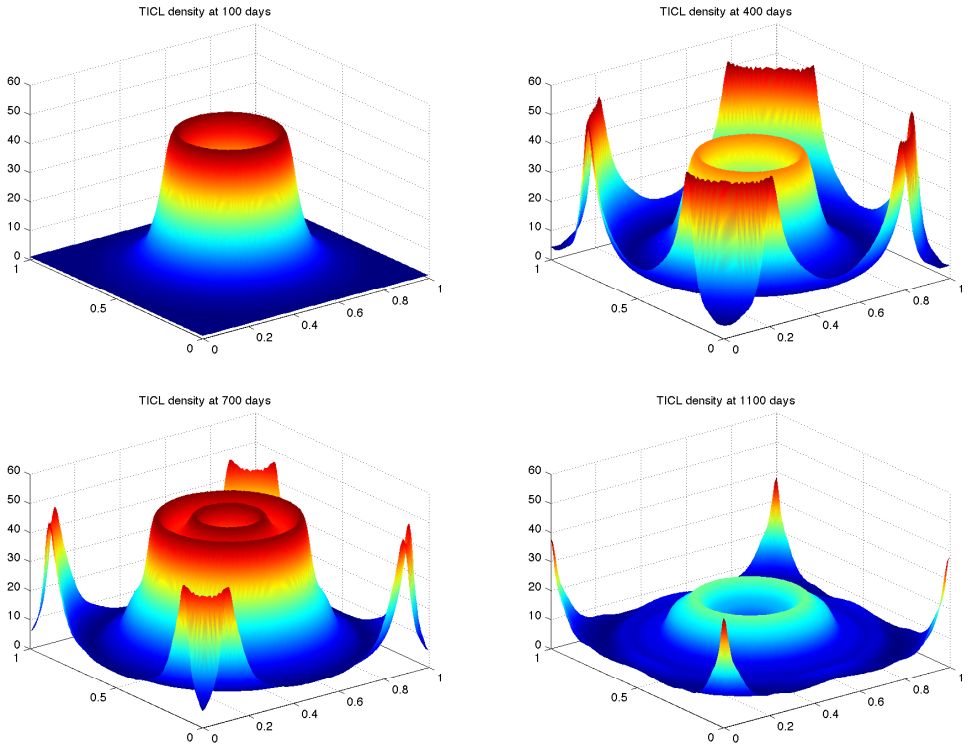

Figure 5.21: Plots showing the spatial distribution of the CTL density within the tissue in a 2-dimensional spatial domain at times corresponding to 100, 400, 700, and 1100 days, respectively, in the baseline case of absence of the immunoevasive mechanism described in this chapter.

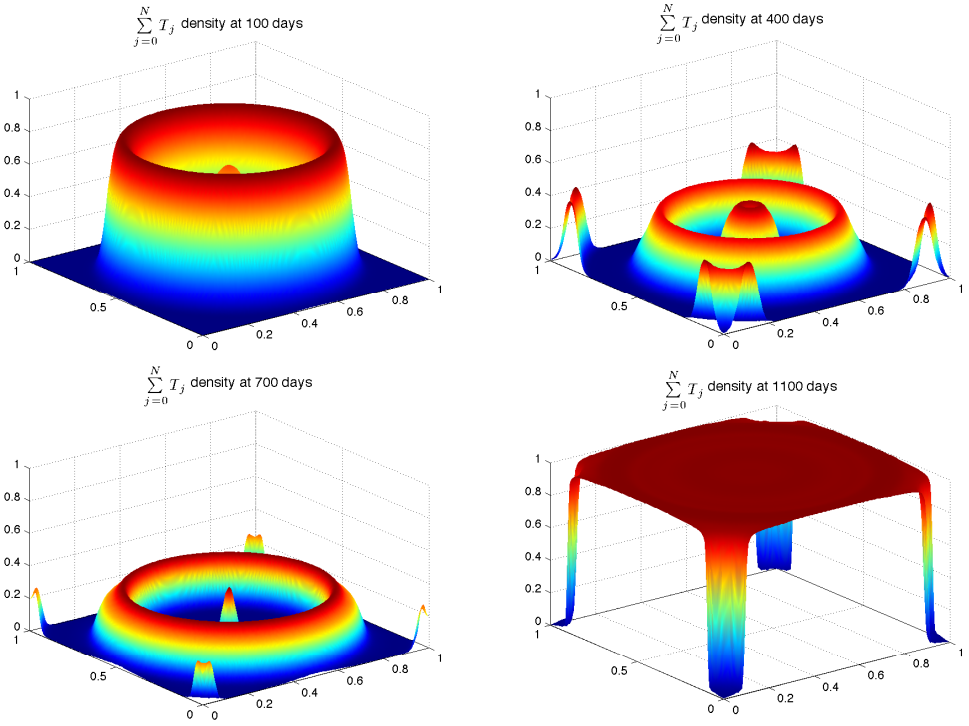

Figure 5.22: Plots showing the spatial distribution of the total tumour cell density ($\sum_{j=0}^{N} T_j$) within the tissue in a 2-dimensional spatial domain at times corresponding to 100, 400, 700, and 1100 days, respectively. These plots illustrate the spatiotemporal onset of immunoevasion. Parameter values $p_N = 0.75$ and k_i^+ is constant.

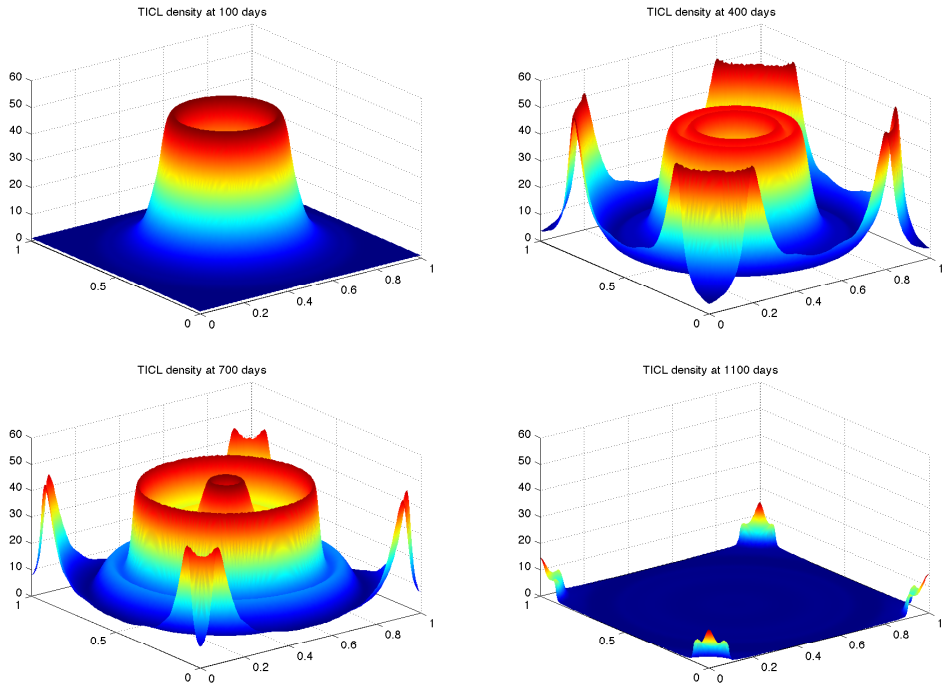

Figure 5.23: Plots showing the spatial distribution of the CTL density within the tissue in a 2-dimensional spatial domain at times corresponding to 100, 400, 700, and 1100 days, respectively. These plots illustrate the spatiotemporal onset of immunoevasion. Parameter values $p_N = 0.75$ and k_i^+ is constant.

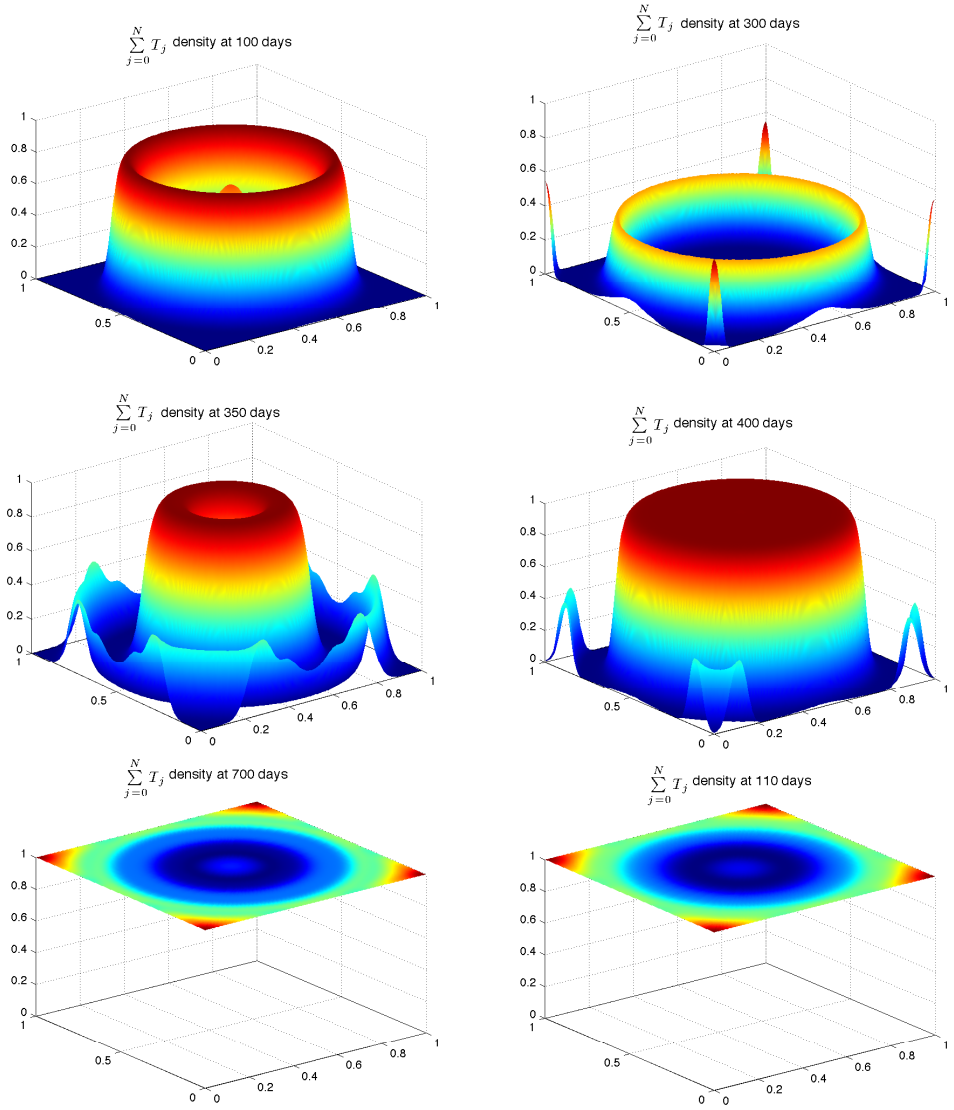

Figure 5.24: Plots showing the spatial distribution of the total tumour cell density ($\sum_{j=0}^{N} T_j$) within the tissue in a 2-dimensional spatial domain at times corresponding to 100, 300, 350, 400, 700, and 1100 days respectively. These plots illustrate the spatiotemporal onset of immunoevasion. Parameter values $p_N = 0.75$ and $k_N^+ = 0$.

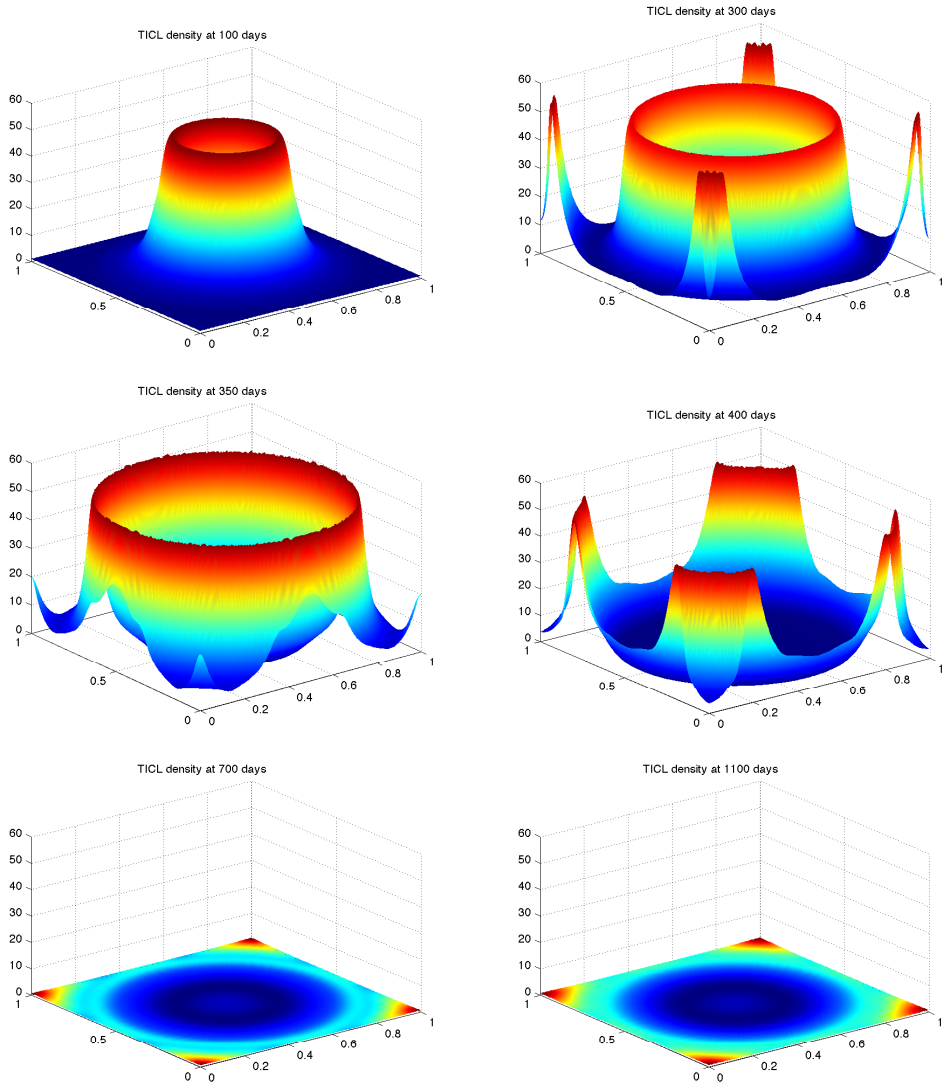

Figure 5.25: Plots showing the spatial distribution of the CTL density within the tissue in a 2-dimensional spatial domain at times corresponding to 100, 300, 350, 400, 700, and 1100 days respectively. These plots illustrate the spatiotemporal onset of immunoevasion. Parameter values $p_N = 0.75$ and $k_N^+ = 0$.

5.7 Discussion and Conclusions

In this chapter we have presented a novel mathematical model of the immune response to cancer, focussing on the specific spatio-temporal response of cytotoxic T-lymphocytes to tumour cells. We have developed and extended ideas originally formulated by Matzavinos et al. (2004) by proposing a possible kinetic mechanism leading to tumour evasion from the immune control. Our model is based on the key concept that a tumour cell which survives the formation of a complex with a cytotoxic T-lymphocyte can develop, with a given probability, an increased probability of surviving further attacks by CTLs. We do not specify whether this so-called 'increased resistance' is genetic or epigenetic. Indeed, from a kinetic point of view, this is immaterial. However, in order to experimentally validate the hypothesis, this distinction would be of paramount relevance.

In this work we have dealt with the spatio-temporal interplay between tumours and a specific immune response from CTLs. We chose this approach because of the experimental evidence on the relevance of CTLs in determining tumour dormancy or the evasion of many important tumours such as melanomas, ovarian carcinomas and colorectal carcinomas, where the presence of infiltrating lymphocytes is a useful prognostic marker (Galon et al., 2006; Zitvogel et al., 2006). However, tumour immunoevasion from dormancy is a multi-faceted phenomenon. We stress here that by no means do we think that ours is an exhaustive theoretical treatment of a such complex phenomenon.

We have built our model based on the tumour dormancy mathematical model of Matzavinos et al. (2004) and Chaplain and Matzavinos (2006), where parameters were fitted to experimental animal (mouse) data. However, embedding the proposed evolutionary mechanism in a more complex setting, where a more detailed description of both

adaptive and innate immunity is included, should lead to results qualitatively similar to those illustrated here.

Our simulations suggest that the proposed mechanism is able to mimic various dynamics of immunoevasion during the lifespan of a mouse. We have also highlighted the differential spatiotemporal contributions to evasion due, respectively, to: *i)* a decrease in the probability p_i of being lethally hit; *ii)* a decrease in the probability, embedded in k_i^+, that a tumour cell is recognized by a CTL. In particular, our model suggests that a decrease in the parameters p_i is needed to produce evasion, which does not occur in the case where p_i remains constant at its baseline level inferred from the experimental data. However, the role of the parameters k_i^+ is important since it can greatly accelerate the simulated process. Moreover, our computational simulations also showed that the proposed mechanism can also deeply affect the spatial patterning of the tumour. In particular, our model suggests that to have a uniform invasion profile for the tumour cells necessitates also having a decrease in the recognition rate, embedded in the parameters k_i^+. These parameters also differentially shape the spatial distribution of the various classes of tumour cells.

Concerning the possible chemorepulsion of CTLs, our computational simulation results showed that, in our biological settings, although it does not affect the spatiotemporal dynamics of the total number of tumour cells, it has a remarkable influence on the spatio-temporal distribution of the different individual classes of tumour cells. Further analysis is needed to ascertain if, with different parameters, the effect of this factor can be different, and in order to understand the behaviour in the current setting.

As far as the key 'immuno-evasion-related' parameters such as θ_i, p_i, and k_i^+ are concerned, we were not able to fit them with experimental data (apart, of course, from the values for p_0 and k_0^+, from Matzavinos et al. (2004); Chaplain and Matzavinos (2006))

because in the literature, to the best of our knowledge, immuno-editing is only illustrated by means of qualitative clinical or molecular experimental findings. In particular, no immuno-evasion-related tumour growth data are available. Indeed, a complete experimental kinetic study of the adaptive evasion from tumour dormancy allowing, for example, the plotting of tumour growth curves would currently be very difficult to undertake. Thus we hope that this theoretical work may contribute to triggering such experimental investigations, which would allow us to validate our model.

From a theoretical point of view, our model, although detailed and focused on a very specific aspect of immuno-oncology, and on some very specific mechanisms, is conceptually in line with the general theories by Bellomo (Bellomo et al., 2004; Bellomo and Delitala, 2008; Bellomo, 2010). Indeed, here also the changes of activities of cells upon encounters between tumour cells and effectors cells of the immune system are central in determining the dynamics of the system.

In this work we essentially were interested in the basic facts of the immune response to tumours. However, a number of immunotherapies have been proposed and also theoretically investigated (see d'Onofrio (2005); Arciero et al. (2004); Kim et al. (2008) and references therein). We believe that both the experimental results concerning immunoevasion of tumours and the theoretical findings we have proposed here might have some implication of interest in clinics. More in general, we share the opinion of Zitvogel et al. (2006), who stressed that recent progress in immuno-oncology have not influenced the way anticancer therapies are conceived and applied in clinics.

The model that was proposed here has to be understood as a detailed model at the level of the kinetics of the cellular populations of a possible mechanism that might enable tumour cells to evade from the control of adaptive immunity. The various specific (and tumour-dependent) strategies deployed by those cells in order to reach their aim, are phenomenologically described by means of the model of the dependence of

the various parameters on the classes of tumour cells, as well as in the macroscopic modelling of the chemorepulsion. This is a first step in a research effort for a more complete description of tumour cell immunoevasion, which will include the detailed modelling of the biological mechanisms underlying those and other specific evasion strategies. Thus, given the complex network of interplaying between inter-cellular and intra-cellular signalling, and given the various temporal scales (from the rapid dynamics of the intracellular pathways involved, to the relatively slow growth of a tumour, up to the very slow onset of immunoevasion) as well as the spatial ones (from individual cells to visible neoplasms), a more detailed model will have to be multiscale. This will involve a wide array of computational tools, from those typical of computational biology and bioinformatics, to more classical analytical and numerical methods of statistical mechanics and mathematical physics.

Chapter 6

A Mathematical Model of the Innate and Adaptive Immune Response to Cancer

6.1 Introduction

In this chapter, we develop a novel, comprehensive model of the interplay between a tumour and both the innate and the cellular part of the adaptive immune system. Our aim is of to assess the role of the kinetic and spatial parameters in influencing the outcome of this interplay: tumour suppression, tumour evasion or transition to a dormant state.

In order to be as realistic as possible, we shall modify and integrate two of the few existing spatiotemporal models of tumour-immune system interplay:

- The Owen-Sherratt model (Owen and Sherratt, 1997), focused on the initial

phases of the growth of a tumour, when it interacts mainly with the innate immune system

- The Matsavinos-Kuznetsov-Chaplain model (Matzavinos et al., 2004), which focused on the later stages of development of a tumour, when it interacts mainly with the adaptive immune system

We shall also take into account the model by de Pillis et al. (2005). These models are characterized by both a good degree of reproduction of the main features in immunoncology, and also for the accurate choice of the parameter values. As will be shown in the following sections, the development of the model does not only require one to simply "cut-and-paste" the above models and merge them: a series of modifications is also needed. One of the major changes is that we include macrophages, which not only can engulf and eliminate tumour cells, but also present antigens to the adaptive immune system.

6.2 The Mathematical Model

The State Variables

The state variables of our PDE model will be the spatial densities of the various cell type and the concentrations of the various chemical involved. We give here the complete list with some overview description:

- T: tumour cells. In absence of the immune response they proliferate with logistic growth. In the presence of the immune response, they may: *i)* be digested by macrophages, with no possibility of survival; *ii)* be induced to apoptosis by

Natural Killer cells (NK); *iii)* form short-lived complexes with the CTLs, which try to kill the tumour cells;

- M^0: macrophages that have never encountered tumour cells. Thus they are unable to present specific antigens of the tumour in order to study the adaptive immune system;

- C_M^0: complexes formed by an M^0 and by a tumour cell. They have a non-null loss rate (due to the toxic chemicals contained in a tumour cell, which can kill the macrophage) that is quite low. Usually, indeed, the macrophage survives (and becomes an M^1 cell). The tumour cell, once engulfed by an M^0, never survives;

- M^1: a macrophage that has encountered $n \geq 1$ times a tumour cell. It has the same features of an M^0, but it also "presents" the antigens of the engulfed tumour cells to the adaptive immune system;

- C_M^1: complexes formed by an M^1 and by a tumour cell. Their behaviour is similar to those of C_M^0 complexes;

- A_M: concentration of the chemoattractant produced by tumour cells and that attracts the macrophages;

- N: natural killer cells. They induce the apoptosis of tumour cells. Their behaviour is similar to that of CTLs, but NKs belongs to the innate immune system;

- C_N: complexes formed by a tumour cell and a natural killer cell;

- A_N: concentration of the chemoattractant produced by tumour cells and that attracts the natural killers;

- E_n: naive T cells. If stimulated by antigen presenting cells (= M^1) they transform to CTLs;

- E: cytotoxic T lymphocytes (CTLs);
- C: complexes formed by a CTL and a Tumour cell;
- A_E: concentration of the chemokine attracting CTLs, which is produced by complexes C.

The equation for the chemoattractant A_M

The tumour cells produce a chemical that attracts the macrophages:

$$\partial_t A_M = D_4 \nabla^2 A_M - \delta_3 A_M + P_1 T, \tag{6.1}$$

where D_4 is the diffusion coefficient, δ_3 is the degradation rate constant, and P_1 is the production rate constant.

The equation for the macrophages M^0

Unlike Owen and Sherratt (1997) and given the different timescales of cell-cell interactions and proliferations, here we do not suppose that macrophages may significantly proliferate, so that their kinetics is given by:

$$\partial_t M^0 = D_2 \nabla^2 M^0 - \chi_1 \nabla \left(M^0 \nabla A_M \right) - \delta_1 M^0 - K_M(A_M) T M^0 + q(A_M), \tag{6.2}$$

where D_2 is the diffusion coefficient of macrophages (equal for both classes), χ_1 is the chemotactic coefficient for macrophages (equal for both classes), δ_1 is the death rate coefficient for macrophages (equal for both classes), $q(A_M) > 0$ is the influx rate of macrophages - we consider this as a linear function of the chemoattactant concentration as in Owen and Sherratt (1997): $q(A_M) = q_0 (1 + \sigma A_M)$, and $K_M(A_M) T M^0$ is

the rate of formation of C_M^0 complexes. The rate coefficient $K_M(A_M)$ depends on the chemoattractant A_M. We may model it as a linear function as in Owen and Sherratt (1997) $K_M(A_M) = k_0 A_M$.

The equation for the complexes C_M^0

The equation describing the dynamics of the complexes C_M^0 is given by the following equation:

$$\partial_t C_M^0 = D_3 \nabla^2 C_M^0 - \delta_2 C_M^0 + K_M(A_M) T M^0 - \beta_1 C_M^0, \tag{6.3}$$

where D_3 is the diffusion coefficient for the complexes, δ_2 is the loss rate (due to the death of the macrophage), and $\beta_1 C_M^0$ is the transition rate: $C_M^0 \rightarrow$ *'digested' Tumour cell* $+ M^1$, where a macrophage M^0 after the encounter with the tumour cells puts the antigens on its surface, so becoming an M^1 macrophage cell that is able to present the antigens to the naive CTL cells.

The equation for the complexes C_M^1

The equation describing the dynamics of the complexes C_M^1 is similar to the equation (6.3):

$$\partial_t C_M^1 = D_3 \nabla^2 C_M^1 - \delta_2 C_M^1 + K_M(A_M) T M^1 - \beta_1 C_M^1 \tag{6.4}$$

only here $\beta_1 C_M^0$ is the rate of returning to the state of non-complexed M^1:

$$C_M^1 \rightarrow \textit{ 'digested' Tumour cell} + M^1$$

The equation for the macrophages M^1

The equation describing the spatiotemporal dynamics of M^1 is given by:

$$\partial_t M^1 = D_2 \nabla^2 M^1 - \chi_1 \nabla \left(M^1 \nabla A_M \right) - \delta_1 M^1 - K_M(A_M) T M^1 + q(A_M) + \beta_1 C_M^0 + \beta_1 C_M^1, \tag{6.5}$$

where $\beta_1 C_M^0$ is the influx rate from the "un-complexing" of complexes C_M^0. The macrophages now have contacted tumour cells at least once, and they have 'exposed' on their own surface the specific antigens of the killed tumour cell. $+\beta_1 C_M^0$ is the influx rate from the un-complexing of complexes C_M^1.

The equation for the naive and activated Cytotoxic T Lymphocytes

Extending the non-spatial model of Moore and Li (2004) (where the amount of antigen presenting cells is considered proportional to the number of tumour cells) we have that the dynamics of naive CTLs is given by:

$$\partial_t E_n = D_7 \nabla^2 E_n - \chi_3 \nabla \left(E_n \nabla A_E \right) + S_n(x) - \mu_n E_n - \gamma(M^1) E_n \tag{6.6}$$

where $S_n(x)$ is a baseline production rate of naive CTLs (concentrated in the lymph nodes), $D_7 \geq 0$ is a diffusion coefficient of the naive CTLs, $\chi_3 \geq 0$ is a chemotactic coefficient of the naive CTLs, μ_n is a loss rate coefficient of the naive CTLs, and $\gamma(M^1)E_n$ is a macrophage-stimulated activation rate, where $\gamma(M^1)$ is an increasing function of M^1 with $\gamma(0) \geq 0$. For example: $\gamma(M^1) = \frac{aM^1}{1+bM^1}$.

Finally, the equation for the activated CTLs is given by:

$$\partial_t E = R(x,T) + \gamma(M^1)E_n + \frac{fC}{g+T} + D_7\nabla^2 E - \chi_3\nabla\left(E\nabla A_E\right) \tag{6.7}$$

$$-\mu E - k^+ TE + k^- C + kpC,$$

where $R(x,T) \geq 0$ is the influx rate of CTLs, $\gamma(M^1)E_n$ is the influx of activated CTLs due to the encounter of naive CTLs with M^1 cells, $fC/(g+T)$ is the rate of recruitment and proliferation stimulated by the presence of the tumour, μ is the baseline death rate of the CTLs, k^+TE is the rate of forming T-CTLs complexes, k^-C is the rate of the transition $C \rightarrow T + CTL$, and p is the probability that a tumour cell dies so that kpC is the rate of the transition $C \rightarrow$ *Dead tumour cell* $+CTL$. The above equations (6.6)-(6.7) have an inherent problem: naive CTLs reside in lymph nodes and not directly to the site of the tumour. To take into account this process, we should include a chemical produced by naive CTLs, which attracts the M^1 macrophages. This first approach is 'exact', and does not require an enormous effort to be included in the model. However, it might make the simulations more difficult since it needs a (elementary maybe) description of the geometry of lymph nodes. In anycase, denoting by A_n this chemoattractant, one has:

$$\partial_t A_n = D_8\nabla^2 A_n - \delta_6 A_n + P_3 E_n, \tag{6.8}$$

and the equation for the M^1 macrophages has to be augmented by including a term describing chemotactic motion towards the naive CTLs:

$$\partial_t M^1 = -\chi_4\nabla\left(M^1\nabla A_n\right) \tag{6.9}$$

$$+D_2\nabla^2 M^1 - \chi_1\nabla\left(M^1\nabla A_M\right) - \delta_1 M^1 - K_M(A_M)TM^1 + q(A_M) + \beta_1 C_M^0 + \beta_1 C_M^1,$$

The equation for the Tumour Cell-CTL Complexes

$$\partial_t C = k^+ TE - k_d C - k^- C - kC, \tag{6.10}$$

where $k_d C$ is the loss rate of complexes (i.e. the rate of the transition $C \rightarrow$ *Dead tumour cell* + *Dead CTL*), and $kC = kpC + k(1-p)C$ is the sum of the rates of the transitions: $C \rightarrow$ *Dead tumour cell* $+CTL$ (occurring with probability p) and $C \rightarrow$ *tumour cell* + *Dead CTL* (occurring with probability $1-p$).

The equations of A_E

The complex produces a chemokine that attracts the activated (and the non-activated) CTLs:

$$\partial_t A_E = D_8 \nabla^2 A_E - \delta_6 A_E + P_4 C, \tag{6.11}$$

where D_8 is the diffusion coefficient, δ_6 is the degradation rate constant, and P_4 is the production rate constant.

The equation for the Natural Killer Cells

The equation describing the spatiotemporal dynamics of NK is given by:

$$\partial_t N = D_5 \nabla^2 N - \chi_2 \nabla (N \nabla A_N) + q(A_N) - \delta_4 N - K_N(A_N) TN + \gamma_N C_N + hwC_N + \pi(T)N, \tag{6.12}$$

where $\gamma_N C_N$ is the influx rate from the "un-complexing" of complexes C_N, and $\pi(T)$ is the natural killer recruitment term. For example: $\pi(T) = \frac{g_1 T^2}{h_1 + T^2}$.

The equation of A_N

The tumour cells produce chemicals that attract the Natural Killer cells:

$$\partial_t A_N = D_6 \nabla^2 A_N - \delta_5 A_N + P_2 T, \tag{6.13}$$

where D_6 is the diffusion coefficient, δ_5 is the degradation rate constant, and P_2 is the production rate constant.

The equation for the Tumour Cell-NK Complexes

$$\partial_t C_N = h^+ TN - h_d C_N - h^- C_N - hC_N, \tag{6.14}$$

where $h_d C_N$ is the loss rate of complexes, i.e. the rate of the transition $C_N \rightarrow$ *Dead tumour cell* + *Dead N* , and $hC_N = hwC_N + h(1-w)C_N$ is the sum of the rates of the transitions: $C_{NK} \rightarrow$ *Dead tumour cell* $+N$ (occurring with probability w) and $C_N \rightarrow$ *tumour cell* + *Dead N* (occurring with probability $1-w$).

The Equation for the Tumour Cells

Considering that the tumour in the absence of the immune response grows with a logistic rate, which is not substantially perturbed by the immune system, and considering that the tumour cells have the possibility of random motion with diffusion coefficient D_1, and using the previous assumptions on the interplay of the tumour with the immune system, one has:

$$\partial_t T = rT(1 - \frac{T}{C_1}) + D_1 \nabla^2 T \tag{6.15}$$

$$-k_M(A_M)T(M^0 + M^1) - h^+ TN + h^- C_N + h(1-w)C_N - k^+ TE + k^- C + k(1-p)C.$$

Thus the full mathematical model is:

$$
\begin{aligned}
\partial_t T &= D_1\nabla^2 T + rT(1-\frac{T}{C_1}) - k_0 A_M T(M^0+M^1) - h^+ TN + h^- C_N \\
&\quad + h(1-w)C_N - k^+ TE + k^- C + k(1-p)C, \\
\partial_t M^0 &= D_2\nabla^2 M^0 - \chi_1\nabla(M^0\nabla A_M) - \delta_1 M^0 - k_0 A_M T M^0 + q_0(1+\sigma A_M), \\
\partial_t C_M^0 &= D_3\nabla^2 C_M^0 - \delta_2 C_M^0 + k_0 A_M T M^0 - \beta_1 C_M^0, \\
\partial_t M^1 &= D_2\nabla^2 M^1 - \chi_1\nabla(M_1\nabla A_M) - \chi_4\nabla(M^1\nabla A_n) - \delta_1 M^1 - k_0 A_M T M^1 \\
&\quad + q_0(1+\sigma A_M) + \beta_1 C_M^0 + \beta_1 C_M^1, \\
\partial_t C_M^1 &= D_3\nabla^2 C_M^1 - \delta_2 C_M^1 + k_0 A_M T M^1 - \beta_1 C_M^1, \\
\partial_t A_M &= D_4\nabla^2 A_M - \delta_3 A_M + P_1 T, \\
\partial_t N &= D_5\nabla^2 N - \chi_2\nabla(N\nabla A_N) + q0(1+\sigma A_N) - \delta_4 N - K_N NT + \gamma_N C_N \\
&\quad + hwC_N + \frac{g_1 T^2}{h_1+T^2}N, \\
\partial_t C_N &= h^+ TN - h_d C_N - h^- C_N - hC_N, \\
\partial_t A_N &= D_6\nabla^2 A_N - \delta_5 A_N + P_2 T, \\
\partial_t E_n &= D_7\nabla^2 E_n - \chi_3\nabla(E_n\nabla A_E) + S_N(x) - \mu_N E_n - \frac{aM_1}{1+bM_1}E_n, \\
\partial_t A_n &= D_8\nabla^2 A_n - \delta_6 A_n + P_3 E_n, \\
\partial_t E &= D_7\nabla^2 E - \chi_3\nabla(E\nabla A_E) + R(x,T) + \frac{aM_1}{1+bM_1}E_n + \frac{fC}{g+T} - \mu E \\
&\quad - k^+ TE + k^- C + kpC, \\
\partial_t C &= k^+ TE - k_d C - k^- C - kC, \\
\partial_t A_E &= D_8\nabla^2 A_E - \delta_6 A_E + P_4 C.
\end{aligned}
\tag{6.16}
$$

Boundary and initial conditions

We consider the model in a fixed 1-dimensional domain [0,1] and close the system by applying appropriate boundary and initial conditions. As far as the boundary conditions are concerned, zero-flux boundary conditions are imposed on all state variables.

The initial conditions are given by:

$$T(x,0) = \begin{cases} 1, & \text{if } x \in [l-\varepsilon, l+\varepsilon], \\ 0, & \text{if } x \notin [l-\varepsilon, l+\varepsilon]. \end{cases}$$

$$\begin{pmatrix} M_0(x,0) \\ M_1(x,0) \\ N(x,0) \\ E_n(x,0) \\ E(x,0) \end{pmatrix} = \begin{cases} 0, & \text{if } x \in [l-\varepsilon, l+\varepsilon], \\ 0.2, & \text{if } x \notin [l-\varepsilon, l+\varepsilon]. \end{cases}$$

where $l = 0.5$ and $\varepsilon = 0.01$, and zero initial conditions for the remaining variables.

6.3 Parameter values

To carry out the computational simulations of the proposed model, we used the values have been reported in the literature. In Table (6.1) we summarise these parameter values with supporting references. Also we suppose $D_5 = D_2$, $D_6 = D_4$, $\chi_2 = \chi_1$, $\chi_4 = \chi_3$, $h^- = k^-$, $h = k$, $h_d = 0$, $k_d = 0$, $\delta_5 = \delta_3$, $P_2 = P_1$, and $P_3 = P_4$.

Table 6.1: A summary of the dimensional parameter estimates

Parameter	Dimensional estimate	Supporting references
D_1	$10^{-6} cm^2 day^{-1}$	(Matzavinos et al., 2004)
r	$0.18\ day^{-1}$	(Matzavinos et al., 2004)
C_1	$0.5 \times 10^9 cells\ cm^{-1}$	(Matzavinos et al., 2004)
k_0	$8.64\ cm^3\ day^{-1}\ M^{-1}$	(Owen and Sherratt 1997)
h^+	$7.13 \times 10^{-10}\ day^{-1}$	(de Pillis et al., 2006)
β_1	$3.45 \times 10^{-2}\ day^{-1}$	(Owen and Sherratt 1997)
w	0.5	-
k^+	$1.3 \times 10^{-7} day^{-1} cells^{-1} cm$	(Matzavinos et al., 2004)
χ_1	$2 \times 10^6\ cm^2\ day^{-1}\ M^{-1}$	(Owen and Sherratt 1997)
k	$7.2\ day^{-1}$	(Matzavinos et al., 2004)
p	0.9997	(Matzavinos et al., 2004)
D_2	$8.64 \times 10^{-7}\ cm^2\ day^{-1}$	(Owen and Sherratt 1997)
k^-	$24\ day^{-1}$	(Matzavinos et al., 2004)
δ_1	$1.728 \times 10^{-2}\ day^{-1}$	(Owen and Sherratt 1997)
q_0	$3.46 \times 10^6\ cm^{-3}\ day^{-1}$	(Owen and Sherratt 1997)
σ	$58 \times 10^{10}\ M^{-1}$	(Owen and Sherratt 1997)
D_3	$4.32 \times 10^{-7}\ cm^2\ day^{-1}$	(Owen and Sherratt 1997)
δ_2	$0.086\ day^{-1}$	(Owen and Sherratt 1997)
D_4	$0.1728\ cm^2\ day^{-1}$	(Owen and Sherratt 1997)
P_1	$4.32 \times 10^{-20}\ M\ cm^3\ day^{-1}$	(Owen and Sherratt 1997)
δ_3	$3.457 \times 10^{-1}\ day^{-1}$	(Owen and Sherratt 1997)
K_N	$7.13 \times 10^{-10}\ day^{-1}$	(de Pillis et al., 2005)
γ_N	$24\ day^{-1}$	(de Pillis et al., 2005)
h_1	$2.02 \times 10^7\ cells$	(de Pillis et al., 2005)
g_1	$4.98 \times 10^{-1}\ day^{-1}$	(de Pillis et al., 2005)
SN	$0.073\ cells\ day^{-1}\ \mu l$	(Moore and Li 2004)
δ_4	$4.12 \times 10^{-2}\ day^{-1}$	(de Pillis et al., 2005)
D_7	$10^{-6} cm^2 day^{-1}$	(Matzavinos et al., 2004)
χ_3	$1.728 \times 10^6\ cm^2 day^{-1}\ M^{-1}$	(Matzavinos et al., 2004)
a	$10^{-5}\ day^{-1}\ cells^{-1}\ \mu l$	(Moore and Li 2004)
μ_n	$0.04\ day^{-1}$	(Moore and Li 2004)
R	$1.36 \times 10^4\ day^{-1} cells\ cm^{-1}$	(Matzavinos et al., 2004)
g	$2.02 \times 10^7\ cells\ cm^{-1}$	(Matzavinos et al., 2004)
μ	$0.0412\ day^{-1}$	(Matzavinos et al., 2004)
f	$0.2988 \times 10^8 day^{-1}\ cells\ cm^{-1}$	(Matzavinos et al., 2004)
b	$10^{-2}\ cells^{-1}\ \mu l$	(Moore and Li 2004)
D_8	$8 \times 10^{-3}\ cm^2\ day^{-1}$	(Matzavinos et al., 2004)
δ_6	$1.155 \times 10^{-2}\ day^{-1}$	(Matzavinos et al., 2004)
P_4	3.03×10^{-18}	(Matzavinos et al., 2004)

6.4 Linear Stability Analysis

We consider the system of ODEs of the underlying spatially homogeneous of model (6.16):

$$\begin{aligned}
\partial_t T &= rT(1-\frac{T}{CC}) - k_0 A_M T(M^0+M^1) - h^+ TN + h^- C_N \\
&\quad + h(1-w)C_N - k^+ TE + k^- C + k(1-p)C, \\
\partial_t M^0 &= -\delta_1 M^0 - k_0 A_M T M^0 + q_0(1+\sigma A_M), \\
\partial_t C_M^0 &= -\delta_2 C_M^0 + k_0 A_M T M^0 - \beta_1 C_M^0, \\
\partial_t M^1 &= -\delta_1 M^1 - k_0 A_M T M^1 + q_0(1+\sigma A_M) + \beta_1 C_M^0 + \beta_1 C_M^1, \\
\partial_t C_M^1 &= -\delta_2 C_M^1 + k_0 A_M T M^1 - \beta_1 C_M^1, \\
\partial_t A_M &= -\delta_3 A_M + P_1 T, \\
\partial_t N &= q0(1+\sigma A_N) - \delta_4 N - K_N NT + \gamma_N C_N + hwC_N + \frac{ggT^2}{hh+T^2}N, \\
\partial_t C_N &= h^+ TN - h_d C_N - h^- C_N - hC_N, \\
\partial_t A_N &= -\delta_5 A_N + P_2 T, \\
\partial_t E_n &= S_N(x) - \mu_N E_n - \frac{aM_1}{1+bM_1}E_n, \\
\partial_t E &= R(x,T) + \frac{aM_1}{1+bM_1}E_n + \frac{fC}{g+T} - \mu E - k^+ TE + k^- C + kpC, \\
\partial_t C &= k^+ TE - k_d C - k^- C - kC,
\end{aligned} \tag{6.17}$$

Using the parameter values described in Table (6.1), it is straightforward to show that there are two positive steady states; free tumour steady state (healthy state) and small tumour steady state (dormant state).

By linearising about each steady state, we find that the first steady state is unstable, and the second steady state is stable.

6.5 Computational Simulation Results

6.5.1 Spatially Homogenous Case

In this first set of simulations, we set all the spatial components of the model to zero and consider only the reaction kinetics. Figure 6.1 shows the plots of the tumour cell, macrophage (M_0, M_1), natural killer, naive and activated CTLs. We observe that there is a slowly damped oscillation in the behaviour of the tumour, natural killer and CTL cells. Also we note that the solution converges to the second steady state where the tumour size is small (dormant state).

In figures 6.2 and 6.3, we changed the values of q_0 and δ_4. This values of parameters gave us two saddle steady states, one with free tumour and the second is with big value of tumour. Also we have a close orbit (limit cycle). We take the time is 10000 days to show the limit cycle. We note that the new shape of solutions with conserve the oscillations.

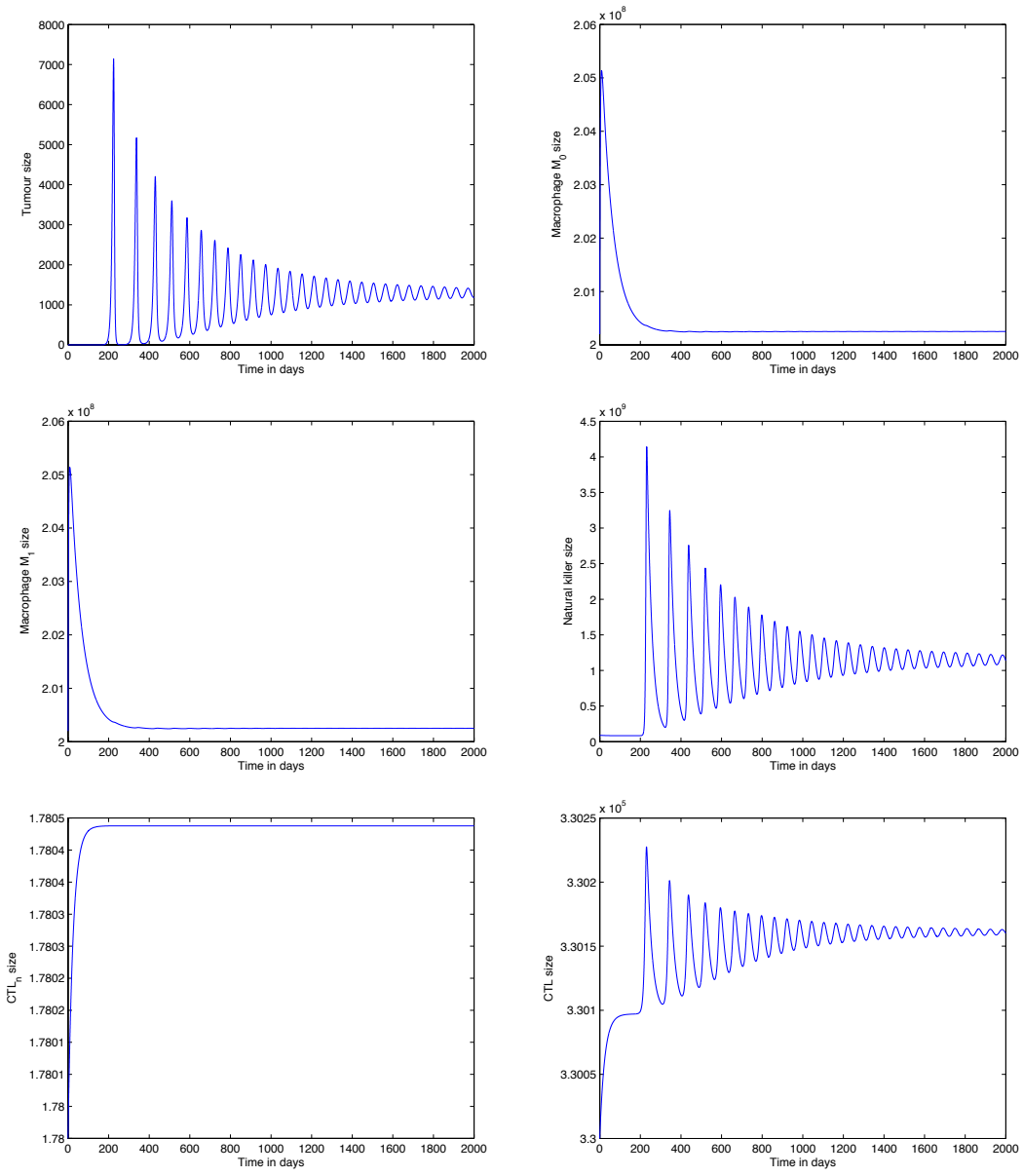

Figure 6.1: Plots showing the growth of the tumour cell population, macrophages M_0, macrophages M_1, natural killer cells, naive CTLs and CTLs over time 2000 days in the case where the spatial components of the model (i.e. all diffusion, taxis terms) have been set to zero. The initial condition is taken close to the first steady state.

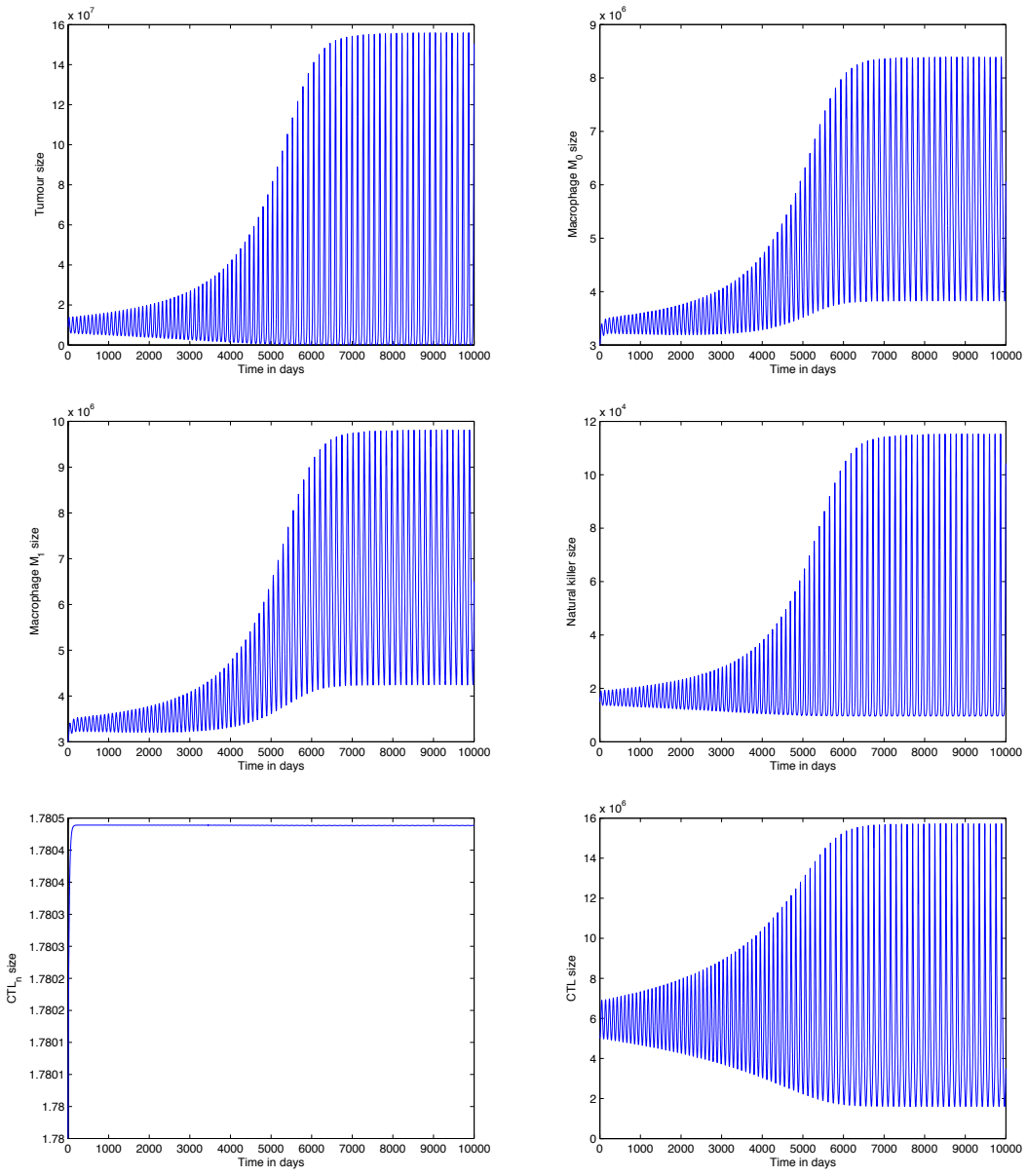

Figure 6.2: Plots showing the growth of the tumour cell population, macrophages M_0, macrophages M_1, natural killer cells, naive CTLs and CTLs over time 10000 days in the case where the spatial components of the model (i.e. all diffusion, taxis terms) have been set to zero, with $q_0 = 3.46 \times 10^4$ and $\delta_4 = 4.12$.

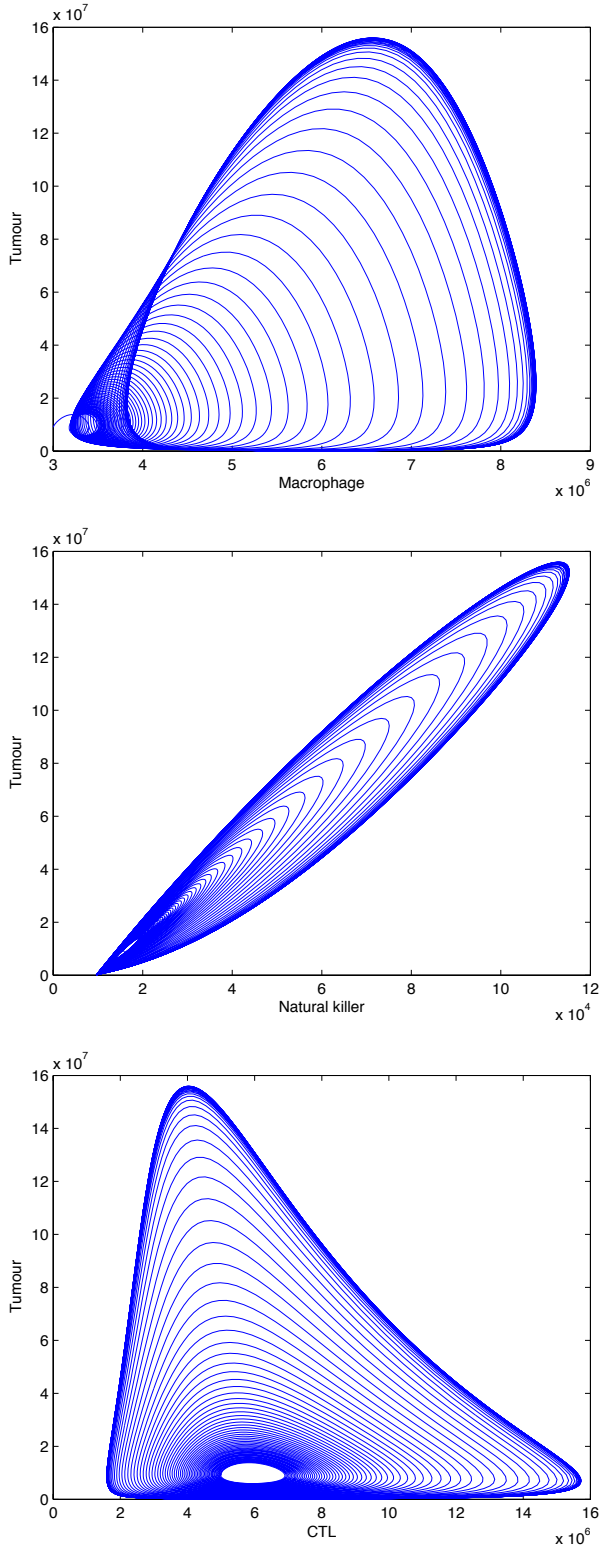

Figure 6.3: Plots showing the solution of the ODE system between (a) macrophages and tumour cells, (b) natural killer cells and tumour cells, and (c) CTLs and tumour cells, with $q_0 = 3.46 \times 10^4$ and $\delta_4 = 4.12$. The plots show there is limit cycle orbit between the variables over time 10000 days.

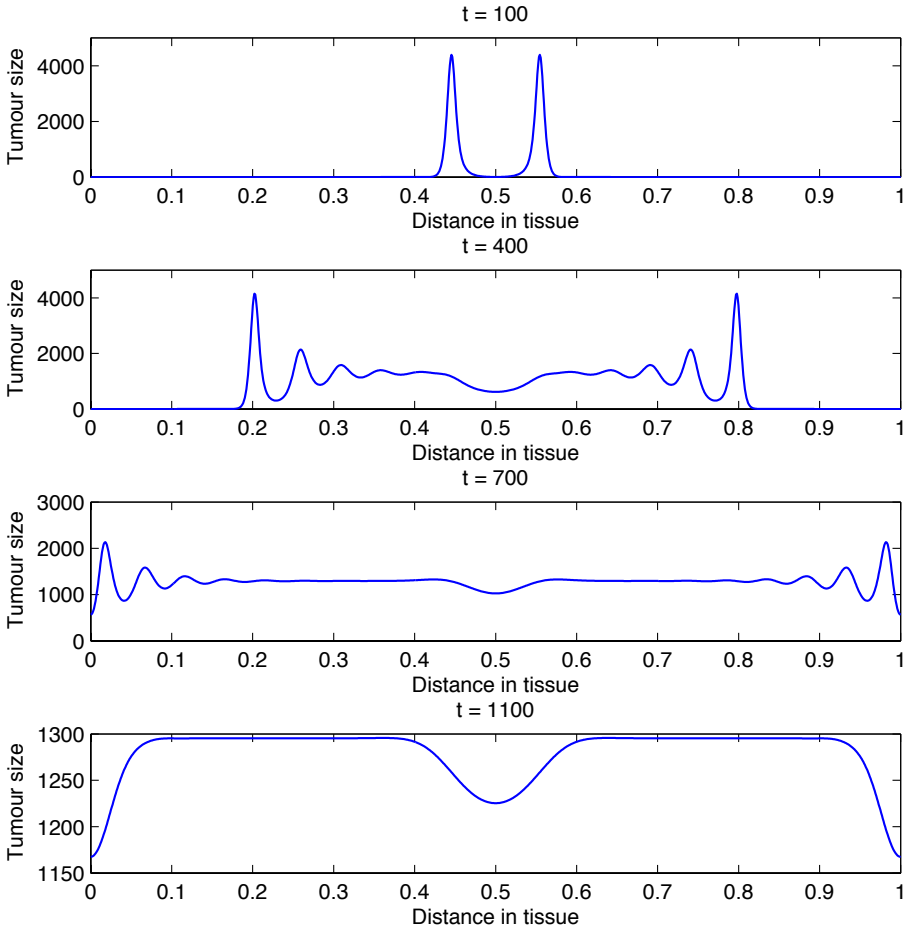

Figure 6.4: Plots showing the distribution of tumour cell density within the tissue at times corresponding to 100, 400, 700, and 1100 days respectively.

6.5.2 Spatiotemporal Case

Now we present the computational simulation results of model (6.16) with the parameter values in Table (6.1). Figure 6.4 shows the spatial distribution of tumour cell density within the tissue at time 100, 400, 700, and 1100 days . These results illustrate that the tumour size is decreasing with time, and is then fixed at the steady state value.

Similarly figures 6.5 and 6.6 shows the macrophage density, the distribution of macrophages

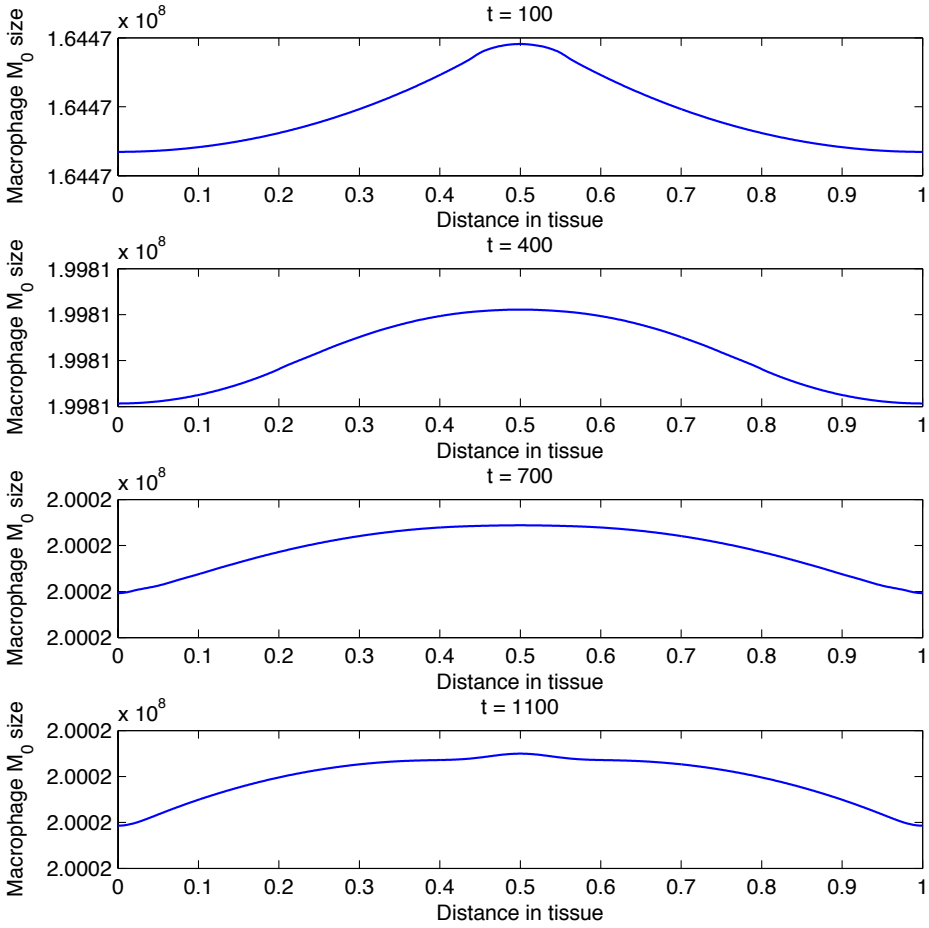

Figure 6.5: Plots showing the distribution of macrophage M_0 cell density within the tissue at times corresponding to 100, 400, 700, and 1100 days respectively.

M_0 is similar to the distribution of macrophages M_1.

Figure 6.7 shows the distribution of the natural killer cells. The behaviour of the solution is similar to the behaviour of the solution for the tumour cells up to time 400 days. However, then the shape of the profile of the natural killer cells changes. Figure 6.8 shows the naive CTL density. We note the solution of the E_n reaches the steady state value after a short time.

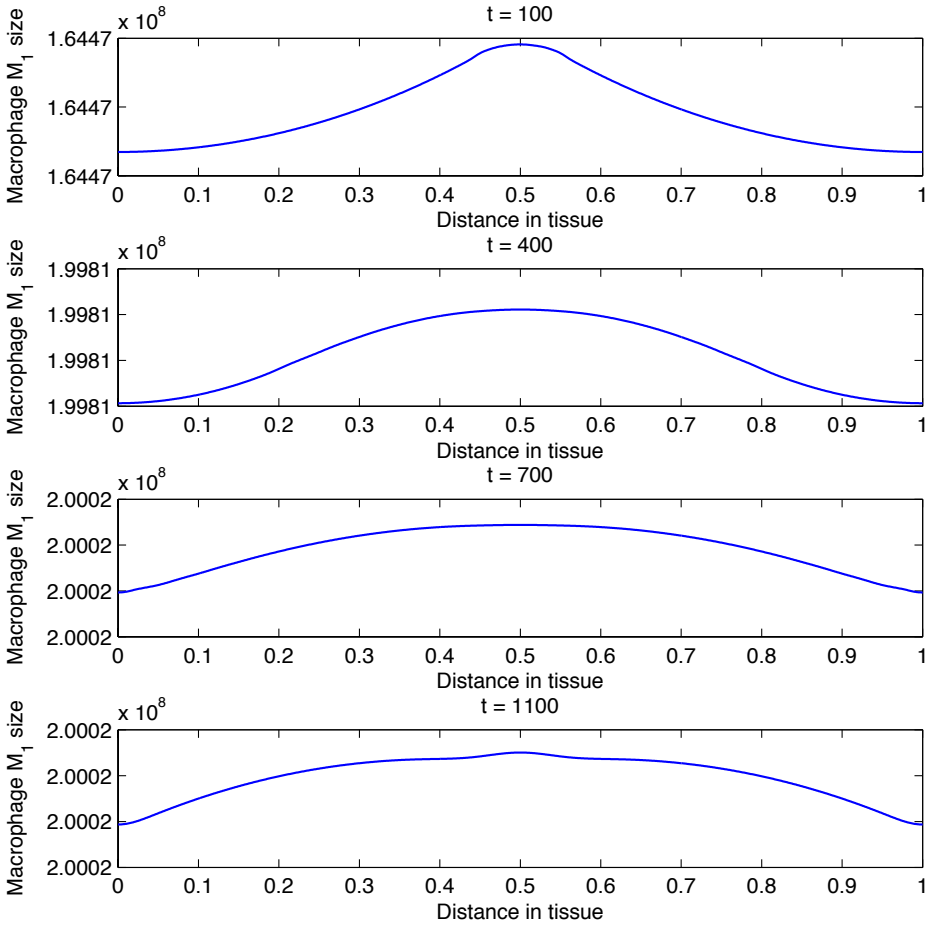

Figure 6.6: Plots showing the distribution of macrophage M_1 cell density within the tissue at times corresponding to 100, 400, 700, and 1100 days respectively.

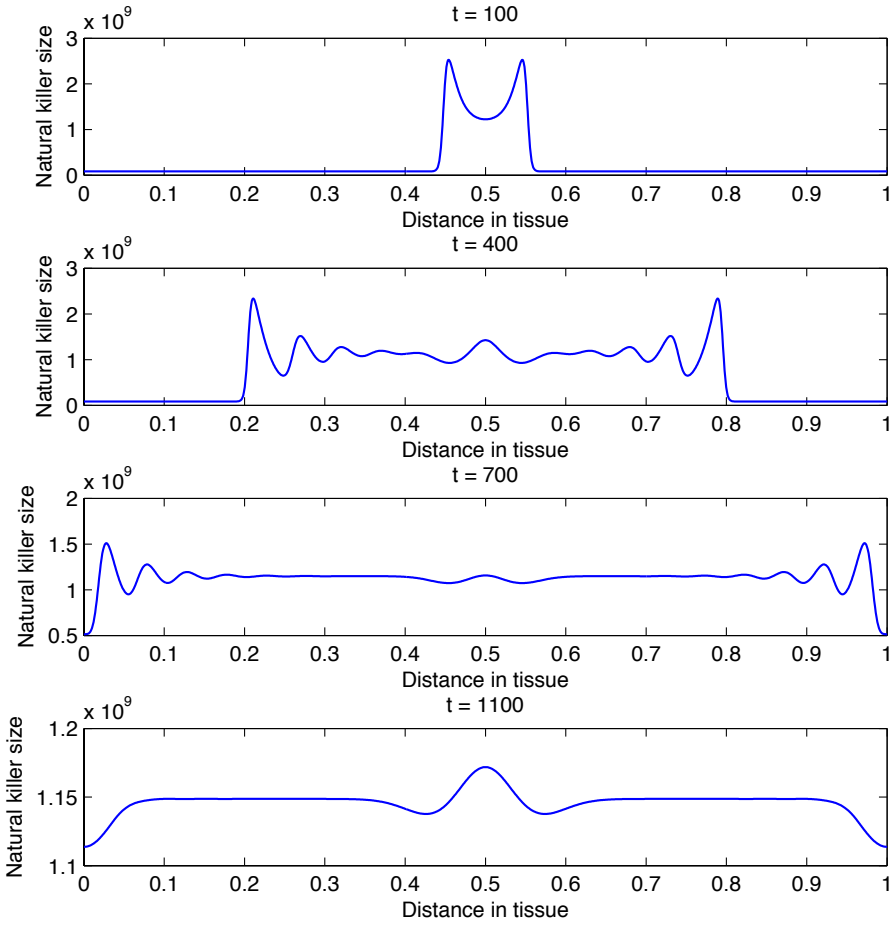

Figure 6.7: Plots showing the distribution of natural killer cell density within the tissue at times corresponding to 100, 400, 700, and 1100 days respectively.

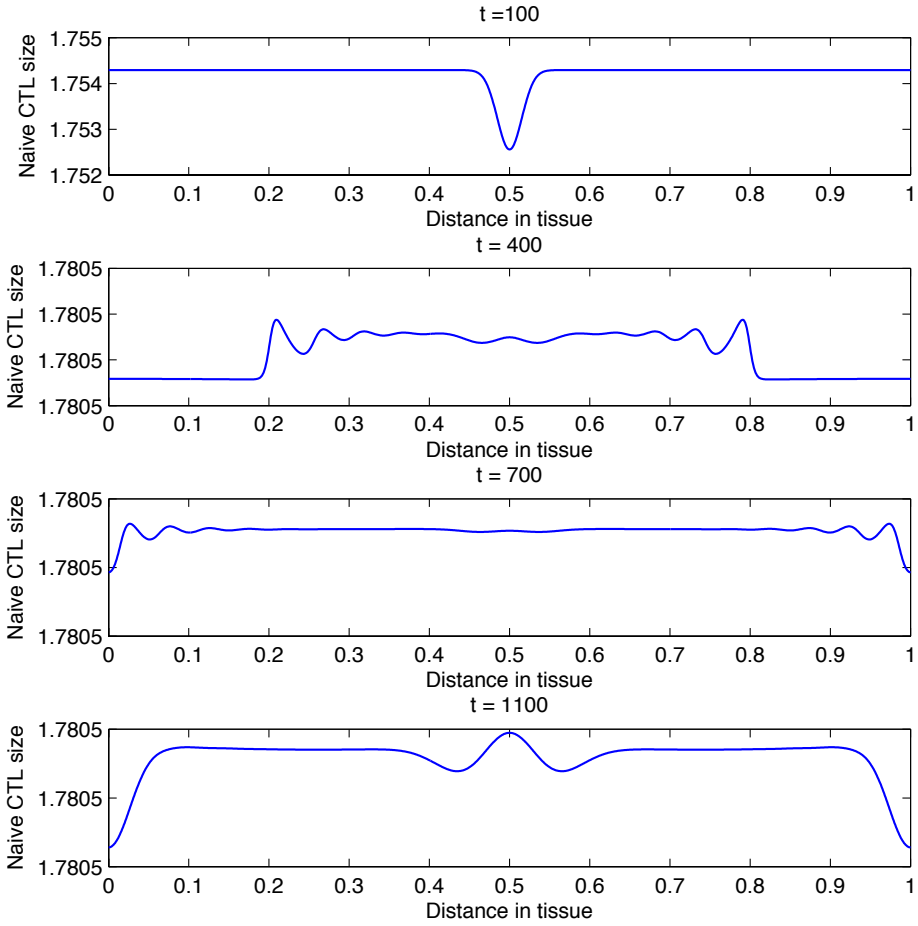

Figure 6.8: Plots showing the distribution of naive CTL cell density within the tissue at times corresponding to 100, 400, 700, and 1100 days respectively.

Finally, figure 6.9 shows the distribution of CTL cell density, again the shape of solution is close to the shape of the tumour solution with different values.

Figure 6.10 shows the spatial distribution of tumour cell density within the tissue at time 100, 400, 700, and 1100 days, with $q_0 = 3.456 \times 4$ and $\delta_4 = 4.12$. We note the size of tumour is different than the previous case (figure 6.4), in additional, we note

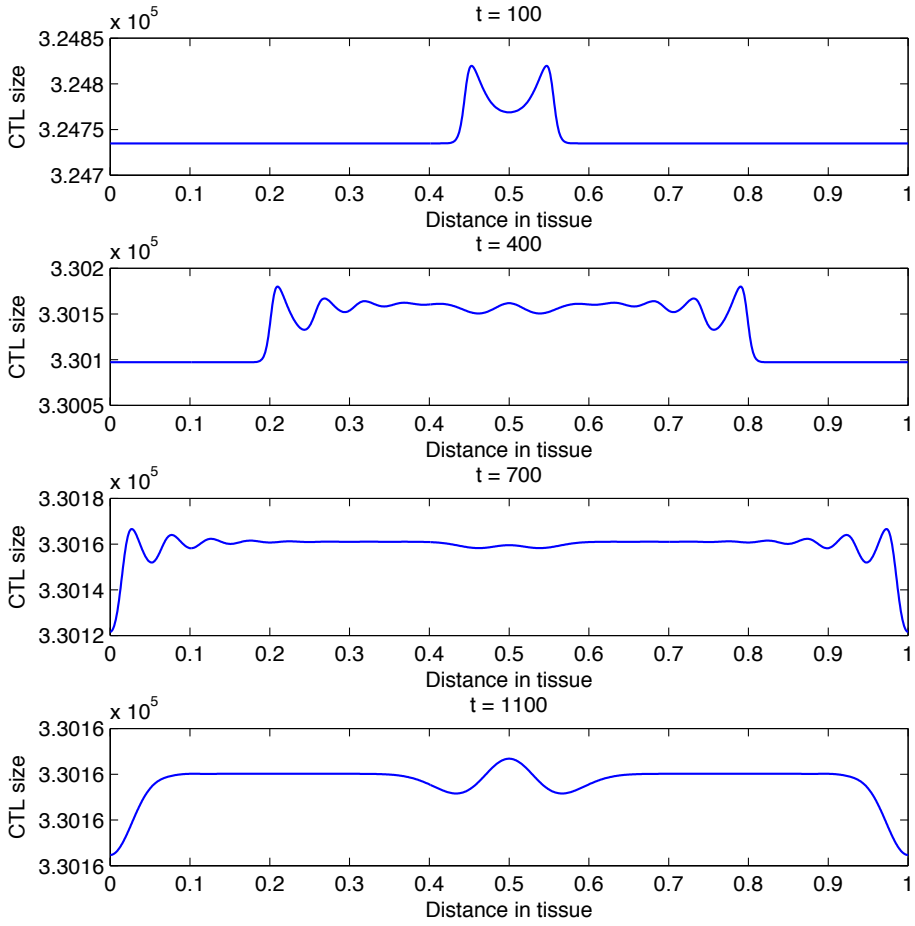

Figure 6.9: Plots showing the distribution of CTL cell density within the tissue at times corresponding to 100, 400, 700, and 1100 days respectively.

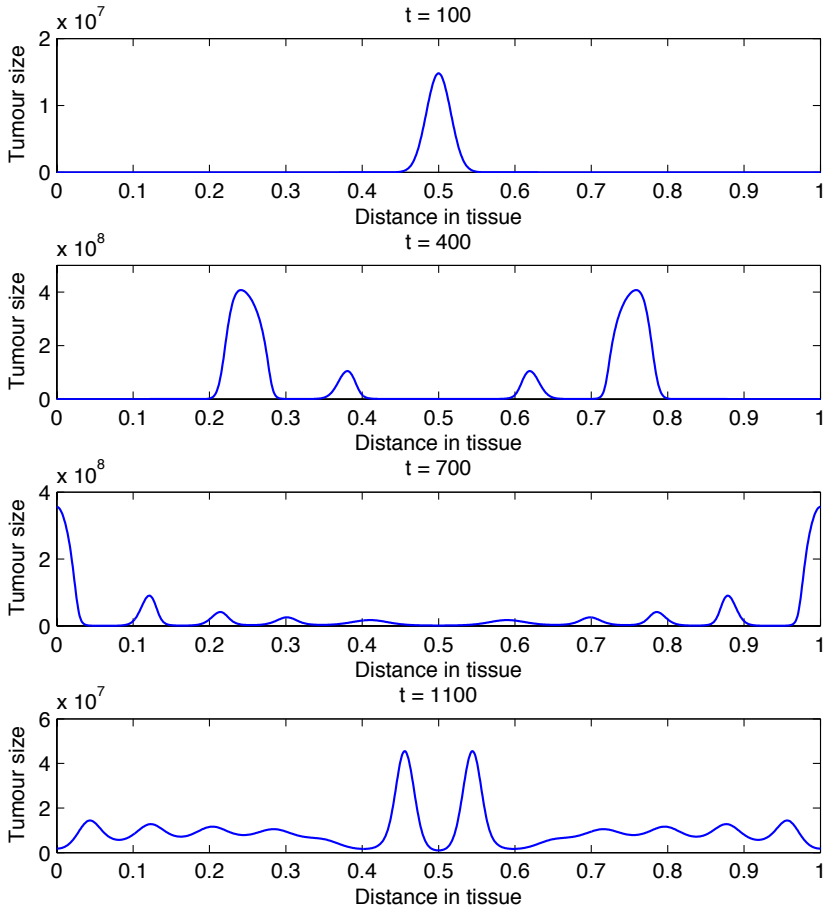

Figure 6.10: Plots showing the distribution of tumour cell density within the tissue at times corresponding to 100, 400, 700, and 1100 days respectively. With $q_0 = 3.456 \times 10^4$ and $\delta_4 = 4.12$.

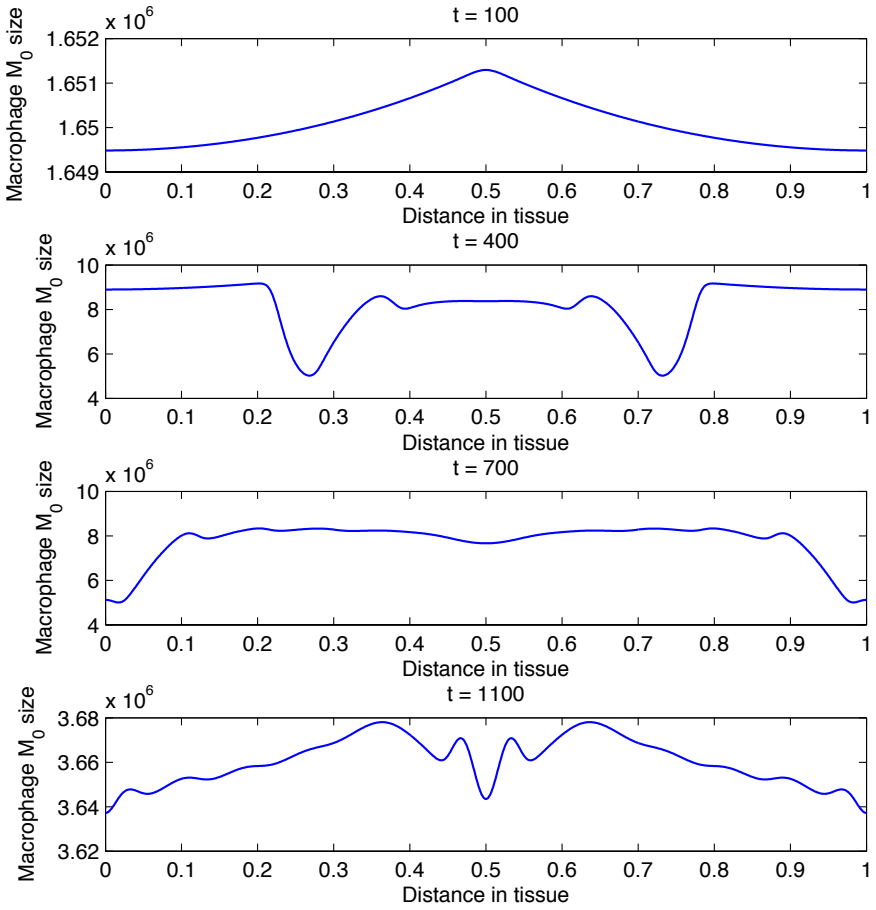

Figure 6.11: Plots showing the distribution of macrophage M_0 cell density within the tissue at times corresponding to 100, 400, 700, and 1100 days respectively. With $q_0 = 3.456 \times 10^4$ and $\delta_4 = 4.12$.

that small clusters of tumour with time 700 days and new clusters of tumour appear with time 1100 days.

Figures 6.11 and 6.12 show the spatial distribution of macrophage M_0 and M_1 cell density within the tissue at time 100, 400, 700, and 1100 days, with $q_0 = 3.456 \times 10^4$ and $\delta_4 = 4.12$. This results illustrate the effect of the limit cycle for the behaviour of the solution if we compare these results with pervious results in figures 6.5 and 6.6.

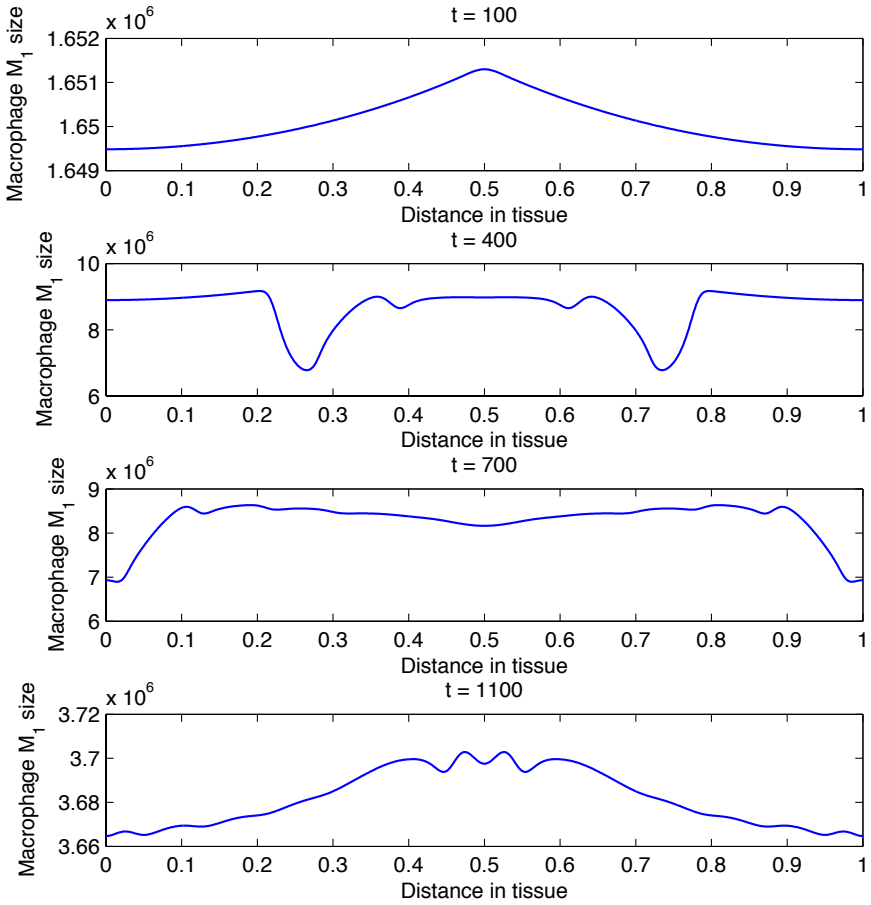

Figure 6.12: Plots showing the distribution of macrophage M_1 cell density within the tissue at times corresponding to 100, 400, 700, and 1100 days respectively. With $q_0 = 3.456 \times 10^4$ and $\delta_4 = 4.12$.

Figure 6.13 shows the spatial distribution of natural killer cell density within the tissue at time 100, 400, 700, and 1100 days, with $q_0 = 3.456 \times 10^4$ and $\delta_4 = 4.12$. The size of natural killer in this figure is smaller than the previous case (figure 6.7), and there is drop in the middle at 1100 days because there is cluster of tumour in the same position and at the same time.

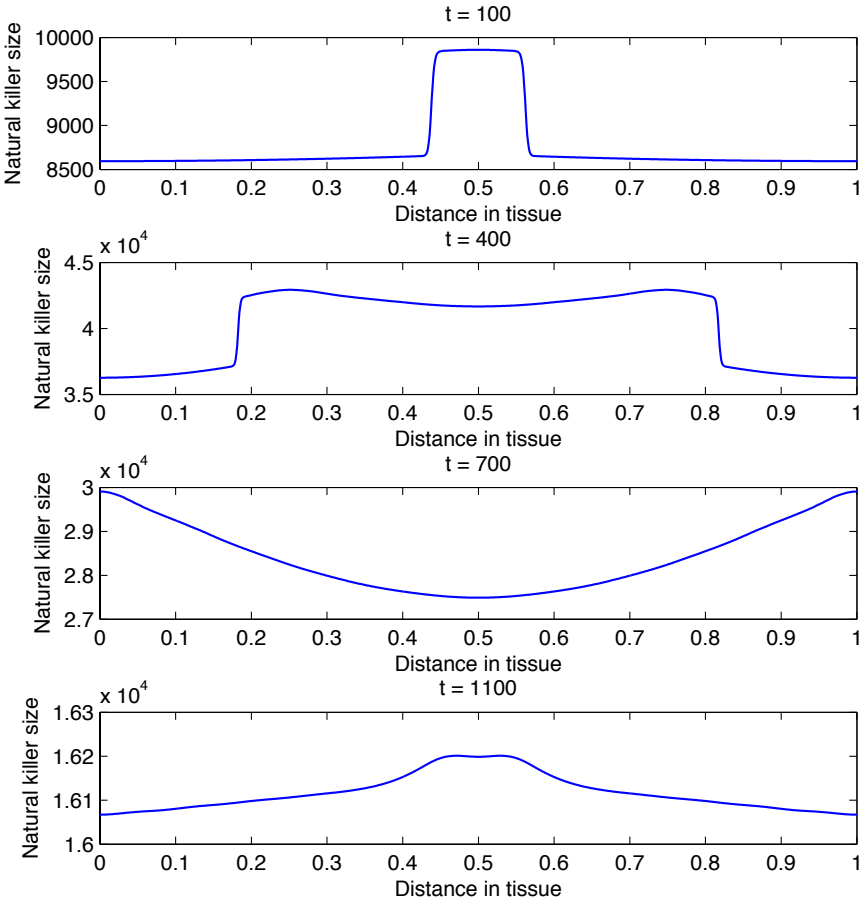

Figure 6.13: Plots showing the distribution of natural killer cell density within the tissue at times corresponding to 100, 400, 700, and 1100 days respectively. With $q_0 = 3.456 \times 10^4$ and $\delta_4 = 4.12$.

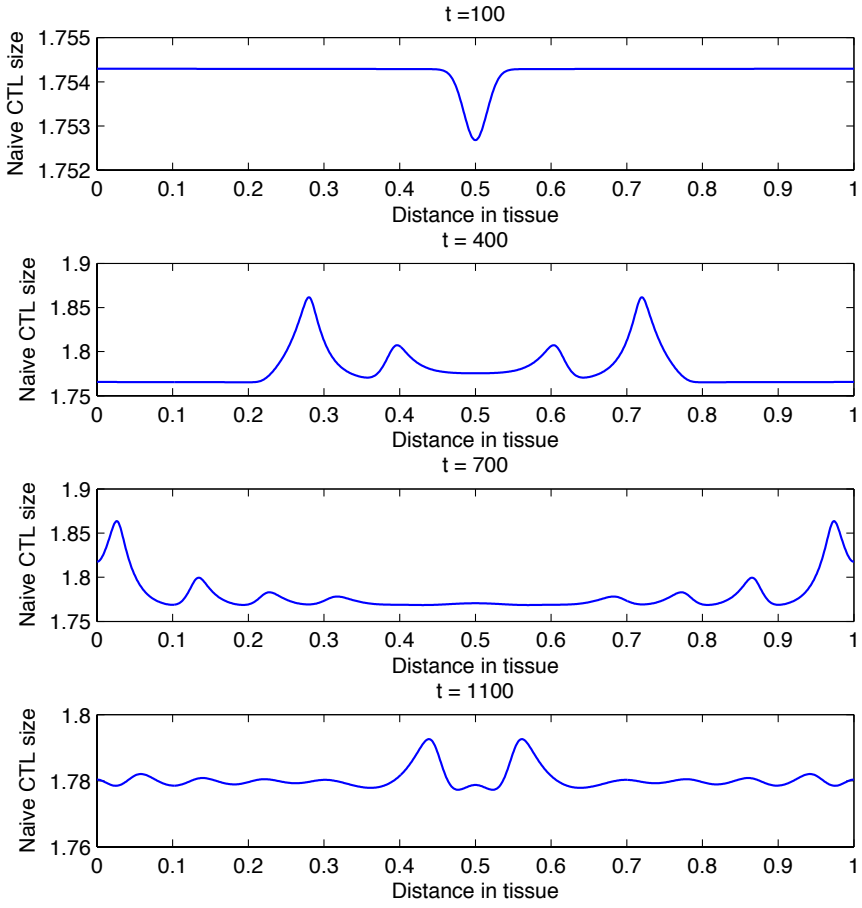

Figure 6.14: Plots showing the distribution of naive CTL cell density within the tissue at times corresponding to 100, 400, 700, and 1100 days respectively. With $q_0 = 3.456 \times 10^4$ and $\delta_4 = 4.12$.

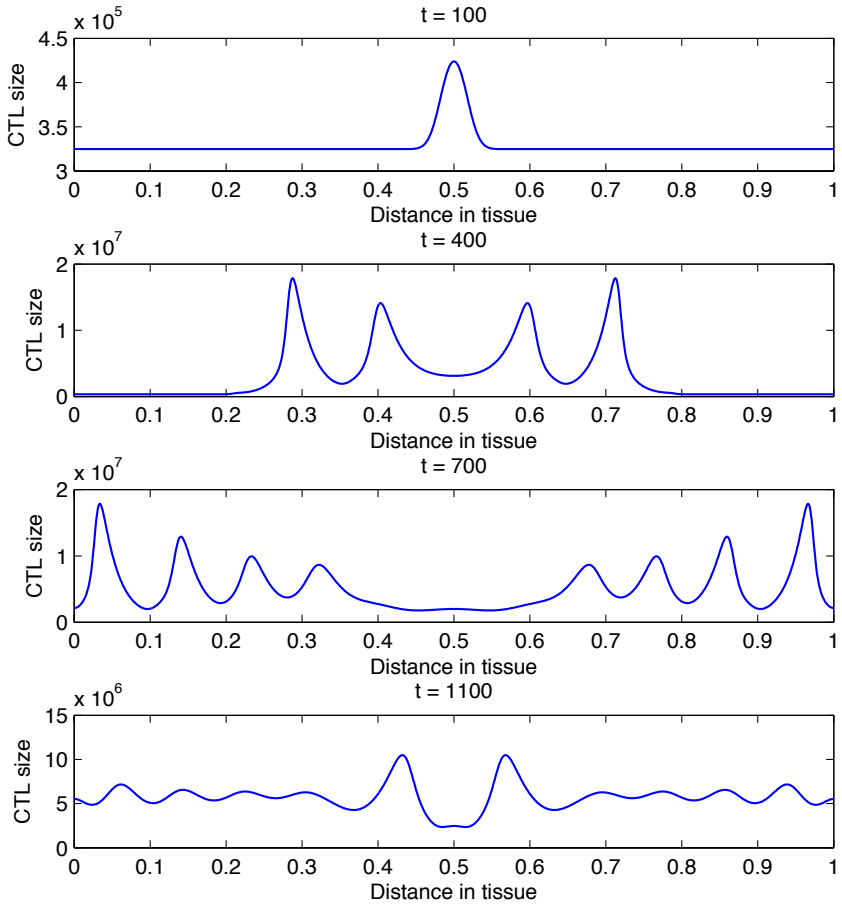

Figure 6.15: Plots showing the distribution of CTL cell density within the tissue at times corresponding to 100, 400, 700, and 1100 days respectively. With $q_0 = 3.456 \times 10^4$ and $\delta_4 = 4.12$.

Figures 6.14 and 6.15 show the spatial distribution of naive and active CTL cell density within the tissue at time 100, 400, 700, and 1100 days, with $q_0 = 3.456 \times 10^4$ and $\delta_4 = 4.12$. Again there are oscillations in the solutions and a drop in the middle of space at time 1100 days for the same reason as that for the natural killer cells. In addition, the size of CTLs is bigger than the previous case (figure 6.9).

6.6 Discussion and Conclusions

In this chapter we have presented a mathematical model of the interplay between a tumour and both the innate and the cellular part of the adaptive immune system. We have developed and extended the ideas originally formulated by Owen and Sherratt (1997), Matzavinos et al. (2004), de Pillis et al. (2005).

In this first set of simulations, we set all the spatial components of the model to zero and consider only the reaction kinetics, then we shows some spatio-temporal simulations which explain the interplay between tumours and macrophages, natural killer cells and cytotoxic T lymphocytes.

We observed that there is a slowly damped oscillation in the behaviour of the tumour, natural killer and CTL cells. Also we note that the solution converges to the second steady state where the tumour size is small (dormant state).

Also we found from the linear stability analysis for the model. there is two positive steady states, the first (free tumour steady state i.e. healthy steady state) is saddle and the second (small tumour steady state i.e. dormant state) is stable.

We changed the stability of this steady states by changed the parameters q_0 and δ_4, where got two saddle positive steady states and the tumour values of the second steady state become big, and the limit cycle still appears.

In the second set of simulations, we found the solution of model (6.16). Following

to the ODE simulations we considered two cases, depending on the parameter values such that the first case in like Table (6.1) and the second case is by change two parameters q_0 and δ_4. In the first case the solution tend to the positive steady state, and the solution of macrophage M_0 is similar to the solution of M_1. The behaviour of the solution of natural killer is similar to the behaviour of the solution for the tumour cells up to time 400 days, then the shape of the profile of the natural killer cells changed. The solution of the E_n reach the steady state value after a short time. The solution of CTL again have the same shape of tumour solution with different values.

In the second case we got the different behaviour of solution because there is limit cycle and oscillation in the shapes of solution and also the values of variables are changed.

Chapter 7

A Mathematical Model of Cancer Invasion of Tissue with an Immune Response

In this chapter we develop a mathematical model of cancer invasion of tissue in the presence of an immune response. We base our cancer invasion model on that of Chaplain and Lolas (2005). This model describes invasive solid tumour growth and how the interactions between cancer cells (C), urokinase plasminogen activator (uPA) (U), plasminogen activator inhibitor-1 (PAI-1) (P), plasmin (M) and the extracellular matrix (ECM) (V) may regulate tumour invasion and metastasis. We derive the new model by including the immune response of effector cells (E) to this model, and we explain the solution of this model for ODEs and PDEs (in 1 and 2 dimensional space). Furthermore, we discuss the stability of the steady states and compute the bifurcation analysis for the parameters.

7.1 Cancer Invasion Model

This model investigates the properties of the urokinase plasminogen activation system and its role in cancer invasion and metastasis.

Cancer cells :- Following Chaplain and Lolas (2005) the "word equation" for the cancer cell density is :

(Rate of change of cell density)
= (random motility) - (chemotaxis due to uPA) - (chemotaxis due to PAI-1)
-(haptotaxis due to V) + (proliferation)
+(extra proliferation due to uPA-cancer cells interactions)
thus the mathematical form of the above equation is:

$$\frac{\partial C}{\partial t} = \underbrace{D_C \frac{\partial^2 C}{\partial x^2}}_{random\ motion} - \frac{\partial}{\partial x}\Big(\underbrace{\chi_C C \frac{\partial U}{\partial x}}_{uPA-chemo} + \underbrace{\zeta_C C \frac{\partial P}{\partial x}}_{PAI-1-chemo} + \underbrace{\xi_C C \frac{\partial V}{\partial x}}_{V-hapto} \Big) + \underbrace{\phi_{13} C U}_{proliferation} + \underbrace{\mu_1 C (1 - \frac{C}{C_0})}_{proliferation},$$

where $D_C, \chi_C, \zeta_C, \xi_C, \mu_1, \phi_{13}$ are the random motility, uPA-mediated chemotaxis, PAI-1-mediated chemotaxis, V-mediated haptotaxis coefficients, the cancer cell proliferation rate and the cancer cell-surface receptors recycling rate respectively.

Extracellular matrix : The "word equation" for ECM is:

(Rate of change of ECM density)
= (degradation due to plasmin formation)+(proliferation)

+ (indirect growth of V due to PAI-1/uPA binding)

- (neutralization due to PAI-1 inhibition)

thus the mathematical equation is :

$$\frac{\partial V}{\partial t} = -\underbrace{\delta VM}_{degradation} + \underbrace{\phi_{21}UP}_{uPA/PAI-1} - \underbrace{\phi_{22}VP}_{PAI-1/V} + \underbrace{\mu_2 V(1-\frac{V}{V_0})}_{proliferation},$$

where $\delta, \mu_2, \phi_{21}, \phi_{22}$, respectively the degradation rate, proliferation rate, production rate of PAI-1/uPA binding and the counterbalancing of PAI-1 binding to V.

Urokinase plasminogen activator-uPA :- The "word equation" of uPA is :

(Rate of change of uPA concentration)

= (motion due to diffusion) + (production due to cancer cells)

- (removal due to PAI-1 inhibition)

- (removal due to binding to cancer cells)

thus the mathematical equation is :-

$$\frac{\partial U}{\partial t} = \underbrace{D_U \frac{\partial^2 U}{\partial x^2}}_{diffusion} - \underbrace{\phi_{31}PU}_{PAI-1/uPA} - \underbrace{\phi_{33}CU}_{uPA/cells} + \underbrace{\alpha_{31}C}_{production},$$

where $D_U, \alpha_{31}, \phi_{31}, and \phi_{33}$ are the uPA diffusion coefficient, rate of production by cancer cells, neutralization by PAI-1 inhibition and rate of binding to cell-surface receptors (uPAR)

Plasminogen activator inhibitor-1 :- The plasminogen activator inhibitor-1 (PAI-1)

conservation equation is similar to that of uPA considered above, and the "word equation" is :-

(Rate of change of PAI-1 concentration)
= (motion due to diffusion)
+ (production due to plasmin activator or cell secretion)
- (loss due to V binding)-(loss due to uPA binding)

thus the mathematical equation is :-

$$\frac{\partial P}{\partial t} = \underbrace{D_P \frac{\partial^2 P}{\partial x^2}}_{diffusion} - \underbrace{\phi_{41} PU}_{PAI-1/uPA} - \underbrace{\phi_{42} PV}_{PAI-1/V} + \underbrace{\alpha_{41} M}_{production},$$

where $D_P, \alpha_{41}, \phi_{41}, \phi_{42}$ respectively the diffusion coefficient, the rate of production as a result of plasmin formation, the neutralization rate by uPA binding and the neutralization rate by V binding.

Plasmin :- The "word equation" of plasmin is :-

(Rate of change of plasmin concentration)
= (motion due to diffusion) + (production by cells)
- (loss due to uPA/PAI-1 binding) + (production due to PAI-1/V binding),
thus the mathematical equation is :-

$$\frac{\partial M}{\partial t} = \underbrace{D_M \frac{\partial^2 M}{\partial x^2}}_{diffusion} - \underbrace{\phi_{51} PU}_{PAI-1/uPA} + \underbrace{\phi_{52} PV}_{PAI-1/V} + \underbrace{\phi_{53} UC}_{uPA/cells},$$

where D_M is the plasmin diffusion coefficient, ϕ_{53} is the rate of production due to

uPA/uPAR binding, ϕ_{52} is the rate of production due to PAI-1/V and ϕ_{51} is the inactivation rate due to uPA inhibition by PAI-1.

Hence the dimensional system of equation describing the interactions of cancer cells, ECM, uPA, PAI-1, and plasmin is :-

$$\begin{aligned}
\frac{\partial C}{\partial t} &= \underbrace{D_C \frac{\partial^2 C}{\partial x^2}}_{random\ motion} - \frac{\partial}{\partial x}\Big(\underbrace{\chi_C C \frac{\partial U}{\partial x}}_{uPA-chemo} + \underbrace{\zeta_C C \frac{\partial P}{\partial x}}_{PAI-1-chemo} + \underbrace{\xi_C C \frac{\partial V}{\partial x}}_{V-hapto}\Big) \\
&\quad + \underbrace{\phi_{13} CU}_{proliferation} + \underbrace{\mu_1 C\left(1 - \frac{C}{C_0}\right)}_{proliferation}, \\
\frac{\partial V}{\partial t} &= -\underbrace{\delta V M}_{degradation} + \underbrace{\phi_{21} UP}_{uPA/PAI-1} - \underbrace{\phi_{22} VP}_{PAI-1/V} + \underbrace{\mu_2 V\left(1 - \frac{V}{V_0}\right)}_{proliferation}, \\
\frac{\partial U}{\partial t} &= \underbrace{D_U \frac{\partial^2 U}{\partial x^2}}_{diffusion} - \underbrace{\phi_{31} PU}_{PAI-1/uPA} - \underbrace{\phi_{33} CU}_{uPA/cells} + \underbrace{\alpha_{31} C}_{production}, \\
\frac{\partial P}{\partial t} &= \underbrace{D_P \frac{\partial^2 P}{\partial x^2}}_{diffusion} - \underbrace{\phi_{41} PU}_{PAI-1/uPA} - \underbrace{\phi_{42} PV}_{PAI-1/V} + \underbrace{\alpha_{41} M}_{production}, \\
\frac{\partial M}{\partial t} &= \underbrace{D_M \frac{\partial^2 M}{\partial x^2}}_{diffusion} - \underbrace{\phi_{51} PU}_{PAI-1/uPA} + \underbrace{\phi_{52} PV}_{PAI-1/V} + \underbrace{\phi_{53} UC}_{uPA/cells}.
\end{aligned} \tag{7.1}$$

In this chapter, we use the modification of this original model given by Andasari et al. (2010) by removing the term ($\phi_{13}CU$) from the cancer equation, removing the ($-\phi_{51}PU$) term from the plasmin equation, and adding the degradation term ($-\phi_{54}M$) to plasmin equation.

7.2 The Mathematical Model of Cancer Invasion in the Presence of an Immune Response

In this section we include the immune response equation to the invasion model (7.1):

Effector cell :- The "word equation" for the effector cell density is:

(Rate of change of cell density)
= (random motility) + (proliferation) -(Immune response)
thus the mathematical form of above equation is:

$$\frac{\partial E}{\partial t} = \underbrace{D_E \frac{\partial^2 C}{\partial x^2}}_{random\ motion} + \underbrace{rE(1-\frac{E}{E_0})}_{proliferation} - \underbrace{\frac{dEC}{E+a}}_{Immune\ response},$$

where D_E, is the random motility.
Also we change the proliferation term of cancer equation to get the close orbit between cancer and effector solutions. This close orbit will give us oscillation for both cancer and effector solution with time, therefore we getting the continuos interactions between

cancer and effector cells. The Model (7.1) becomes:

$$
\begin{aligned}
\frac{\partial E}{\partial t} &= \underbrace{D_E \frac{\partial^2 E}{\partial x^2}}_{diffusion} + \underbrace{rE(1-\frac{E}{E_0})}_{proliferation} - \underbrace{\frac{dEC}{E+a}}_{Immune\ response}, \\
\frac{\partial C}{\partial t} &= \underbrace{D_C \frac{\partial^2 T}{\partial x^2}}_{diffusion} - \frac{\partial}{\partial x}(\underbrace{\chi_C C \frac{\partial U}{\partial x}}_{uPA-chemo} + \underbrace{\zeta_C C \frac{\partial P}{\partial x}}_{PAI-1-chemo} + \underbrace{\xi_C C \frac{\partial V}{\partial x}}_{V-hapto}) \\
&\quad + \underbrace{bC(1-\frac{hC}{E+a})}_{proliferation}, \\
\frac{\partial V}{\partial t} &= - \underbrace{\delta V M}_{degradation} + \underbrace{\phi_{31} U P}_{uPA/PAI-1} - \underbrace{\phi_{32} V P}_{PAI-1/V} + \underbrace{\mu_2 V(1-\frac{V}{V_0})}_{proliferation}, \qquad (7.2) \\
\frac{\partial U}{\partial t} &= \underbrace{D_U \frac{\partial^2 U}{\partial x^2}}_{diffusion} - \underbrace{\phi_{41} P U}_{PAI-1/uPA} - \underbrace{\phi_{43} T U}_{uPA/cells} + \underbrace{\alpha_{41} T}_{production}, \\
\frac{\partial P}{\partial t} &= \underbrace{D_P \frac{\partial^2 P}{\partial x^2}}_{diffusion} - \underbrace{\phi_{51} P U}_{PAI-1/uPA} - \underbrace{\phi_{52} P V}_{PAI-1/V} + \underbrace{\alpha_{51} M}_{production}, \\
\frac{\partial M}{\partial t} &= \underbrace{D_M \frac{\partial^2 M}{\partial x^2}}_{diffusion} + \underbrace{\phi_{62} P V}_{PAI-1/V} + \underbrace{\phi_{63} U T}_{uPA/cells} - \underbrace{\phi_{64} M}_{decay}.
\end{aligned}
$$

Following Chaplain and Lolas (2005), we consider a spatial domain $\Omega = [0, 2L]$, where L=0.1 cm, and time with $\tau = \frac{L^2}{D}$ (where D represents a chemical diffusion coefficient $\sim 10^{-6} cm^2 s^{-1}$).

The dependent variables and key parameters are rescaled thus:

$$
\tilde{t} = \frac{t}{\tau}, \qquad \tilde{x} = \frac{x}{L}, \qquad \tilde{E} = \frac{E}{E_0} \qquad \tilde{C} = \frac{C}{C_0}, \qquad \tilde{V} = \frac{V}{V_0}, \qquad \tilde{U} = \frac{U}{U_0}, \qquad \tilde{P} = \frac{P}{P_0},
$$

$$
\tilde{M} = \frac{M}{M_0} \qquad \tilde{D_E} = \frac{D_E}{D}, \qquad \tilde{D_C} = \frac{D_C}{D}, \qquad \tilde{D_U} = \frac{D_U}{D}, \qquad \tilde{D_P} = \frac{D_P}{D}, \qquad \tilde{D_M} = \frac{D_M}{D},
$$

$$
\tilde{\chi_C} = \chi_C \frac{U_0}{D}, \qquad \tilde{\xi_C} = \xi_C \frac{V_0}{D}, \qquad \tilde{\zeta_C} = \zeta_C \frac{P_0}{D}, \qquad \tilde{b} = b\tau, \qquad \tilde{\mu_2} = \mu_2 \tau, \qquad \tilde{d} = \frac{dC_0\tau}{E_0}
$$

$$\tilde{r} = r\tau \qquad \tilde{a} = \frac{a}{E_0} \qquad \tilde{h} = \frac{hC_0}{E_0} \qquad \tilde{\delta} = \delta\frac{M_0\tau}{V_0}, \qquad \tilde{\alpha_{31}} = \alpha_{31}\frac{C_0}{U_0}\tau, \qquad \tilde{\alpha_{41}} = \alpha_{41}\frac{M_0}{P_0}\tau,$$

$$\tilde{\phi_{21}} = \phi_{21}\frac{U_0P_0}{V_0}\tau, \qquad \tilde{\phi_{22}} = \phi_{22}P_0\tau, \qquad \tilde{\phi_{31}} = \phi_{31}P_0\tau. \qquad \tilde{\phi_{33}} = \phi_{33}C_0\tau$$

$$\tilde{\phi_{41}} = \phi_{41}U_0\tau, \qquad \tilde{\phi_{42}} = \phi_{42}V_0\tau, \qquad \tilde{\phi_{51}} = \phi_{51}\frac{U_0P_0}{M_0}\tau, \qquad \tilde{\phi_{53}} = \phi_{53}\frac{U_0C_0}{M_0}\tau$$

Dropping the tildes for notational convenience, we obtain the non-dimensional system of equations:

$$\begin{aligned}
\frac{\partial E}{\partial t} &= D_E\frac{\partial^2 E}{\partial x^2} + rE(1-E) - \frac{dEC}{E+a}, \\
\frac{\partial C}{\partial t} &= D_C\frac{\partial^2 T}{\partial x^2} - \frac{\partial}{\partial x}(\chi_C C\frac{\partial U}{\partial x} + \zeta_C C\frac{\partial P}{\partial x} + \xi_C C\frac{\partial V}{\partial x}) + bC(1-\frac{hC}{E+a}), \\
\frac{\partial V}{\partial t} &= -\delta VM + \phi_{31}UP - \phi_{32}VP + \mu_2 V(1-V), \\
\frac{\partial U}{\partial t} &= D_U\frac{\partial^2 U}{\partial x^2} - \phi_{41}PU - \phi_{43}CU + \alpha_{41}C, \\
\frac{\partial P}{\partial t} &= D_P\frac{\partial^2 P}{\partial x^2} - \phi_{51}PU - \phi_{52}PV + \alpha_{51}M, \\
\frac{\partial M}{\partial t} &= D_M\frac{\partial^2 M}{\partial x^2} + \phi_{62}PV + \phi_{63}UC - \phi_{64}M.
\end{aligned} \tag{7.3}$$

where the non-dimensional values of parameter as in Table (7.1).

Table 7.1: List of parameter values

Parameter	Description	Estimate Value
D_E	Random motility of effector cell	$3.5 \times 10^{-}4$
D_T	Random motility of tumour cell	$3.5 \times 10^{-}4$
D_U	Diffusion coefficient of uPA	$2.5 \times 10^{-}3$
D_P	Diffusion coefficient of PAI-1	$3.5 \times 10^{-}3$
D_M	Diffusion coefficient of plasmin	$4.91 \times 10^{-}3$
χ_T	uPA-mediated chemotaxis coefficient	$3.05 \times 10^{-}2$
ξ_T	PAI-1-mediated chemotaxis coefficient	$2.85 \times 10^{-}2$
ζ_T	V-mediated haptotaxis coefficient	$3.75 \times 10^{-}2$
δ	Degradation rate of V by plasmin	8.15
ϕ_{31}	Production rate of PAI-1/uPA binding	0.75
ϕ_{32}	Counterbalancing of PAI-1 binding V	0.55
μ	Proliferation rate of V	0.85
ϕ_{41}	Neutralization rate by PAI-1 inhibition binding	0.75
ϕ_{43}	rate of binding to cell-surface receptors(uPAR)	0.3
α_{41}	Production rate of uPA by cancer cells	0.215
ϕ_{51}	Neutralization rate by uPA binding	0.75
ϕ_{52}	Neutralization rate by V binding	0.55
α_{51}	Production rate of PAI-1 by plasmin	0.5
ϕ_{62}	Production rate due to PAI-1/V	0.11
ϕ_{63}	Production rate due to uPA/uPAR binding	0.75
ϕ_{64}	Decay rate of plasmin	0.5
h	Constant	1.4
a	Constant	0.1
b	Proliferation rate of tumour	0.15
d	Constant	0.95
r	Proliferation rate of effector cell	0.8

For boundary conditions, we impose zero-flux boundary conditions for all the variables of the model at x = 0 and x = 2.

The initial conditions are given by:

$$E(x,0) = \begin{cases} 0, & \text{if } 0 \le x \le l, \\ 1 - \exp(-1000(x-l)^2), & \text{if } l < x \le 2, \end{cases}$$

$$T(x,0) = \begin{cases} 1 - \exp(-1000(x-l)^2), & \text{if } 0 \le x \le l, \\ 0, & \text{if } l < x \le 2, \end{cases}$$

$$\begin{aligned} V(x,0) &= 1 - \frac{1}{2}\exp(\frac{-x^2}{\varepsilon}), && x \in [0,2] \quad \textit{and} \quad \varepsilon > 0 \\ U(x,0) &= \frac{1}{2}\exp(\frac{-x^2}{\varepsilon}), && x \in [0,2] \quad \textit{and} \quad \varepsilon > 0 \\ P(x,0) &= \frac{1}{20}\exp(\frac{-x^2}{\varepsilon}), && x \in [0,2] \quad \textit{and} \quad \varepsilon > 0 \\ M(x,0) &= 0, && x \in [0,2], \end{aligned}$$

where $\varepsilon = 0.01, \quad l = 0.2$.

7.3 Computational Simulation Results

7.3.1 Spatially Homogeneous Simulation

In this section, we set all spatial components of the model to zero and consider only the reaction kinetics in order to compare between the behaviour of our model and the model of Chaplain and Lolas (2005) with time 1000 ($\sim$3000 hours), i.e. t=1 ($\sim$3 hours). Figure 7.1 shows the dynamics of effector, tumour, ECM, uPA, PAI-1, and plasmin over time. We observe that there is a regular oscillation for all species. This occurs because there is a limit cycle between the effector cells and the tumour cells (see section 7.4). Figure 7.2 shows the behaviour of the solutions of the model of Chaplain and Lolas (2005). We observe the solution going to a stable steady state.

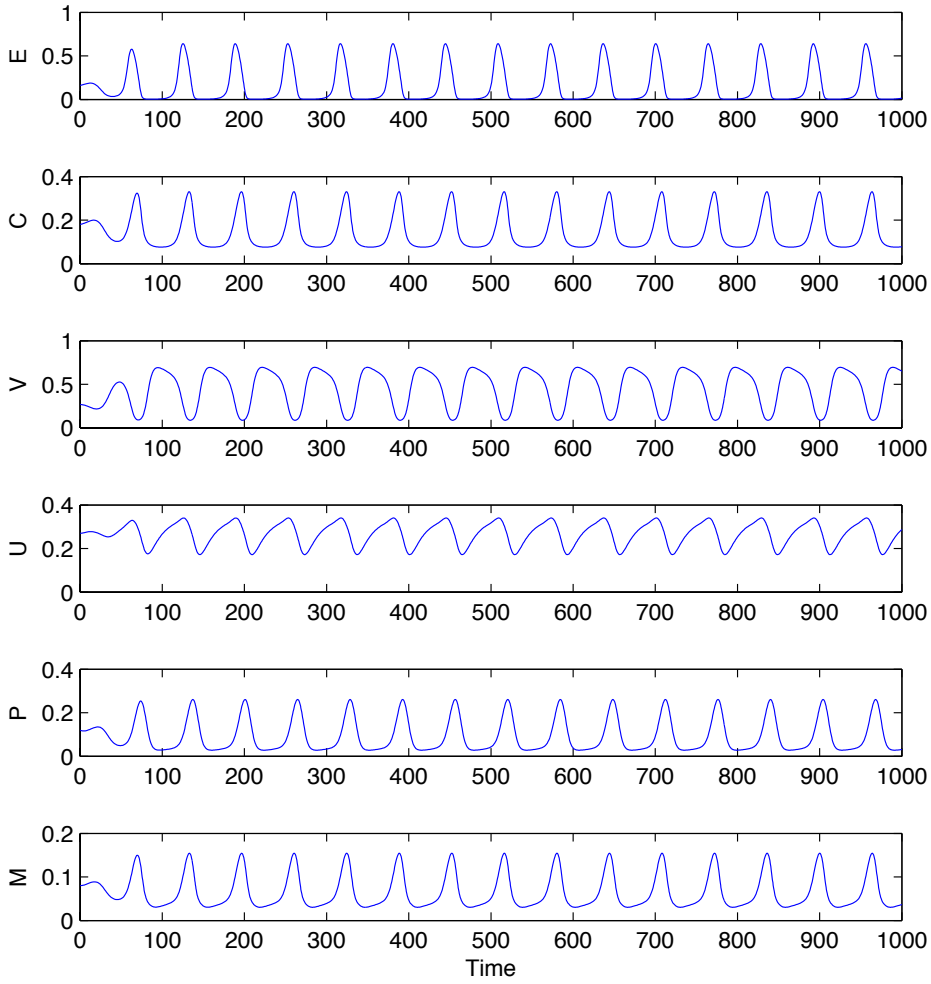

Figure 7.1: Plots showing the growth of the tumour, effector, ECM, uPA, PAI-1, and plasmin over time in the case where the spatial components of the model (i.e. all diffusion, taxis terms) have been set to zero. The initial conditions were taken near the non-trivial steady state.

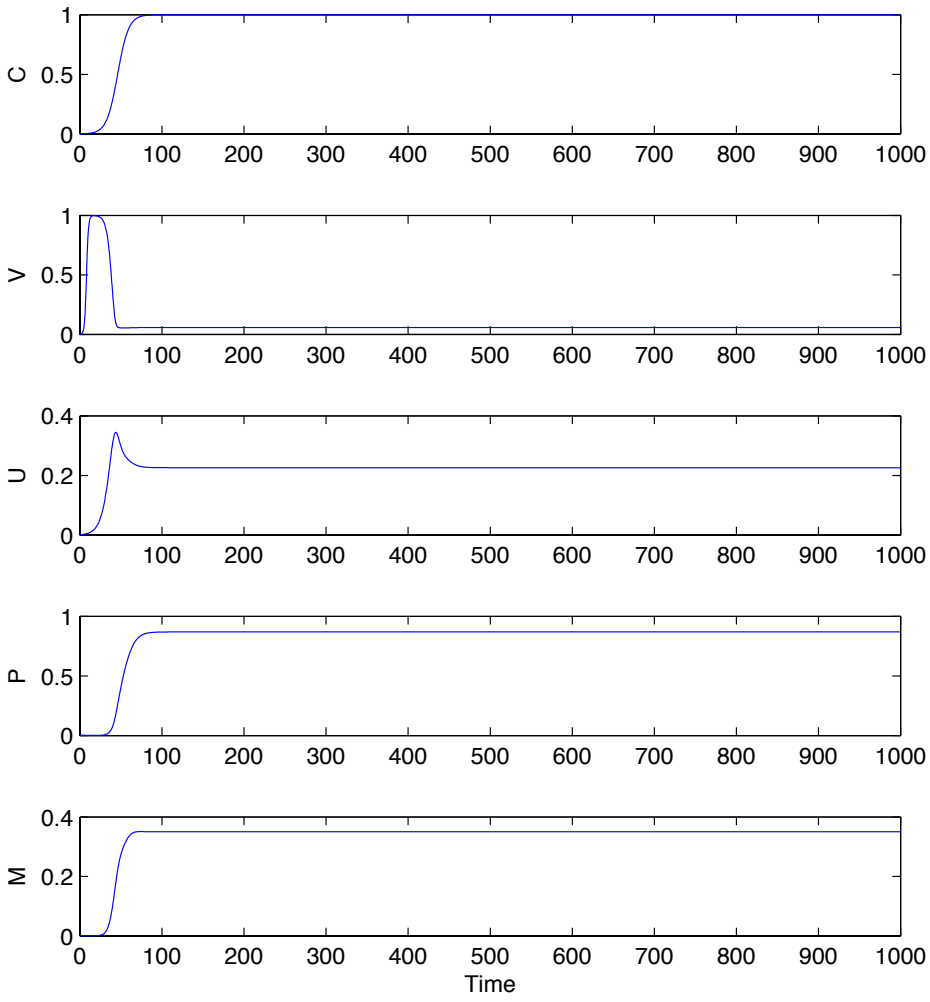

Figure 7.2: Plots showing the growth of the tumour, ECM, uPA, PAI-1, and plasmin from Chaplain and Lolas (2005) over time in the case where the spatial components of the model (i.e. all diffusion, taxis terms) have been set to zero. The initial conditions were taken near the trivial steady state.

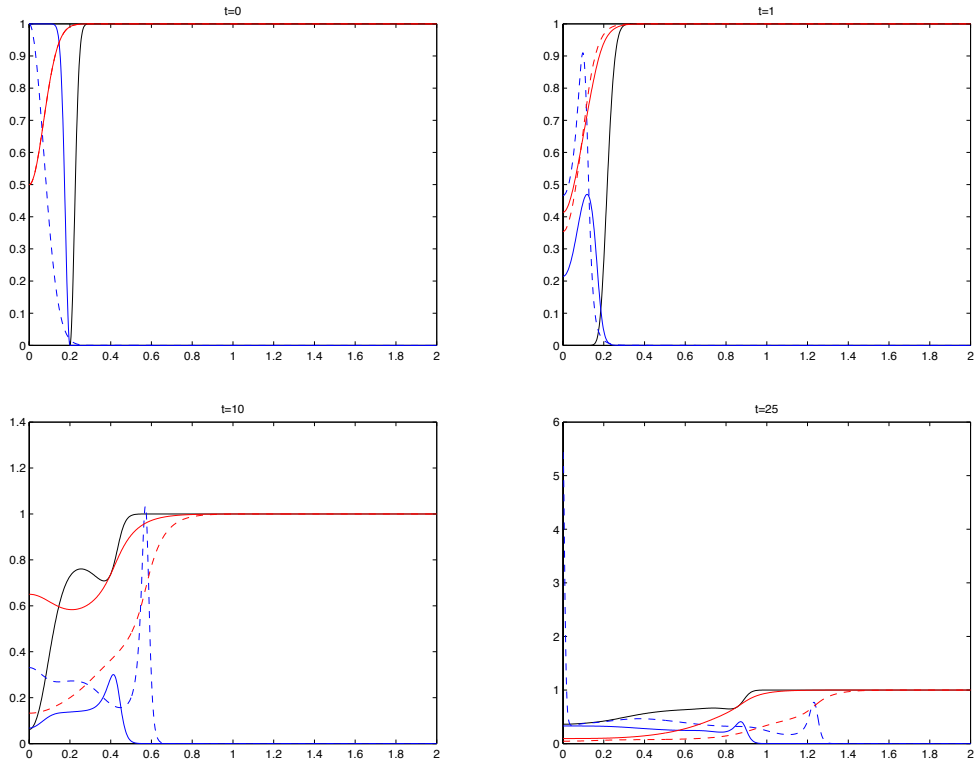

Figure 7.3: Plots showing the distribution of tumour cell density, effector cell density, and ECM within the tissue at times corresponding to 0, 1, 10, and 25 respectively. The red lines represent the ECM, the blue lines represent the tumour, and the black lines represent the effector cell. The dash line represents the results of Chaplain and Lolas (2005), the solid line represents the model (7.1).

7.3.2 Spatiotemporal Simulations

In this section, we present the computational results of model (7.3). Figure 7.3 shows the spatial distribution of effector cell, tumour cell, and ECM from t=0-25 with comparing between the results of model (7.3) and the model of Chaplain and Lolas (2005). We note that the tumour of our model is smaller than the tumour of Chaplain and Lolas model, in additional to the degrading of ECM of our model is less than the degrading of Chaplain and Lolas Model. This means that the existence of the effector cells bounded the growth of the tumour cells, and therefore reduces the degradation of ECM.

Figure 7.4 also shows that the effect of the effector cells is to reduce the size of the

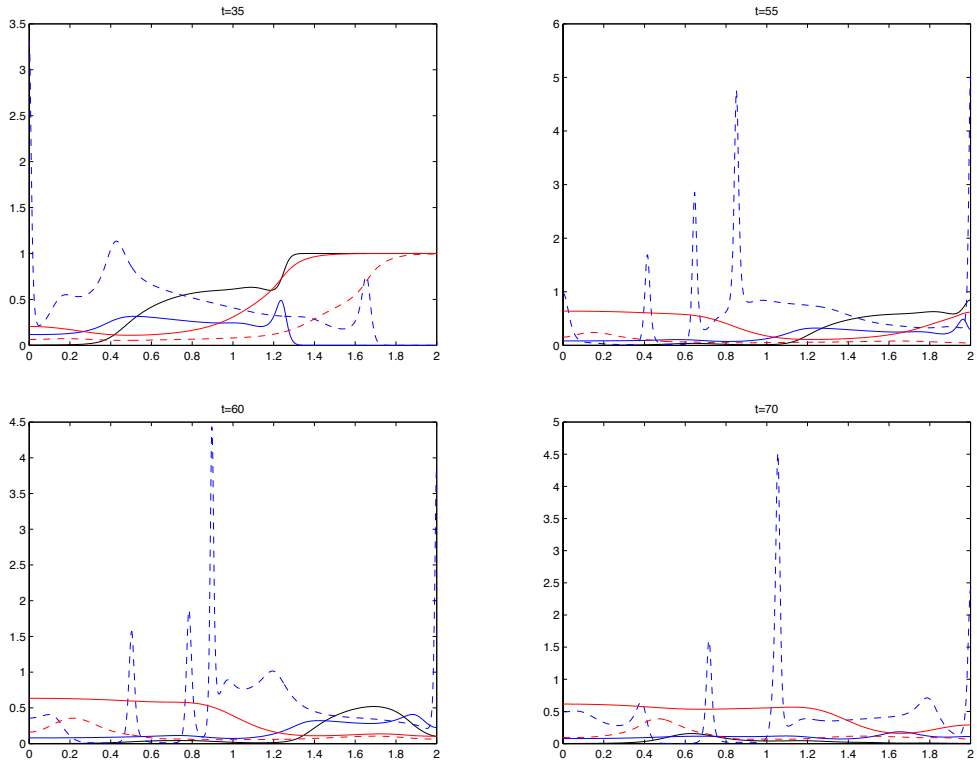

Figure 7.4: Plots showing the distribution of tumour cell density, effector cell density, and ECM within the tissue at times corresponding to 35, 55, 60, and 70 respectively. The red lines represent the ECM, the blue lines represent the tumour, and the black lines represent the effector cell, the dash line represents the results of Chaplain and Lolas (2005), the solid line represents the model (7.1).

tumour compared to the invasion model of Chaplain and Lolas. We note that the ECM is still degraded but at a lower rate than the Chaplain and Lolas model.

Figure 7.5 shows the tumour cluster of Chaplain and Lolas model is increased and greater than the tumour clusters of our model.

In figure 7.6 more clusters are appeared in Chaplain and Lolas model and bigger effector cell and ECM of our model. And the same behaviour in figure 7.7 and 7.8.

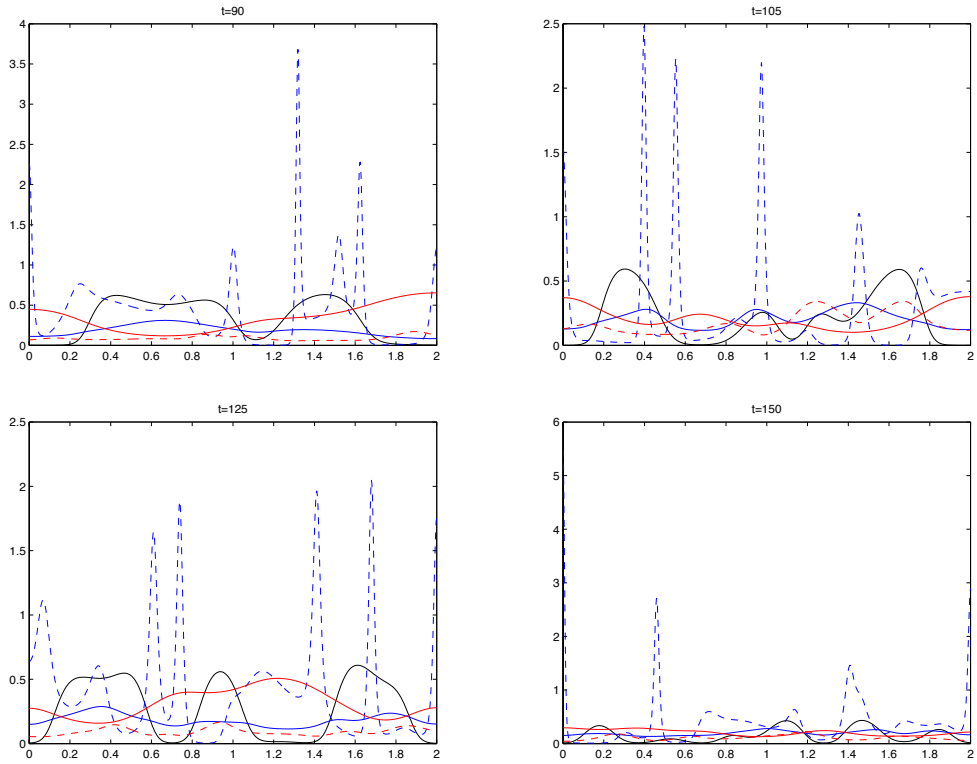

Figure 7.5: Plots showing the distribution of tumour cell density, effector cell density, and ECM within the tissue at times corresponding to 90, 105, 125, and 150 respectively. The red lines represent the ECM, the blue lines represent the tumour, and the black lines represent the effector cell, the dash line represents the results of Chaplain and Lolas (2005), the solid line represents the model (7.1).

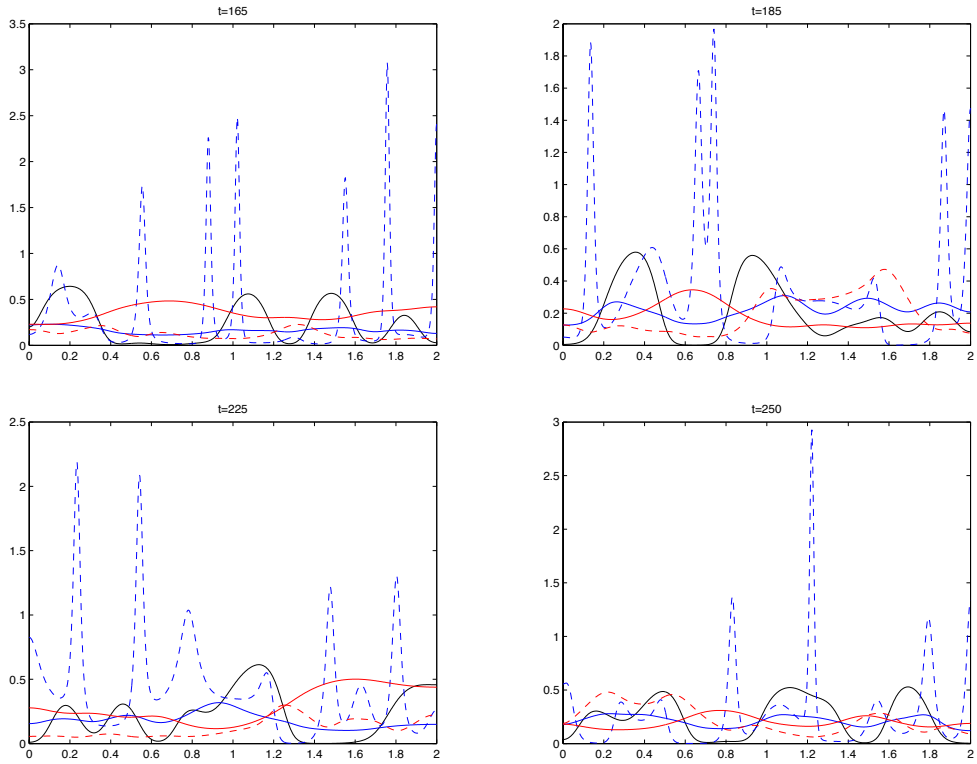

Figure 7.6: Plots showing the distribution of tumour cell density, effector cell density, and ECM within the tissue at times corresponding to 165, 185, 225, and 250 respectively. The red lines represent the ECM, the blue lines represent the tumour, and the black lines represent the effector cell, the dash line represents the results of Chaplain and Lolas (2005), the solid line represents the model (7.1).

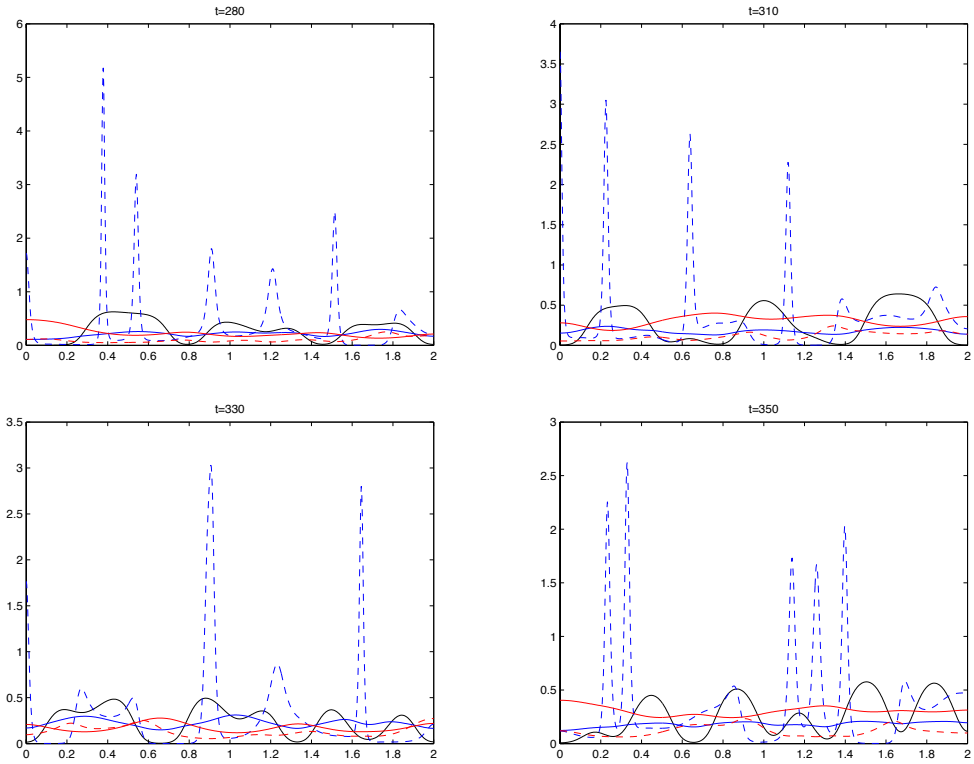

Figure 7.7: Plots showing the distribution of tumour cell density, effector cell density, and ECM within the tissue at times corresponding to 280, 310, 330, and 350 respectively. The red lines represent the ECM, the blue lines represent the tumour, and the black lines represent the effector cell, the dash line represents the results of Chaplain and Lolas (2005), the solid line represents the model (7.1).

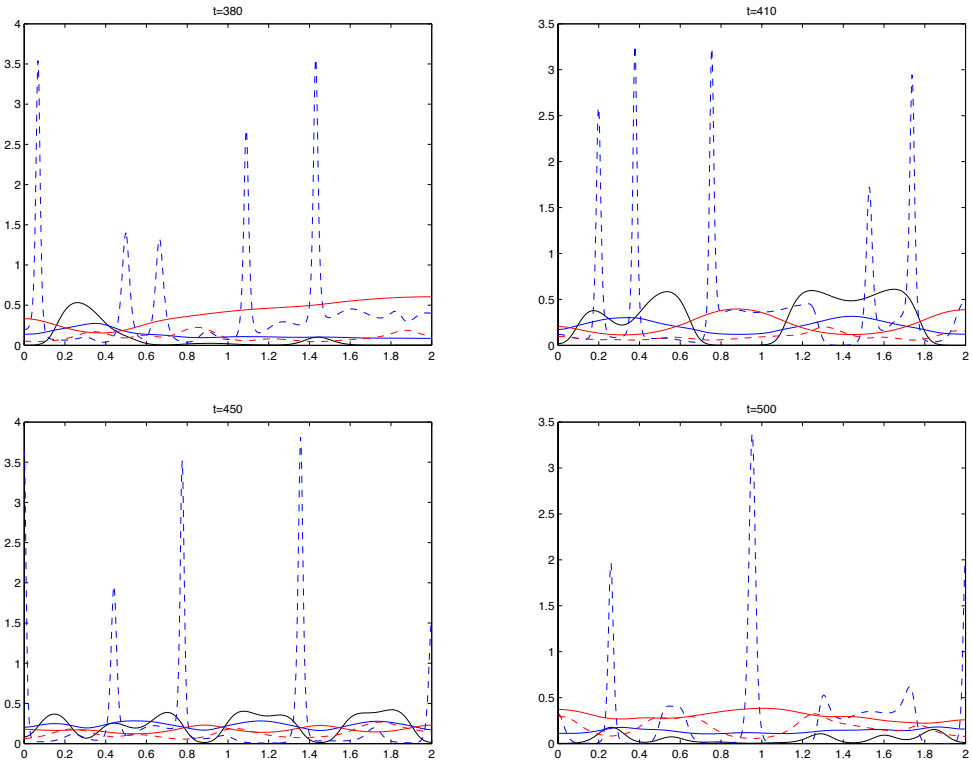

Figure 7.8: Plots showing the distribution of tumour cell density, effector cell density, and ECM within the tissue at times corresponding to 380, 410, 450, and 500 respectively. The red lines represent the ECM, the blue lines represent the tumour, and the black lines represent the effector cell, the dash line represents the results of Chaplain and Lolas (2005), the solid line represents the model (7.1).

7.4 Linear Stability Analysis

The system (7.3) has trivial (all species are zero), semi-trivial (free tumour steady state i.e. healthy steady state), and non-trivial steady states. All these steady states are saddle, the semi steady states are 'healthy', i.e., only ECM or only effector sell, and we don't have full malignant steady state. The non-trivial steady state has complex eigenvalues, four with negative real part, and two with positive real part. We consider the ODE equations of tumour and effector cell

$$\begin{aligned} \frac{\partial E}{\partial t} &= rE(1-E) - \frac{dEC}{E+a}, \\ \frac{\partial C}{\partial t} &= bC(1 - \frac{hC}{E+a}). \end{aligned} \tag{7.4}$$

The results of the numerical computations in this direction are present in figure 7.9, we note there is limit cycle, and in figure 7.10 we note the oscillation behaviour of the numerical solution of tumour and effector over time.

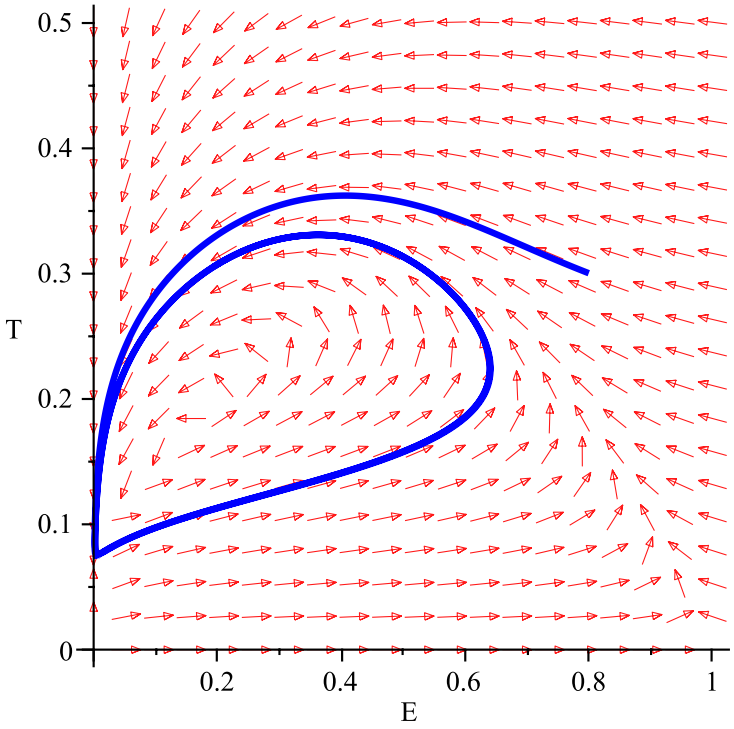

Figure 7.9: Plot showing the orbit of the ODE system (7.4) with initial condition near the non-trivial steady state, converging to the limit cycle.

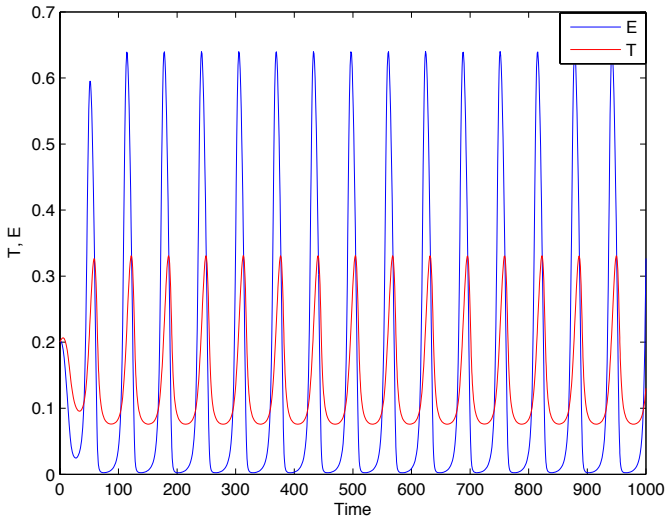

Figure 7.10: Plots showing the numerical solution of model (7.4) over time. The blue line is effector cells and red line is tumour cells. There are regular oscillations in both the tumour cell and effector cell numbers over time.

7.5 Bifurcation Analysis

In this section, we show a numerical bifurcation of system (7.4) with respect to parameters h and a. The bifurcation diagrams presented here have been generated by the numerical continuation routine AUTO that is implemented within the XPP package (Ermentrout, 2002). AUTO provides implementation of numerical algorithms for tracking Hopf bifurcation and therefore, establishing the existence of limit cycle.

Figures 7.11, 7.12, and 7.13, shows the bifurcation diagram of tumour density versus the parameters h and a, and effector density versus the parameter a. Figure 7.11shows the Hopf bifurcation was detected at $h = 1.766$. The solid dote represent the maximum and minimum values of the periodic solutions that emerge when h lies in a particular interval. Figure 7.12 and 7.13, shows the Hopf bifurcation was detected at $a = 0.2277$.

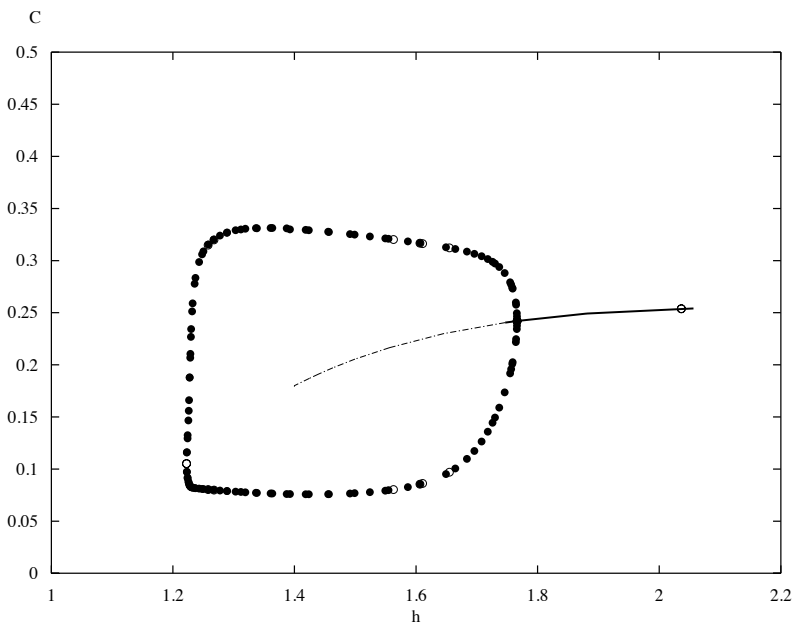

Figure 7.11: Bifurcation diagram of a tumour density versus parameter h.

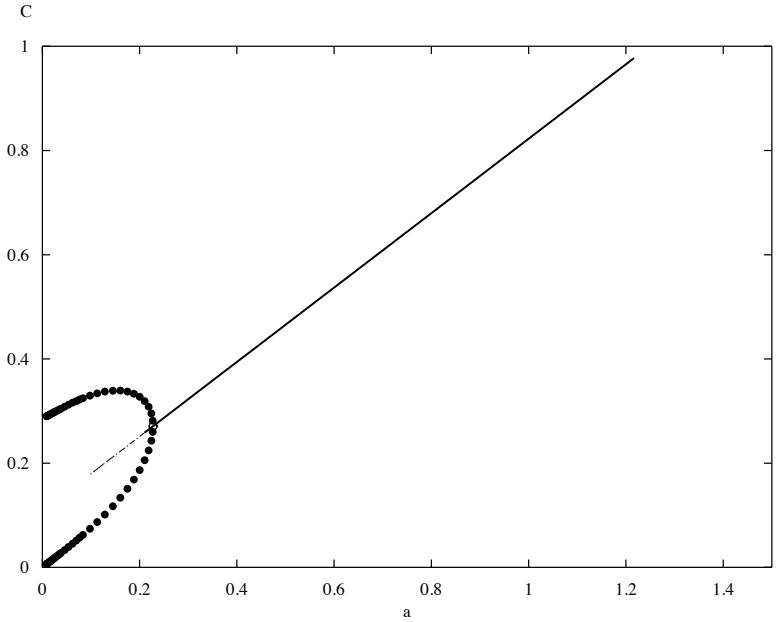

Figure 7.12: Bifurcation diagram of a tumour density versus parameter a.

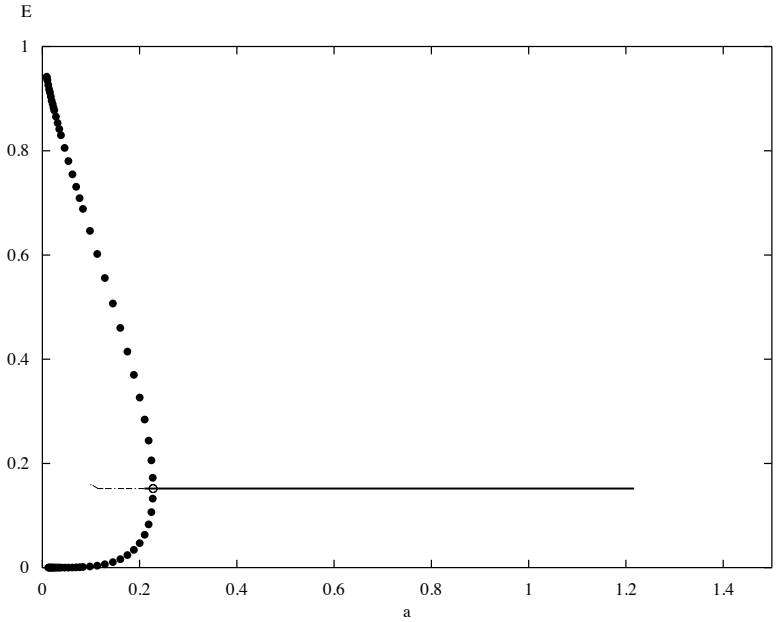

Figure 7.13: Bifurcation diagram of effector density versus parameter a.

7.6 2D Simulations

In this section, we present computational simulation results of model (7.3) on a two-dimensional square domain, with homogeneous and heterogeneous ECM. We consider the rectangular domain: $\Omega = (0,2)^2$, with zero-flux boundary conditions. The simulations were performed using COMSOL Multiphysics which uses a finite element approach to solve PDEs.

7.6.1 2D simulations with homogeneous ECM

We assume the initial condition for effector cell, tumour cell, ECM, uPA, PAI-1, and plasmin given as:

$$\begin{aligned} E(x,y,0) &= 1-exp(-100((x-1)^2-(y-1)^2)), \\ C(x,y,0) &= exp(-100((x-1)^2-(y-1)^2)), \\ V(x,y,0) &= 1-\frac{1}{2}exp(-100((x-1)^2-(y-1)^2)), \\ U(x,y,0) &= \frac{1}{2}exp(-100((x-1)^2-(y-1)^2)), \\ P(x,y,0) &= \frac{1}{20}exp(-100((x-1)^2-(y-1)^2)), \\ M(x,y,0) &= 0. \end{aligned} \tag{7.5}$$

Following the 1-dimensional results, figures 7.14, 7.15, and 7.16 shows respectively, the spatial distribution of effector cells, tumour cells, and ECM, with time 100, 200, 300, and 400 respectively.

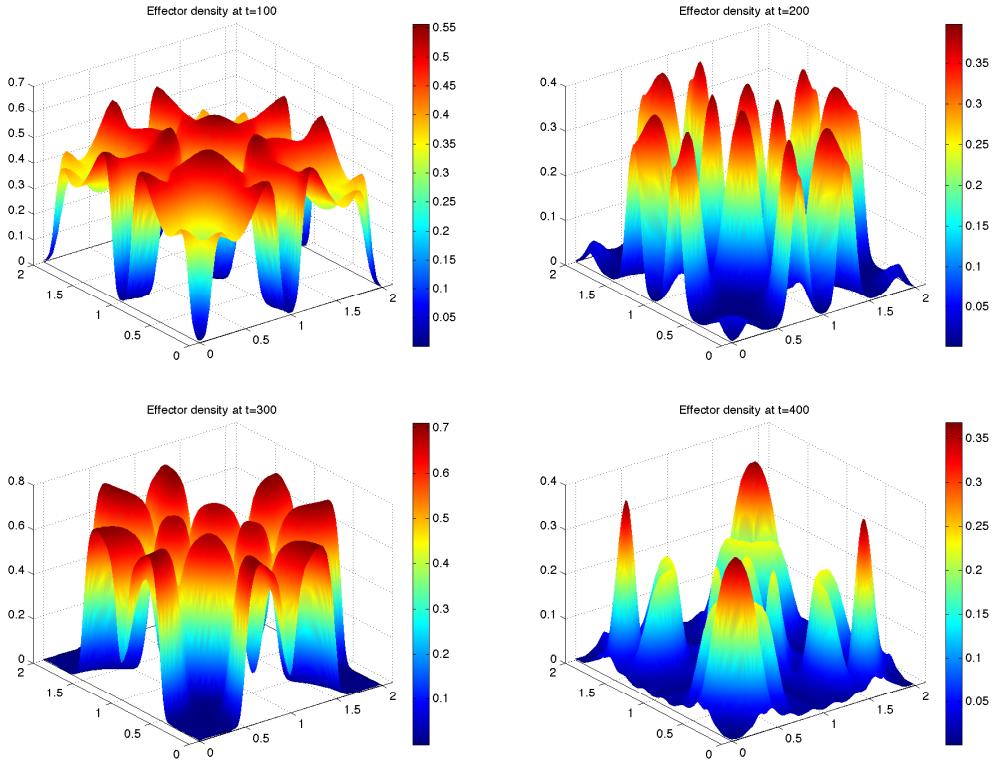

Figure 7.14: Plots showing the spatial distribution of effector cell density within the tissue in a 2-dimensional spatial domain at time corresponding to 100, 200, 300, and 400, respectively (homogeneous ECM).

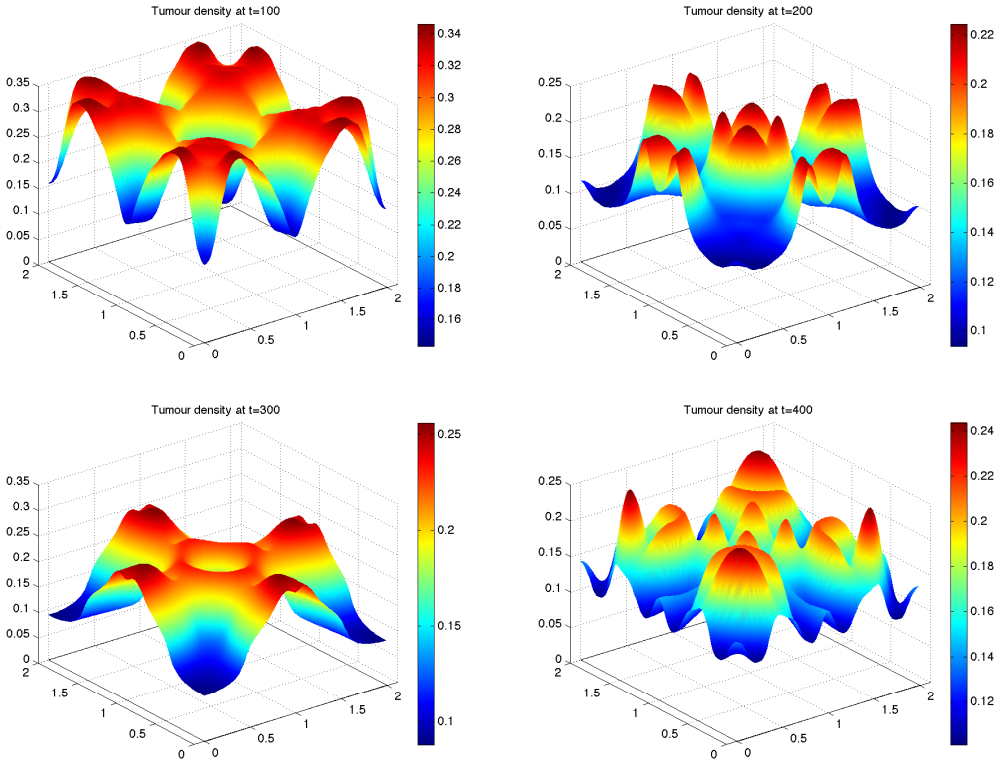

Figure 7.15: Plots showing the spatial distribution of tumour cell density within the tissue in a 2-dimensional spatial domain at time corresponding to 100, 200, 300, and 400, respectively (homogeneous ECM).

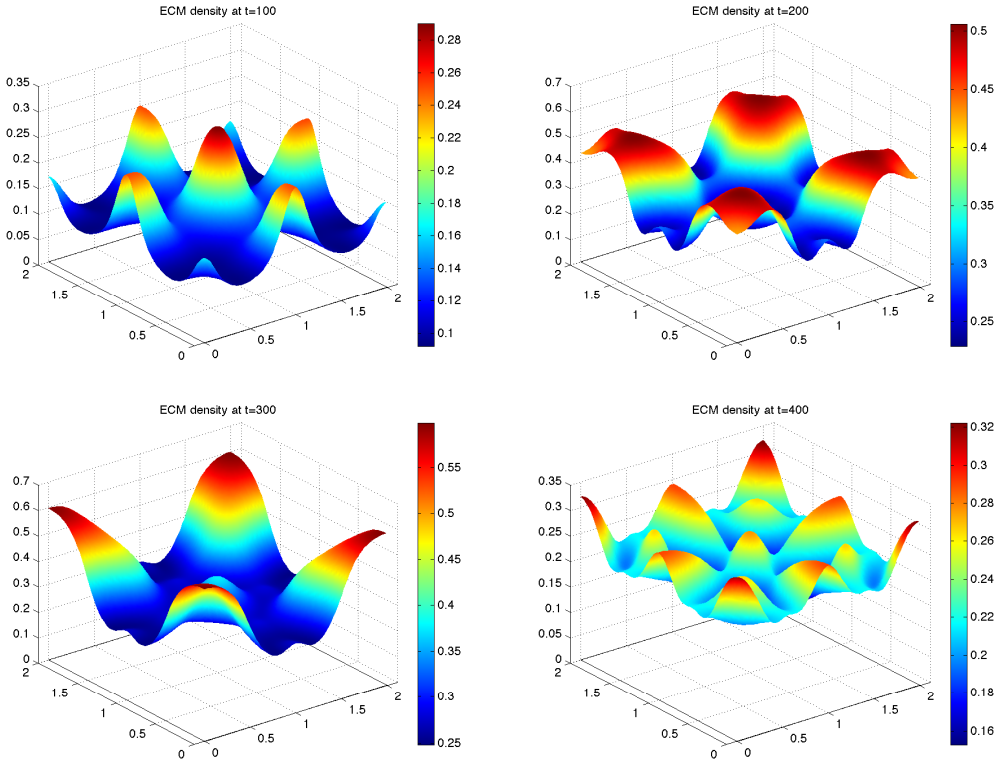

Figure 7.16: Plots showing the spatial distribution of ECM density within the tissue in a 2-dimensional spatial domain at time corresponding to 100, 200, 300, and 400, respectively (homogeneous ECM).

7.6.2 2D simulations with a heterogeneous ECM

We focus in this section to explore the numerical results of our model in 2D domain with a heterogeneous ECM density environment. To this end, we use the initial data for the effector, cancer, uPA, PAI-1, and plasmin as given in (7.5) and the ECM initial condition as figure 7.17.

Figures 7.18, 7.19, and 7.20 shows respectively, the spatial distribution of effector

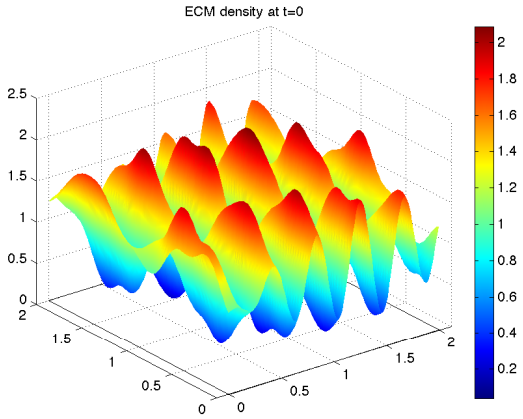

Figure 7.17: Heterogeneous ECM initial conditions.

cells, tumour cells, and ECM, with time 100, 200, 300, and 400 respectively. We note the tumour with heterogeneous ECM is close to the tumour with homogeneous ECM, with different behaviour.

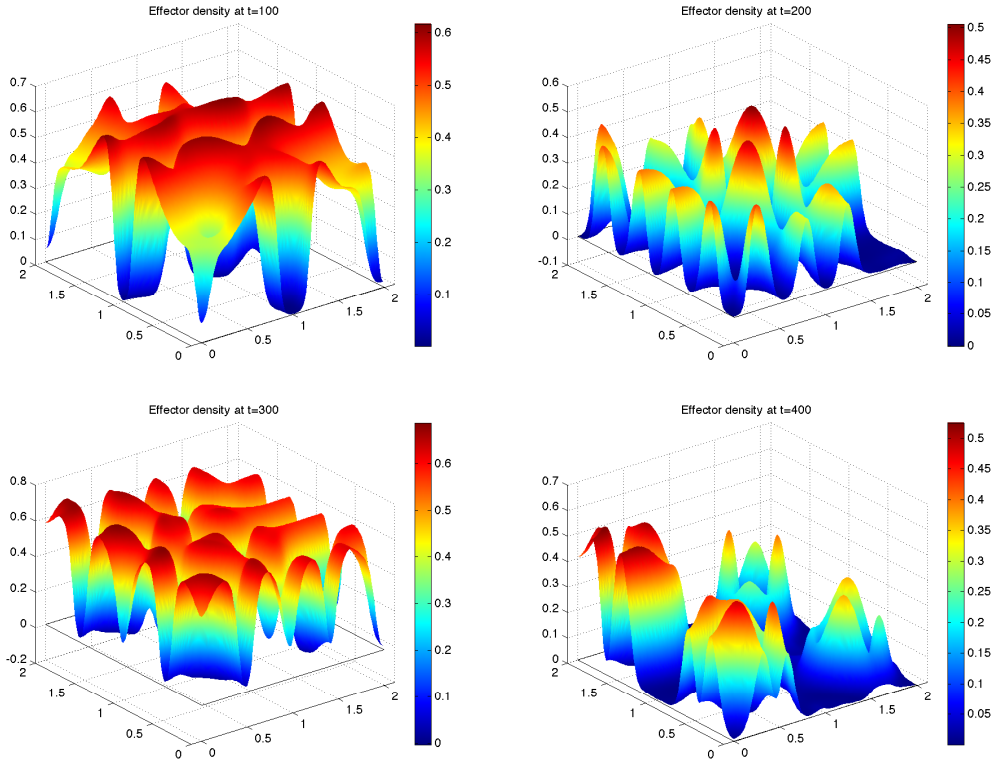

Figure 7.18: Plots showing the spatial distribution of effector cell density within the tissue in a 2-dimensional spatial domain at time corresponding to 100, 200, 300, and 400, respectively. Heterogeneous ECM initial conditions 7.17.

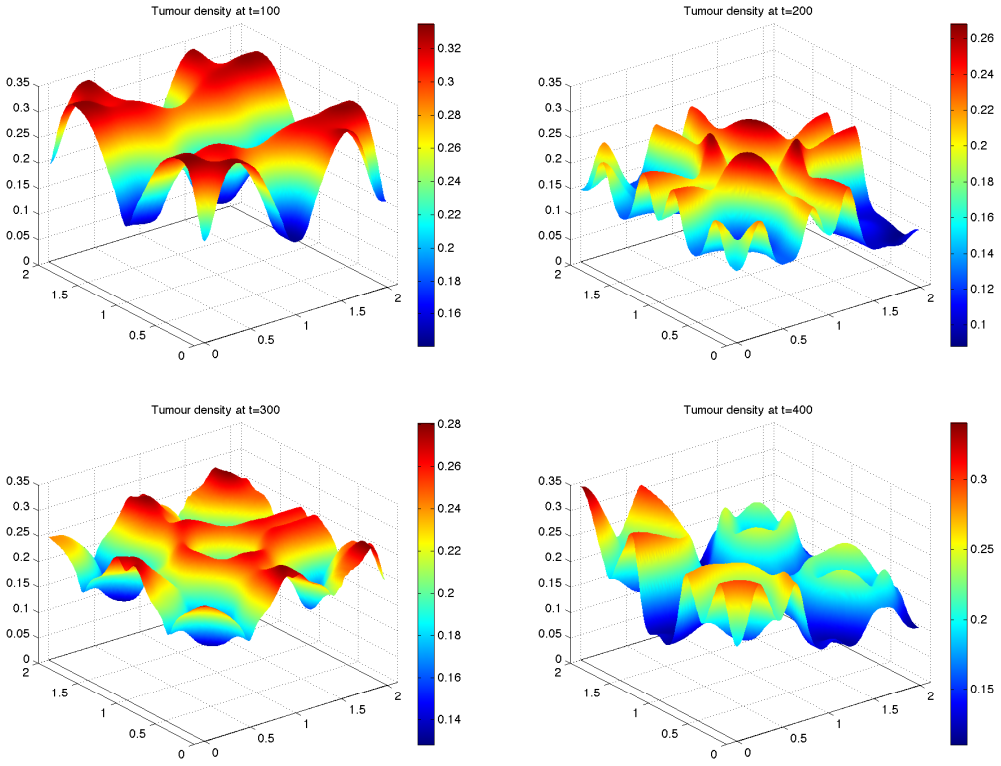

Figure 7.19: Plots showing the spatial distribution of tumour cell density within the tissue in a 2-dimensional spatial domain at time corresponding to 100, 200, 300, and 400, respectively. Heterogeneous ECM initial conditions.

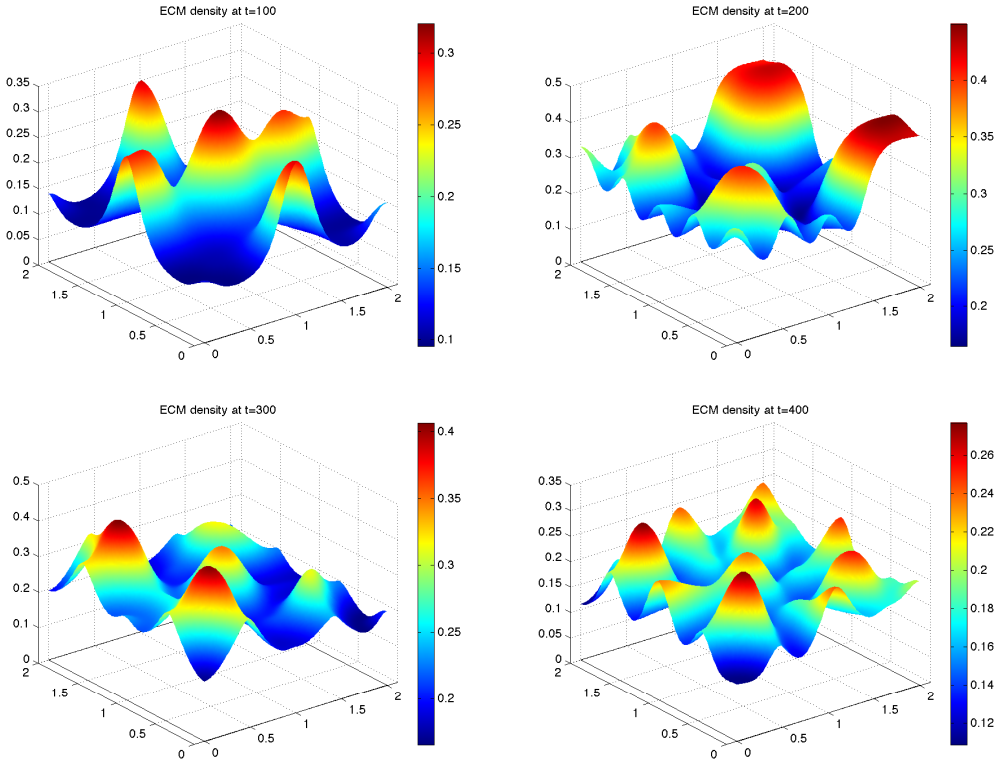

Figure 7.20: Plots showing the spatial distribution of ECM density within the tissue in a 2-dimensional spatial domain at time corresponding to 100, 200, 300, and 400, respectively. Heterogeneous ECM initial conditions.

7.7 Discussion and Conclusions

The work we have presented in this chapter has developed a mathematical model for tumour invasion with an immune response using a continuum model in 1 and 2 space dimensions. This model consists of a system of nonlinear partial differential equations and examines the effector cell response the tumour invasion. This model consists of effector cells, tumour cells, ECM, uPA, PAI-1, and plasmin. First, we set all spatial components of the model to zero and considered only the reaction kinetics in order to compare between the behaviour of our model and the original Chaplain and Lolas model. The spatial homogeneous simulation showed the behaviour of solutions have regular oscillations (figure 7.10), because there is a closed orbit (limit cycle figure 7.9). This was also explained by using bifurcation analysis.

Figure **??** explained the Hopf bifurcation with respect to the parameters h and a. The results from the one dimensional model simulation compared the results of the Chaplain and Lolas model (Chaplain and Lolas, 2005) with our model.

Second, we presented the computational results of the spatio-temporal model, and we noted from these simulations that the tumour size of our model is smaller than the tumour size of the Chaplain and Lolas model because the immune cells are interacting with the tumour cells, and also the degradation of ECM is less than that in the Chaplain and Lolas model. In addition, the number of tumour cell clusters in our model is less than those in the Chaplain and Lolas model. Also we found the tumour clusters of the mathematical model which was discussed in this chapter to have the same range than the tumour clusters of the Chaplain and Lolas model.

We calculated the steady states of the mathematical model and showed the linear stability analysis of these steady states. The mathematical model had trivial, semi-trivial, and non-trivial steady states. All these steady states are saddle, the semi steady states are healthy, i.e., only ECM or only effector sell, and we dont have a fully malignant

steady state. The non-trivial steady state has complex eigenvalues, four with negative real part, and two with positive real part.

The bifurcation analysis was applied in this chapter to explain the Hopf bifurcation with respect the parameters h and a. The bifurcation diagram shows the bifurcation was detected at $h = 1.766$, and at $a = 0.2277$.

Following the one-dimensional spatial model, we solved the model (7.2) in two-dimensional space, with homogeneous and hetrogeneous ECM.

Chapter 8

Controlling Cancer Growth through Competition for Space

In this chapter, we consider a Lotka-Volterra-type competition model that consists firstly of two cell types in competition for space: effector cells and tumour cells. We then extend the model to also include the effect of competition for space with extracellular matrix (ECM). The Lotka-Volterra competition model describes two populations that affect each other in a negative fashion. This model assumes that each species in the absence of the other grows logistically to some carrying capacity.

8.1 Mathematical Model

The model system we consider is:

$$\begin{aligned} \frac{\partial E}{\partial t} &= D_E \nabla^2 E + f(E,T), \\ \frac{\partial T}{\partial t} &= D_T \nabla^2 T + g(E,T), \end{aligned} \tag{8.1}$$

where E denotes the density of effector cells, T the density of tumour cells,

$$f(E,T) = E(1-E-\beta T), \qquad g(E,T) = rT(1-T-\gamma E)$$

and D_E, D_T, β, γ, and r are positive constants. In this model we consider that f and g satisfy the following conditions (cf. Alzahrani et al. (2010)):

1. $f(0,T) = 0 = g(E,0)$.
2. (8.1) has exactly two stable, uniform equilibria S_- = (0,1) and S_+ = (1,0) and two unstable, uniform equilibria (0,0) and (E_s, T_s).
3. $f_T(E,T) < 0$, $g_E(E,T) < 0$ for $(E,T) \in (0,1)^2$.
4. The non-trivial solution (E,T) of $g(E,T) = 0$ are given by $E = \Gamma(T)$ for a monotonically decreasing function Γ. Setting $\Gamma(1) = 0$ and $\Gamma(0) = \hat{E}$, where $0 < \hat{E} < 1$, Γ has an inverse $\hat{\Gamma} \in C^1([0,\hat{E}],[0,1])$, which can be extended trivially to a function $\gamma \in C^0([0,1],[0,1])$ where

$$\gamma(E) = \begin{cases} \hat{\gamma}, & E \in [0,\hat{E}], \\ 0, & E \in (\hat{E},1]. \end{cases}$$

Model (8.1) has four steady states:

$$(0,0), \qquad (1,0), \qquad (1,0), \qquad (\frac{\beta-1}{\gamma\beta-1}, \frac{\gamma-1}{\gamma\beta-1}).$$

The first steady state is unstable, the second steady state is stable if $\beta > 1$ and a saddle if $\beta < 1$, the third steady state is stable if $\gamma > 1$, and a saddle if $\gamma < 1$. Finally, the fourth steady state is stable if $\beta, \gamma < 1$ and a saddle if $\beta, \gamma > 1$. In this chapter, we choose $\beta, \gamma > 1$.

8.2 Computational Simulation Results

In this section, we solve model (8.1) numerically by using MATLAB.

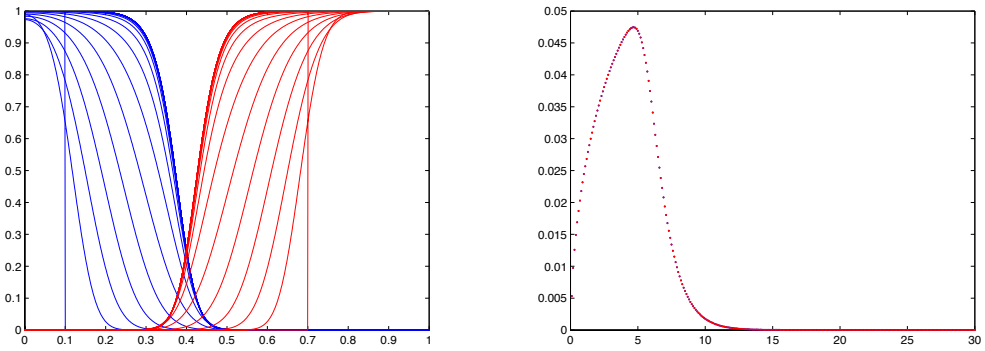

(a) (b)

Figure 8.1: Plots showing the distribution of tumour and effector cell density within the tissue at times from 0 up to final time 30. These plots illustrate the (a) standing wave of tumour and effector cell, and (b) wave speed. The blue lines represent the tumour cell , and the red lines represent the effector cell. The parameters are: $D_E = D_T = 0.001$, $\beta = \gamma = 5$, r=1.

Figure 8.1(a) shows the spatial distribution of tumour and effector cells within the tissue at time from 0 to 30. We note that the solution of model (8.1) is a travelling wave. These results show that the wave of effector cells stops the wave of tumour cells when they meet. Also figure 8.1 (b) shows that the wave speed is positive before the effector wave meets the tumour wave, and then it becomes zero after meeting. Figure 8.2 shows when $\beta > \gamma$, the travelling wave solution moves to the right and does not stop, i.e. the tumour occupies the space (the positive sign of the speed of the invading tumour cells refers to a tumour increasing, and the negative sign of the speed refers to the decreasing of effector cells). Figure 8.3 shows when $\gamma > \beta$, the solution moves to the left, i.e. the effector cells occupy the space. The positive sign of speed refers to the increasing of effector cells, and the negative refers to the decreasing of tumour cells.

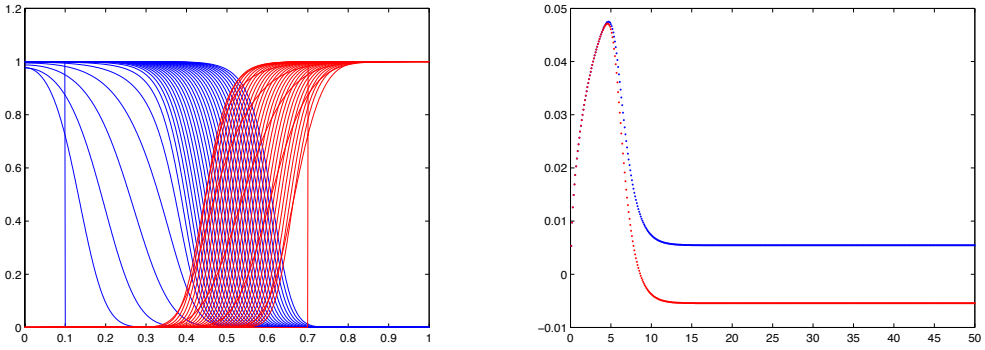

(a) (b)

Figure 8.2: Plots showing the distribution of tumour and effector cell density within the tissue at times from 0 up to final time 30. These plots illustrate the (a) standing wave of tumour and effector cell, and (b) wave speed. The blue lines represent the tumour cell , and the red lines represent the effector cell. The parameters are: $D_E = D_T = 0.001$, $\beta = 7, \gamma = 5$, r=1.

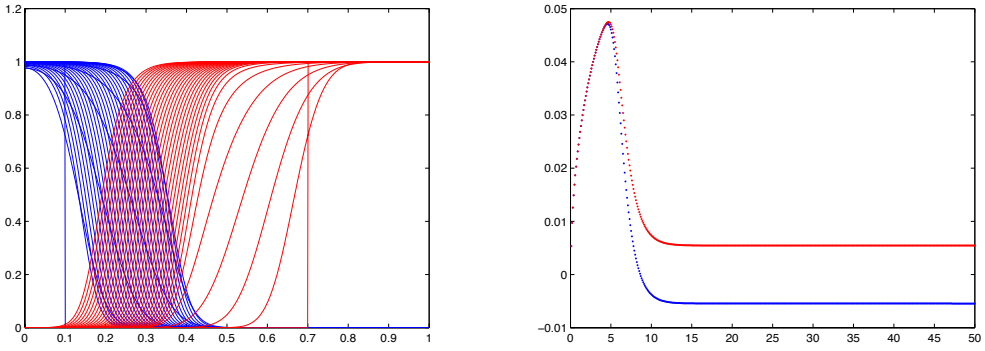

(a) (b)

Figure 8.3: Plots showing the distribution of tumour and effector cell density within the tissue at times from 0 up to final time 30. These plots illustrate the (a) standing wave of tumour and effector cell, and (b) wave speed. The blue lines represent the tumour cell , and the red lines represent the effector cell. The parameters are: $D_E = D_T = 0.001$, $\beta = 5, \gamma = 7$, r=1.

If $D_E \neq D_T$, then to get the standing wave between the two species E and T we need to change the relationship between β and γ. Suppose D_E is fixed, and the system has standing wave solutions by fixing γ and varying β: if $D_T << D_E$, then $\beta = \gamma^2$, if $D_T = D_E$, this is the case above ($\beta = \gamma$), and if $D_T >> D_E$, then $\beta = \sqrt{\gamma}$ (Alzahrani, 2011).

8.3 Tumour Mutation Model

We now suppose that the tumour cells will mutate into a new class of tumour cells, and therefore model (8.1) becomes:

$$\begin{aligned} \frac{\partial T_1}{\partial t} &= D_{T_1}\nabla^2 T_1 + r_1 T_1(1 - T_1 - \beta_2 T_2 - \gamma E) - \lambda T_1 H(t - t^*), \\ \frac{\partial T_2}{\partial t} &= D_{T_2}\nabla^2 T_2 + r_2 T_2(1 - T_2 - \beta_1 T_1 - \gamma E) + \lambda T_1 H(t - t^*), \\ \frac{\partial E}{\partial t} &= D_E \nabla^2 E + E(1 - E - \beta_1 T_1 - \beta_2 T_2), \end{aligned} \tag{8.2}$$

where T_1 denotes the the sub-population 1 of tumour cell, T_2 the sub-population 2, H is a Heaviside function, $r_2 > r_1$ and $D_{T_2} = D_{T_1}$. In the above model (8.2), we have assumed that the cancer cells of sub-population 1 are converted into cancer cells of sub-population 2 after time $t = t^*$. The difference between the two sub-populations is the proliferation rates. Cells of sub-population 2 proliferate more rapidly than cells of sub-population 1, i.e. $r_2 > r_1$.

We impose zero-flux boundary conditions and the initial conditions are:

$$T_1(x,0) = exp(-100x^2),$$

$$T_2(x,0) = 0,$$

$$E(x,0) = \begin{cases} 0, & \text{if } 0 \leq x < 0.3, \\ 1 - \exp(-100(x-0.3)^2), & \text{if } 0.3 \leq x \leq 1. \end{cases}$$

Figure 8.4 (a) shows the results of a computational simulation of model (8.2) where $t < t^*$. This means the cancer cells meet the effector cells but the mutation has not occurred, i.e. before the standing wave happens. In figure 8.4 (b) the cancer cells of sub-population 1 start to convert to those of sub-population 2, and the sub-population 2 start to invade the effector cells. In figure 8.4 (c) the sub-population 1 of cancer cells becomes zero, i.e. all sub-population 1 is converted to sub-population 2. Finally, in figure 8.4, the subpopulation 2 continues to occupy the tissue and is close to arriving at the other edge.

8.4 The Mutation Model with ECM Included

In this section, we add an equation modelling the interactions of ECM to model (8.2), and we get:

$$\begin{aligned} \frac{\partial T_1}{\partial t} &= D_{T_1}\nabla^2 T_1 + r_1 T_1(1 - T_1 - \beta_2 T_2 - \gamma E - \alpha V) - \lambda T_1 H(t - t^*), \\ \frac{\partial T_2}{\partial t} &= D_{T_2}\nabla^2 T_2 + r_2 T_2(1 - T_2 - \beta_1 T_1 - \gamma E - \alpha V) + \lambda T_1 H(t - t^*), \\ \frac{\partial E}{\partial t} &= D_E \nabla^2 E + E(1 - E - \beta_1 T_1 - \beta_2 T_2 - \alpha V), \\ \frac{\partial V}{\partial t} &= \mu V(1 - V - \beta_1 T_1 - \beta_2 T_2 - \gamma E). \end{aligned} \tag{8.3}$$

We find the numerical simulation of model (8.3) with two initial conditions as in figure 8.5, and we apply the standing wave into two ways, first by the effector cells, second by the ECM, depending on the relationship between parameters α, β_1, β_2 and γ, such as:

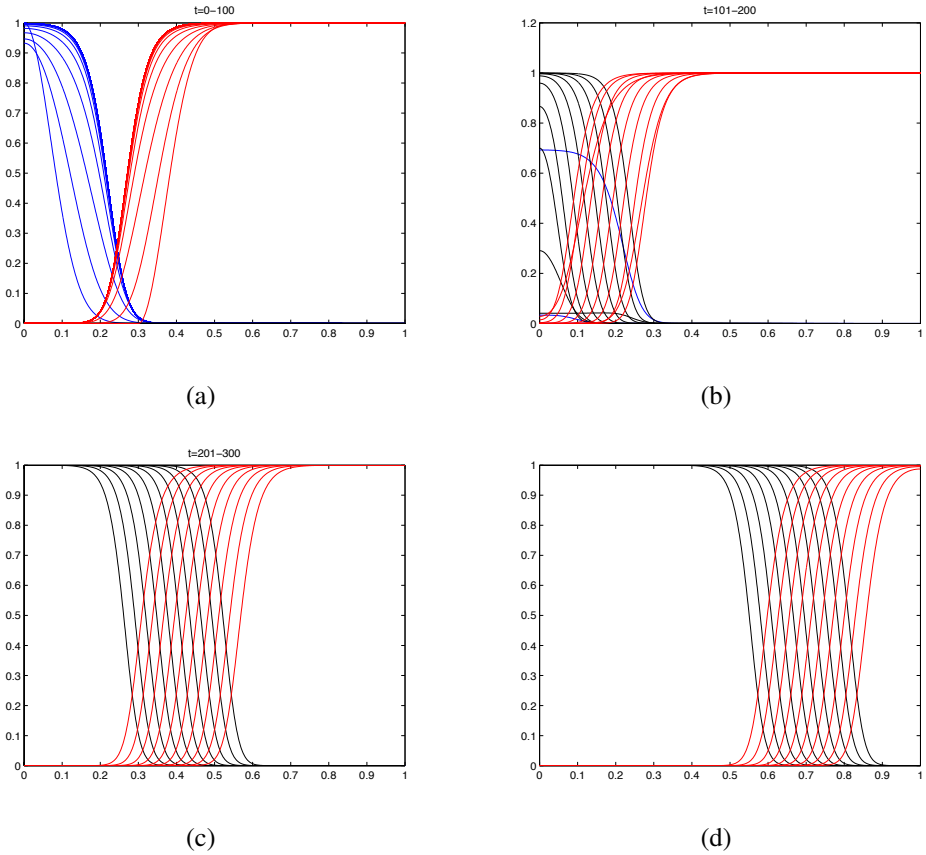

Figure 8.4: Plots showing the distribution of tumour and effector cell density within the tissue at times from 0 up to final time 300. These plots illustrate the standing wave of tumour and effector cell at (a) t=0-100, (b)t=101-200, (c) t=201-300, and (d) t=301-400. The blue lines represent the sub-population 1 of tumour cells, black line represent the sub-population 2 of tumour cells, and the red lines represent the effector cell. The parameters are: $D_E = D_{T_1} = D_{T_2} = 0.001$, $\beta_1 = \gamma = 5$, $\beta_2 = 7$,$r_1 = 1$, $r_2 = 2$, $\lambda = 0.3$.

If $\alpha < \beta_1 = \gamma$, then we get a behaviour similar to the behaviour of model (8.1) such

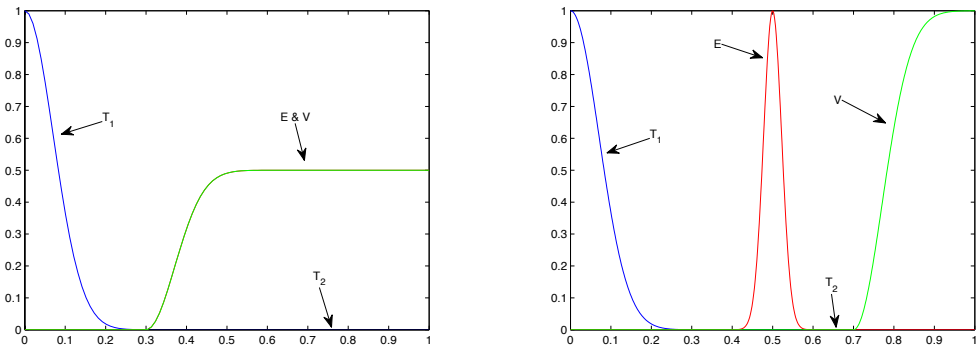

(a) (b)

Figure 8.5: Plots showing the initial conditions of tumour cells, effector cells and ECM.

that the ECM tends to zero, and the standing wave appears between the effector cells and tumour cells, then the mutation of cancer cells occurs and the more aggressive phenotype starts to invade the effector cells. Figure 8.6 (a) shows this case with initial 8.5 (a).

If $\beta_1 = \sqrt{\alpha}$, and $\gamma < \alpha$, then the effector cells tend to zero and the standing wave happens between the tumour cells and ECM. In addition, the mutation of cancer cells occurs and the new sub-population starts to invade the tissue. This phenotype is illustrated in figure 8.6 (b) with initial condition 8.5(a). We apply the initial condition 8.5 (b) for the two cases above. Figure 8.7 (a) shows the case $\alpha < \beta_1 = \gamma$. We note that the solution does not change from the initial conditions because there is standing wave between the tumour cells and effector cells and between effector cells and ECM. After the new sub-population appears, the tumour cells invade the effector cells until these vanish. The tumour cells then invade the ECM. Figure 8.7 (b) shows the case $\beta_1 = \sqrt{\alpha}$, and $\gamma < \alpha$, where the standing wave happens between the effector cells and tumour cells, but the effector cells invade the ECM from the other edge, therefore, the ECM disappears and the new sub-population of tumour cells invades the effector cells.

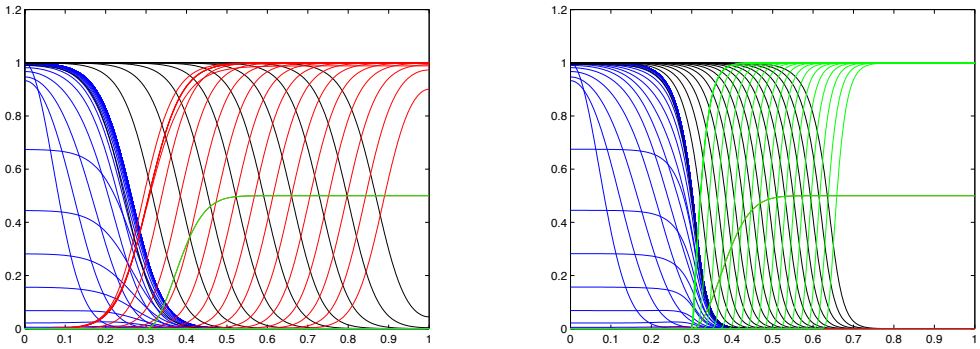

(a) (b)

Figure 8.6: Plots showing the distribution of tumour and effector cell density within the tissue at times from 0 up to final time 300. The blue lines represent the sub-population 1 of tumour cells, black line represent the sub-population 2 of tumour cells, red lines represent the effector cell, and green line represent the ECM. The parameters are: $D_E = D_{T_1} = D_{T_2} = 0.001$,(a) $\beta_1 = \gamma = 2$, $\alpha = 1.5$, $\beta_2 = 2.5$, $r_1 = 1$, $r_2 = 2$, $\lambda = 0.3$, (b) $\beta_1 = \gamma = 2$, $\alpha = 4$, $\beta_2 = 2.5$, $r_1 = 1$, $r_2 = 2$, $\lambda = 0.3$. The two figures with initial condition 8.5 (a).

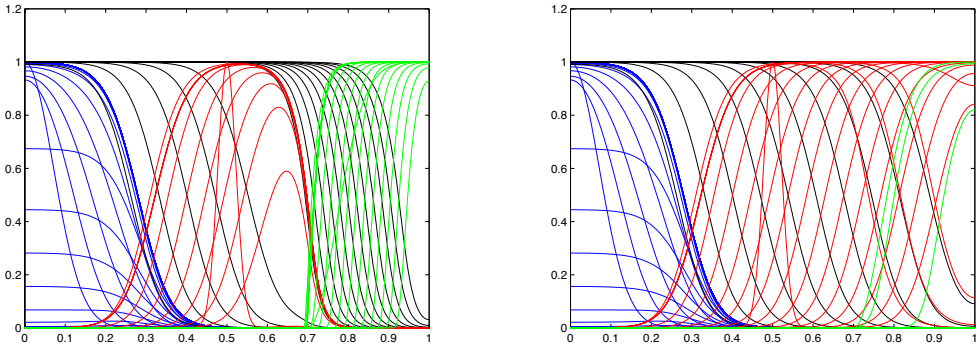

(a) (b)

Figure 8.7: Plots showing the distribution of tumour and effector cell density within the tissue at times from 0 up to final time 300. The blue lines represent the sub-population 1 of tumour cells, black line represent the sub-population 2 of tumour cells, red lines represent the effector cell, and green line represent the ECM. The parameters are: $D_E = D_{T_1} = D_{T_2} = 0.001$,(a) $\beta_1 = \gamma = 2$, $\alpha = 1.5$, $\beta_2 = 2.5$, $r_1 = 1$, $r_2 = 2$, $\lambda = 0.3$, (b) $\beta_1 = \gamma = 2$, $\alpha = 4$, $\beta_2 = 2.5$, $r_1 = 1$, $r_2 = 2$, $\lambda = 0.3$. The two figures with initial condition 8.5 (b).

8.5 Mutation Model with ECM and Matrix Degrading Enzyme

The last model we discuss in this chapter is

$$\begin{aligned}
\frac{\partial T_1}{\partial t} &= D_{T_1}\nabla^2 T_1 + r_1 T_1(1 - T_1 - \beta_2 T_2 - \alpha V) - \lambda T_1 H(t - t^*), \\
\frac{\partial T_2}{\partial t} &= D_{T_2}\nabla^2 T_2 + r_2 T_2(1 - T_2 - \beta_1 T_1 - \alpha V) + \lambda T_1 H(t - t^*), \\
\frac{\partial V}{\partial t} &= -\eta V M + \mu V(1 - V - \beta_1 T_1 - \beta_2 T_2), \\
\frac{\partial M}{\partial t} &= D_M \nabla^2 M + \delta T_2 - \omega M,
\end{aligned} \tag{8.4}$$

where M is a matrix degrading enzyme (MDE) of the ECM, and H is the Heaviside function. We impose zero-flux boundary conditions and the initial conditions are

$$T_1(x,0) = exp(-100x^2),$$

$$T_2(x,0) = 0,$$

$$V(x,0) = \frac{1}{2}exp(-100x^2),$$

$$M(x,0) = 0.$$

The numerical simulation of model (8.4) is illustrated in figure 8.8, where the degrading enzyme product depends on the sub-population 2 of tumour cells, i.e. there is no degradation of ECM before the mutation of sub-population 1 of tumour cells to sub-population 2 because the ECM stops the invasion. Similar to the previous results the sub-population 2 of tumour cells invades the ECM and occupy the space.

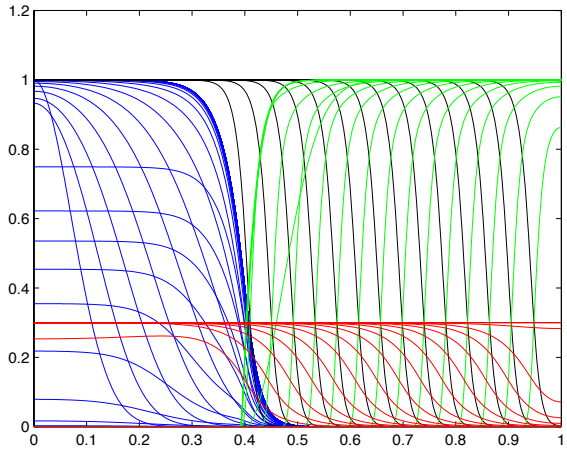

Figure 8.8: Plots showing the distribution of tumour and ECM density within the tissue at times from 0 up to final time 300. The blue lines represent the sub-population 1 of tumour cells, black line represent the sub-population 2 of tumour cells, red lines represent the degrading enzyme of ECM, and green line represent the ECM. The parameters are: $D_{T_1} = D_{T_2} = 0.001$,(a) $\alpha = 4$, $\beta_1 = \sqrt{\alpha}$, $\beta_2 = 2.5$, $r_1 = 1$, $r_2 = 2$, $\lambda = 0.3$, $\eta = 2$, $\omega = 0.5$, $\mu = 1$, $\delta = 0.15$.

8.6 Discussion and Conclusion

The Lotka-Volterra model is a phenomenological (holistic) model. It describes the possible effects of competition between two species (in terms of coexistence or competitive exclusion).

The numerical simulations discussed in this chapter were essentially associated with the initial model of two equations representing the effector cells and tumour cells, such that there is a standing wave between these species. We note that the solution of the mathematical model was a travelling wave and also had a standing wave solution (i.e. the wave of effector cells stops the wave of tumour cells when they meet). This phenomenon happened when the two diffusion coefficients are the same and $\beta = \gamma$, i.e. the waves stop and do not go either to the right or left. Also we showed that when $\beta > \gamma$, the travelling wave solution moved to the right and did not stop, i.e. the tumour

occupied the space, and when $\gamma > \beta$, the solution moved to the left, i.e. the effector occupied the space.

We calculated the wave speed to illustrate that the speed tended to zero when the two waves met - the positive speed of tumour cells refers to an invading tumour, and the negative sign of speed refers to the decreasing of effector cells. After that we modified the model by adding the equation for a second cancer cells population T_2, which is the sub-population 2 of tumour cells. This was to reflect the fact that cancer is a progressive disease, and as such it becomes more malignant as the cancer cells undergo successive mutations. We showed in this case how the new type of cancer cells start to invade the effector cells after the failure of the first type.

The third model discussed in this chapter was arrived at by adding the ECM equation to the second model, and it explained how the standing wave arose from two types of equations - the first one contained diffusion, and the second one without diffusion. The second case was satisfied by choosing $\beta_1 = \sqrt{\alpha}$, and this model was discussed with two types of initial conditions as in figure 8.5.

If $\beta_1 = \sqrt{\alpha}$ and $\gamma < \alpha$, then the effector cells tend to zero and the standing wave happens between tumour cells and ECM. In addition, the mutation of cancer cells is satisfied and the new sub-population starts to invade the tissue. We note that the solution does not changed from the initial condition because there is a standing wave between the tumour cells and effector cells, and between the effector cells and ECM. After the second cancer cell sub-population appears, the tumour invades the effector cells until they vanish, and then then the cancer cells invade the ECM.

In the other case when $\alpha < \beta_1 = \gamma$, the standing wave happens between the effector cells and the tumour cells, but the effector cells invade the ECM from the other edge, therefore, the ECM disappears and the new sub-population of tumour cells invades the effector cells.

Finally, we formulated a mathematical model which contained the ECM with cancer cells but also added an equation describing the effect of matrix degrading enzymes. These enzyme depend on the sub-population 2 of cancer cells, i.e. the enzymes appear after the mutation of sub-population 1 to sub-population 2.

Chapter 9

Conclusions and Future Directions

We conclude this thesis with a brief summary of the major points and some possible avenues of future exploration. Of course, this is by no means exhaustive, and we refer the reader to the appropriate chapters for a more detailed account.

9.1 General Conclusions

In the framework of this thesis we have examined spatio-temporal mathematical models describing the growth of a solid tumour in the presence of an immune system response. In the first chapter, we focussed on the spatio-temporal response of cytotoxic T-lymphocytes to tumour cells. We have developed and extended ideas originally formulated by Matzavinos et al. (2004) by proposing a possible kinetic mechanism leading to tumour evasion from the immune control.

Our model is based on the key concept that a tumour cell which survives the formation of a complex with a cytotoxic T-lymphocyte can develop, with a given probability, an

increased probability of surviving further attacks by CTLs. We do not specify whether this so-called increased resistance is genetic or epigenetic. Indeed, from a kinetic point of view, this is immaterial. However, in order to experimentally validate the hypothesis, this distinction would be of paramount relevance. In this work we have dealt with the spatio-temporal interplay between tumours and a specific immune response from CTLs. We chose this approach because of the experimental evidence on the relevance of CTLs in determining tumour dormancy or the evasion of many important tumours such as melanomas, ovarian carcinomas and colorectal carcinomas, where the presence of infiltrating lymphocytes is a useful prognostic marker (Galon et al., 2006; Zitvogel et al., 2006). However, tumour immunoevasion from dormancy is a multi-faceted phenomenon. We stress here that by no means do we think that ours is an exhaustive theoretical treatment of a such complex phenomenon.

We have built our model based on the tumour dormancy mathematical model of Matzavinos et al. (2004); Chaplain and Matzavinos (2006), where parameters were fitted to experimental animal (mouse) data. However, embedding the proposed evolutionary mechanism in a more complex setting, where a more detailed description of both adaptive and innate immunity is included, should lead to results qualitatively similar to those here illustrated.

Our simulations suggest that the proposed mechanism is able to mimic various dynamics of immunoevasion during the lifespan of a mouse. We have also highlighted the differential spatiotemporal contributions to evasion due, respectively, to: *i)* a decrease in the probability p_i of being lethally hit; *ii)* a decrease in the probability, embedded in k_i^+, that a tumour cell is recognized by a CTL. In particular, our model suggests that a decrease in the parameters p_i is needed to produce evasion, which does not occur in the case where p_i remains constant at its baseline level inferred from the experimental

data. However, the role of the parameters k_i^+ is important since it can greatly accelerate the simulated process. Moreover, our computational simulations also showed that the proposed mechanism can also deeply affect the spatial patterning of the tumour. In particular, our model suggests that to have a uniform invasion profile for the tumour cells necessitates also having a decrease in the recognition rate, embedded in the parameters k_i^+. These parameters also differentially shape the spatial distribution of the various classes of tumour cells.

Concerning the possible chemorepulsion of CTLs, our computational simulation results showed that, in our biological settings, although it does not affect the spatiotemporal dynamics of the total number of tumour cells, it has a remarkable influence on the spatio-temporal distribution of the different individual classes of tumour cells. Further analysis is needed to ascertain if, with different parameters, the effect of this factor can be different, and in order to understand the behaviour in the current setting.

As far as the key 'immuno-evasion-related' parameters such as θ_i, p_i, and k_i^+ are concerned, we were not able to fit them with experimental data (apart, of course, from the values for p_0 and k_0^+, from Matzavinos et al. (2004); Chaplain and Matzavinos (2006)) because in the literature, to the best of our knowledge, immuno-editing is only illustrated by means of qualitative clinical or molecular experimental findings. In particular, no immuno-evasion-related tumour growth data are available. Indeed, a complete experimental kinetic study of the adaptive evasion from tumour dormancy allowing, for example, the plotting of tumour growth curves would currently be very difficult to undertake. Thus we hope that this theoretical work may contribute to triggering such experimental investigations, which would allow us to validate our model.

From a theoretical point of view, our model, although detailed and focused on a very specific aspect of immuno-oncology, and on some very specific mechanisms, is conceptually in line with the general theories by Bellomo (Bellomo et al., 2004; Bellomo

and Delitala, 2008; Bellomo, 2010). Indeed, here also the changes of activities of cells upon encounters between tumour cells and effectors cells of the immune system are central in determining the dynamics of the system.

In this work we essentially were interested in the basic facts of the immune response to tumours. However, a number of immunotherapies have been proposed and also theoretically investigated (see d'Onofrio (2005); Arciero et al. (2004); Kim et al. (2008) and references therein). We believe that both the experimental results concerning immunoevasion of tumours and the theoretical findings we have proposed here might have some implication of interest in clinics. More in general, we share the opinion of Zitvogel et al. (2006), who stressed that recent progress in immuno-oncology have not influenced the way anticancer therapies are conceived and applied in clinics.

The model that was proposed here has to be understood as a detailed model at the level of the kinetics of the cellular populations of a possible mechanism that might enable tumour cells to evade from the control of adaptive immunity. The various specific (and tumour-dependent) strategies deployed by those cells in order to reach their aim, are phenomenologically described by means of the model of the dependence of the various parameters on the classes of tumour cells, as well as in the macroscopic modelling of the chemorepulsion. This is a first step in a research effort for a more complete description of tumour cell immunoevasion, which will include the detailed modelling of the biological mechanisms underlying those and other specific evasion strategies. Thus, given the complex network of interplaying between inter-cellular and intra-cellular signalling, and given the various temporal scales (from the rapid dynamics of the intracellular pathways involved, to the relatively slow growth of a tumour, up to the very slow onset of immunoevasion) as well as the spatial ones (from individual cells to visible neoplasms), a more detailed model will have to be multiscale. This will involve a wide array of computational tools, from those typical of computational

biology and bioinformatics, to more classical analytical and numerical methods of statistical mechanics and mathematical physics.

The second chapter discussed in this thesis is a mathematical model of the interplay between a tumour and both the innate and the cellular part of the adaptive immune system. We have developed and extended the ideas originally formulated by Owen and Sherratt (1997); Matzavinos et al. (2004); de Pillis et al. (2005).

In this first set of simulations, we set all the spatial components of the model to zero and consider only the reaction kinetics, then we shows some spatio-temporal simulations which explain the interplay between tumours and macrophages, natural killer cells and cytotoxic T lymphocytes.

We observed that there is a slowly damped oscillation in the behaviour of the tumour, natural killer and CTL cells. Also we note that the solution converges to the second steady state where the tumour size is smaller than the second stable steady state (fourth steady state).

Also we discussed in this chapter the effect of the initial conditions to the solution of ODE system, since we have multi-stable system, we should take the initial condition of the ODE system close to the steady state.

We found there is a oscillation when we take the initial conditions close to the fourth steady state and the oscillation are continuous with time increasing. This behaviour means that there is a closes orbit around the steady state (limit cycle).

The model which discussed in this chapter is sensitive to the initial condition, because when we multiplied the initial condition by 0.999, the shape of solution is changed and some some sort of transient chaos, but the solution going after that to the steady state.

Also we found from the linear stability analysis for the model. there is four positive steady state s, two are stable and two are saddle. We changed the stability of this steady states by changed the parameters q_0 and δ_4, where got two saddle positive steady states.

and the limit cycle still appears.

In the second set of simulations, we found the solutions of model 6.16. Following to the ODE simulations we considered two cases, depending on the parameter values such that the first case in like table 6.1 and the second case is by changed two parameters q_0 and δ_4. In the first case the solution tended to the positive steady state, and the solution of macrophage M_0 is similar to the solution of M_1. The behaviour of the solution of natural killer is similar to the behaviour of the solution for the tumour cells up to time 400 days, then the shape of the profile of the natural killer cells changed. The solution of the E_n reach the steady state value after a short time. The solution of CTL again have the same shape of tumour solution with different values.

In the second case we got the different behaviour of solution because there is limit cycle and oscillation in the shapes of solution and also the values of variables are changed.

The third chapter developed a mathematical model for tumour invasion with immune response using a continuum model in 1 and 2 space dimensions. This model consists of a system of nonlinear partial differential equations and examines how the effector cell response the tumour invasion. This model consists of effector cell, tumour cell, ECM, uPA, PAI-1, and plasmin. First, we set all spatial components of the model to zero and consider only the reaction kinetics in order to compare between the behaviour of our model and the Chaplain and Lolas model. The spatial homogeneous simulation showed the behaviour of solutions have regular oscillation, because there is a close orbit (limit cycle), this is also explained by using the bifurcation analysis.The results from the one dimensional model simulation comparing the results of Chaplain and Lolas (2005) with our model.

Second, we presented the computational results of spatio-temporal model, we noted from this simulations the tumour size of our model is smaller than the tumour size of Chaplain and Lolas model because there is an immune cell interacting with tumour

cells, and also the degrading of ECM is less than the degrading of Chaplain and Lolas model. In additional to the number of cluster of our model is less than the cluster of Chaplain and Lolas model. Also we found the tumour clusters of the mathematical model which discussed in this chapter are have the same range than the tumour clusters of Chaplain and Lolas model.

We calculated the steady states of the mathematical model and showed the linear stability analysis of these steady states. The mathematical model had trivial, semi-trivial, and non-trivial steady states. All these steady states are saddle, the semi steady states are healthy, i.e., only ECM or only effector sell, and we dont have full malignant steady state. The non-trivial steady state has complex eigenvalues, four with negative real part, and two with positive real part.

The bifurcation analysis was applied in this chapter to explained the Hopf bifercation with respect the parameters h and a. The bifurcation diagram shows the bifurcation was detected at $h = 1.766$, and at $a = 0.2277$. Following to the one-dimensional space, we solved the model in two-dimensional space, with homogeneous and hetrogeneous ECM.

In the last chapter we formulated a mode where competition for space was the key feature. The Lotka-Volterra model is a phenomenological (holistic) model. It describes the possible effects of competition between two species (in terms of coexistence or competitive exclusion).

The numerical simulations discussed in this chapter were essentially associated with the model of two equations represented the effector cells and tumour cells, such that there is a standing wave between these species.

We note that the solutions of the mathematical model was a travelling wave and also a standing wave (i.e. the wave of effector cells stops the wave of tumour cells when they meet). This behaviour happened when the diffusion coefficients are the same and

$\beta = \gamma$, i.e. the waves stop going either to the right or left. Also we showed when $\beta > \gamma$, the travelling wave solution moved to the right and did not stop, i.e. the tumour occupies the space, and when $\gamma > \beta$, the solution move to the left, i.e. the effector cells occupy the space.

We calculated the wave speed to illustrate that the speed tended to zero when the two waves met, the positive sign of the speed of tumour cells referring to an invading tumour, and the negative sign of speed refers to the decreasing of effector cells. After that we modified the model by adding an equation for a second sub-population of cancer cells T_2. Since cancer is a progressive disease, it is becomes more malignant as the cancer cells undergo successive mutations. We showed in this case how the new type of cancer cells start to invade the effector cells after the failure of the first type.

The third model discussed in this chapter was formulated by adding the ECM equation to the second model, and explained how the standing waves arose from two types of equations - the first one contained diffusion, and the second one without diffusion. The second case was satisfied by choosing $\beta_1 = \sqrt{\alpha}$. This model was discussed with two types of initial conditions.

If $\beta_1 = \sqrt{\alpha}$ and $\gamma < \alpha$, then the effector cells tend to zero and the standing wave happens between the tumour cells and ECM. In addition, the mutation of cancer cells is satisfied and the new sub-population starts to invade the tissue. We note that the solution does not change from the initial conditions because there is a standing wave between tumour cells and effector cells and between effector cells and ECM. After the new cancer sub-population appears, the tumour invades the effector cells until they vanish, then the cancer cells invade the ECM.

In the other case when $\alpha < \beta_1 = \gamma$, the standing wave happens between the effector cells and tumour cells, but the effector cells invade the ECM from the other edge. Therefore, the ECM disappeared and the new sub-population of tumour cells invaded the effector cells.

Finally, we presented a mathematical model containing the ECM with cancer cells, and added the equation of matrix degrading enzymes. These enzymes depended on the sub-population 2 of cancer cells, i.e. the enzymes are secreted after mutation of sub-population 1 to the sub-population 2.

9.2 Future Directions

One further aspect of immunoevasion that we would like to investigate in the future is to extend the ideas of chapter five to the model of Owen Sherratt (Owen and Sherratt, 1997, 1999) and include here the interplay with the innate immune system. Our idea would be to describe the immunoevasion from the initial control of the macrophages. The tumour cells would form a complex with the macrophages, acquire an advantage and thus transit to a class of more resistant cells T_1, ... etc. Also we may try to modify the results in chapter six, for the innate and adaptive immune response with cancer.

As we have seen, uncontrolled proliferation and abnormal cell migration are two of the main characteristics of tumour growth. The tumour cells change their phenotype due to mutations that are acquired during cancer progression. Initially, mutations alter the proliferation control of the cells which leads to uncontrolled cell division Hanahan and

Weinberg (2000). Then the transformed cells form a neoplastic lesion and the tumour can grow up to a size at which the diffusion-driven oxygen supply becomes insufficient (hypoxia) to support further growth.

Experiments with cultures of glioma cells (Giese et al., 2003) have shown a relationship between migratory and proliferative behaviour. Especially, cell motion and proliferation are mutually exclusive processes and highly motile glioma cells tend to have lower proliferation rates, i.e. cells proliferate only when they do not move (resting phase). This phenomenon is known as the migration/proliferate dichotomy (or the 'Go or Grow' mechanism) (Giese et al., 996a,b).

In the future, we would like to test the idea of standing waves which was discussed in chapter eight to the stationary mobile model with a switch between them (Lewis and Schmitz, 1996).

The mathematical model would be represented in this case by a system of PDEs of the form:

$$\partial_t s = rs(1-\frac{s}{k}) + \lambda_{ms} m - \lambda_{sm} s,$$

$$\partial_t m = D\frac{\partial^2 m}{\partial x^2} - \mu m - \lambda_{ms} m + \lambda_{sm} s,$$

where $s(x,t)$ is the density of cells in the stationary state and $m(x,t)$ is the density of cells in the mobile state, λ_{sm} is the rate of switching from stationary to mobile state and λ_{ms} is the rate of switching from a mobile to stationary state.

Bibliography

Abbas, A. K. and Lichtman, A. H. (2009). *Basic immunology: functions and disorders of the immune system*. Saunders Elsevier, third edition edition.

Adam, J. A. and Bellomo, N. (1997). *A Survey of Models for Tumor-Immune System Dynamics*. Birkhauser.

Alberts, B., Bray, D., Lewis, J., Raff, M., Roberts, K., and Watson, J. D. (1994). *Molecular Biology of the Cell*. Garland Publishing.

Alzahrani, E. (2011). *Travelling Waves in Lotka-Volterra Competition Models*. PhD thesis, Dundee University.

Alzahrani, E., Davidson, F., and Dodds, N. (2010). Travelling waves in near-degenerate bistable competition models. *Math. Model. Nat. Phenom.*, 5(5):13–35.

Andasari, V., Gerisch, A., Lolas, G. South, A., and Chaplain, M. A. J. (2010). Mathematical modeling of cancer cell invasion of tissue: Biological insight from mathematical analysis and computational simulation. *J. Math. Biol.*, 63(1):141–171.

Anderson, A., Chaplain, M. A. J., Newman, E., Steele, R., and Thompson, A. (2000). Mathematical modelling of tumour invasion and metastasis. *J. Theor. Biol.*, 2:129–154.

Arciero, J. C., Jackson, T. L., and Kirschner, D. E. (2004). A mathematical model of tumour-immune evasion and sirna treatment. *Disc. Cont. Dyn. Sys. Series B*, 4:39–58.

Bellomo, N. (2010). Modelling the hidinglearning dynamics in large living systems. *Appl. Math. Lett.*, 23:907–911.

Bellomo, N., Bellouquid, A., and Delitala, M. (2004). Mathematical topics on the modelling complex multicellular systems and tumor immune cell competition. *Math. Mod. Meth. Appl. Sci.*, 14:1683–1733.

Bellomo, N. and Delitala, M. (2008). From the mathematical kinetic, and stochastic game theory for active particles to modelling mutations, onset, progression and immune competition of cancer cells. *Phy. Life Rev.*, 5:183–206.

Berezhnaya, N. M. (2010). Interaction between tumor and immune system: The role of tumor cell biology. *Exp. Oncol.*, 32(3):159–166.

Caravagna, G., A., d., Milazzo, P., and Barbuti, R. (2010). Antitumour immune surveillance through stochastic oscillations. *J. Theor. Biol.*, 265(3):336–345.

Chaplain, M. A. J. (1995). The mathematical modelling of tumour angiogenesis and invasion. *Acta Biotheor.*, 43:387–402.

Chaplain, M. A. J. and Lolas, G. (2005). Mathematical modeling of cancer cell invasion of tissue: hhe role of the urokinase plasminogen activation system. *Math. Meth. Mod. Appl. Sci.*, 15(11):1685–1734.

Chaplain, M. A. J. and Matzavinos, A. (2006). Mathematical modelling of spatio-temporal phenomena in tumour immunology. *Lecture Notes in Mathematics*, 1872:131–183.

de Pillis, L., Radunskaya, A., and Wiseman, C. (2005). A validated mathematical model of cell-mediated immune response to tumor growth. *Cancer Res.*, 65:7950–7958.

Delves, P., Martin, S., Burton, D., and Roitt, I. (2006). *Essential Immunology*. Blackwell Publishing Ltd.

d'Onofrio, A. (2005). A genaral framework for modeling tumor-immune system competition and immunotherapy: Analysis and medical inferences. *Phys. D*, 208:220–235.

d'Onofrio, A. (2006). The role of the proleferation rate of effectors in the tumor-immune system competition. *Math. Mod. Meth. Appl. Sci.*, 16:1375–1401.

d'Onofrio, A. (2007). Tumor evasion from immune control: Strategies of a miss to become a mass. *Chaos Sol. Fractal*, 31:261–268.

d'Onofrio, A. (2008). Metamodeling tumor-immune system interaction, tumor evasion and immunotherapy. *Math. Comp. Mod.*, 47:614–637.

d'Onofrio, A. (2010). Tumour evasion from imune system control as bounded-noise induced transition. *Phys. Rev. E*, 81:art. n. 021923.

Du, L.-C. and Mei, D.-C. (2010). The critical phenomenon aand the re-entrance phenomenon in the anti-tumor model induced by the time delay. *Phy. Lett. A*, 374:3275–3279.

Dunn, G., Old, L., and Schreiber, R. (2004). The three es of cancer immunoediting. *Ann. Rev. Immun.*, 22:329–360.

Eftimie, R. and Bramson, J. (2011). Interactions between the immune system and cancer: Abrief review of non-spatial mathematical models. *Bull. Math. Biol.*, 73:2–32.

Ehrlich, P. (2009). Ueber den jetzigen stand der karzinomforschung. *Ned. Tijdschr. Geneeskd.*, 53:273–290.

Fang, J., Gillies, R., and Gatenby, R. (2008). Adaptation to hypoxia and acidosis in carcinogenesis and tumor progression. *Semin. Cancer Biol.*, 18:330–337.

Gabrilovich, D. I. and Hurwitz, A. A. (2008). *Tumor-Induced Immune Suppression*. Springer.

Galon, J., Costes, A., Sanchez-Cabo, F., Kirilovsky, A., Mlecnik, B., Lagorce-Pages, C., Tosolini, M., Camus, M., A., B., Wind, A., Zinzindohou, F., Bruneval, P., Cugnenc, P., Trajanoski, Z., Fridmanl, W., and Pags, F. (2006). Type, density, and location of immune cells within human colorectal tumors predict clinical outcome. *Science*, 313:1960–1964.

Garay, R. and Lefever, R. (1978). A kinetic approach to immunology of cancer: stationary states properties of effector-target cell reactions. *J. Theor. Biol.*, 73:417–438.

Giese, A., Bjerkvig, R., Berens, M., and Westphal, M. (2003). Cost of cigration: invasion of malignant gliomas and implications for treatment. *J. Clin. Oncol.*, 21:1624–1636.

Giese, A., Kluwe, L., Laube, B., and Berens, M. (1996a). Migration of human glioma cells on myelin. *Neurosurgery*, 38:755–764.

Giese, A., Loo, M., Tran, D., Haskett, S., and Coons, B. (1996b). Dichotomy of astrocytoma migration and proliferation. *Int. J. Cancer*, 67:275–282.

Hanahan, D. and Weinberg, R. A. (2000). The hallmarks of cancer. *Cell*, 100:57–70.

Horsthemke, W. and Lefever, R. (1977). Phase transitions induced by external noise. *Phy. Lett. A.*, 64:19–21.

Keener, J. and Sneyd, J. (2003). *Mathematical Physiology*. Springer-Verlag.

Kim, P. S., Lee, P. P., and Levy, D. (2008). Dynamics and potential impact of the immune response to chronic myelogenous leukemia. *PLoS Comput. Biol*, 4(6):e1000095.

Kim, R., Emi, M., and Tanabe, K. (2007). Cancer immunnoediting from immune surveillance to immune escape. *Immunology*, 121:1–14.

Kindt, T., Osborne, B., and Goldsby, R. (2006). *Kuby Immunology*. W. H. Freeman.

King, R. J. B. (2000). *Cancer Biology*. Prentice Hall.

Kirschner, D. and Panetta, J. (1998). Modelling immunotherapy of the tumout-immune interaction. *J. Math. Biol.*, 37:235–252.

Koebel, C. M., Vermi, W., Swann, J. B., Zerafa, N., Rodig, S. J., Old, L. J., Smyth, M. J., and Schreiber, R. D. (2007). Adaptive immunity maintains occult cancer in an equilibrium state. *Nature*, 450:903–907.

Kogan, Y., Forys, U., Shukron, O., Kronik, N., and Agur, Z. (2010). Cullular immunotherapy for high grade gliomas: Mathematical analysis deriving efficacious infusion rates based on patient requirement. *SIAM J. Appl. Math.*, 70:1953–1976.

Kronick, N., Kogan, Y., Elishmereni, M., Halevi-Tobias, K., Vuk Pavlovic, S., and Agur, Z. (2010). Predicting effect of prostate cancer immunotherapy by personalized mathematical models. *PLoS One*, 5(12):e15482.

Kuznetsov, V. and Knott, G. (2001). Modeling tumor regrowth and immunotherapy. *Math. Comp. Mod.*, 33:1275–1287.

Kuznetsov, V. A., Makalkin, I. A., Taylor, M. A., and Perelson, A. S. (1994). Nonlinear dynmamics of immunogenic tumors: Parameter estimation and global bifercation analysis. *Bull. Math. Biol.*, 56(2):295–321.

Lefever, R., J., H., Urbain, J., and Meyers, P. (1992). On the kinetics and optimal specificity of cytotoxic reactions mediated by t-lymphocyte clones. *Bull. Math. Biol.*, 59:263–294.

Lejeune, O., Chaplain, M. A. J., and Akili, I. (2008). Oscillations and bistability in the dynamics of cytotoxic reactions mediated by the response of immune cells to solid tumours. *MAth. and Comp. Mod.*, 47:649–662.

Lewis, M. and Schmitz, G. (1996). Biological invasion of an organism with separate mobile and stationary states: Modeling and analysis. *Forma*, 11(1):1–25.

Matzavinos, A., Chaplain, M. A. J., and Kuznetsov, V. (2004). Mathematical modelling of the spatio-temporal response of cytotoxic t-lymphocyte to a solid tumour. *Math. Med. Biol. IMA*, 21:1–34.

Mendez, V., Fedotov, S., and Horsthemke, W. (2010). *Reaction-Transport Systems*. Springer-Verlag.

Moore, H. and Li, N. K. (2004). A mathematical model for chronic myelogenous leukemia (cml) and t cell interaction. *J. Theor. Biol.*, 227:513–523.

Murphy, K., Travers, P., and Walport, M. (2008). *Janeway's Immunobiology*. Garland Science Publishing, seventh edition edition.

Murray, J. D. (2002). *Mathematical Biology I: An Introduction*. Springer-Verlag, third edition edition.

Owen, M. and Sherratt, J. (1997). Pattern formation and spatiotemporal irregularity in a model for macrophage-tumour interactions. *J. Theor. Biol.*, 189:63–80.

Owen, M. and Sherratt, J. (1999). Mathematical modelling of macrophage dynamics in tumours. *Math. Meth. Mod. Appl. Sci.*, 9:513–539.

Pardoll, D. (2003). Does the immune system see tumors as foreign or self ? *Ann. Rev. Immun.*, 21:807–839.

Parham, P. (2009). *The Immune System*. Garland Science, Taylor and Francis Group, LLC, third edition edition.

Skeel, R. and Berzins, M. (1990). A method for the spatial discretisation of parabolic equations in one space variable. *SIAM J. Sci. Stat. Comp.*, 11:1–32.

Sompayrac, L. (2008). *How the Immune System Works*. Blackwell Publishing Ltd, third edition edition.

Stepanova, N. (1980). Course of the immune reaction during the development of a malignant tumor. *Biophysics*, 24:917–923.

Stewart, T. J. and Abrams, S. I. (2008). How tumour escape mass destruction. *Oncogene*, 27:5894–5903.

Swann, J. and Smyth, M. (2007). Immune surveillance of tumors. *J. Clin. Inv.*, 117:1137–1146.

Szymanska, Z. (2003). Analysis of immunotherapy model in the context of cancer dynamics. *Appl. Math. Comput. Sci.*, 13:407–418.

Todd, I. and Spickett, G. (2005). *Immunology*. Blackwell Publishing Ltd, fifth edition edition.

Uhr, J. and Marches, R. (2001). Dormancy in a model of murine b cell lymphoma. *Sem. Canc. Biol.*, 11:277–283.

Vianello, F., Papeta, N., Chen, T. Kraft, P., White, N., Hart, W., Kircher, M., Swart, E., Rhee, S., Pal, G., Irimia, D., M., T., R., W., and Poznansky, M. (2006). Murine b16 melanomas expressing high levels of the chemokine stromal-derived factor-1/cxcl12

induce tumor-specific t cell chemorepulsion and escape from immune control. *J Immunol.*, 176:2902–2914.

Webb, S., Sherratt, J., and Fish, R. (2002). Cells behaving badly: a therotical model for the fas/fasl system in tumour immunology. *Math. Biosci.*, 179:113–129.

Yefenov, E. (2008). *Innate and Adaptive Immunity in the Tumor Microenvironment*. Springer.

Zitvogel, L., Tesniere, A., and Kroemer, G. (2006). Cancer despite immunosurveillance: Immunoselection and immunosubversion. *Nat. Rev. Imm.*, 6:715–727.